An antenna for a satellite communication ground station (provisional electrical design)

th e

An antenna for a satellite communication ground station
(provisional electrical design)

by

J. Dijk, M. Jeuken, and E.J. Maanders

TECHNISCHE HOGESCHOOL
EINDHOVEN NEDERLAND

AFDELING ELEKTROTECHNIEK

TECHNOLOGICAL UNIVERSITY
EINDHOVEN NETHERLANDS
DEPARTMENT OF ELECTRICAL
ENGINEERING

An antenna for a satellite communication ground station (provisional electrical design)

by

J.Dijk, M.Jeuken and E.J.Maanders

TH-report 68-E-01
March 1968

Contents

Contents

Acknowledgement.

This work was initiated on January 26, 1967 and completed in September 1967 as part of a provisional design for a satellite communication ground station in the Netherlands.

The authors wish to thank Prof.ir.B. van Dijl and Prof.dr.ir. A.A.Th.M. van Trier for their permission to carry out this investigation and for many encouraging conversations on this subject.

The authors are very grateful to Mr. A. Geurts and Mr. H. Willemsen of the Department of Mathematics of the Eindhoven Technological University for their help in preparing computer programmes.

The authors appreciate the able assistance of the technical staff of the Department of Electrical Engineering of the University of Eindhoven, notably Mr. K. Holleboom and Mr. A. v.d. Vorst for their continual help in calculating, drawing and correcting this work, and Mr. M. Knoben and Mr. A. Mulders for the measurements carried out on feeds and sub-reflectors. Finally they thank the personnel of the University's workshop for the models manufactured, Miss M.P. Verhoeven for the careful preparations of this report and Mr. H.J.A. van Beckum for his assistance in preparing the english text.

Summary.

This report deals with the provisional electrical design of an antenna suitable for satellite communications in the frequency band of 3.700 - 4.200 Mc/s for receiving, and 5.900 - 6,400 Mc/s for transmitting.

It is shown that with respect to noise properties an antenna according to the cassegrain principle is more favourable than the focal point fed paraboloid.

In chapter 3 the properties of the cassegrain antenna are discussed in detail. Much attention is paid to the blocking and diffraction problems. Analytical expressions are deduced to calculate the decrease in antenna efficiency caused by blocking and diffraction. A measuring arrangement is set up to measure the diffraction effects at the sub-reflector. It appears that the angular aperture has practically no influence on the performance of the antenna.

A theoretical treatment is given of the loss of energy due to blocking and means are discussed to minimise this blocking energy by introducing some irregularities in the surface of the subreflector. The noise properties of the cassegrain antenna are also studied in detail.

In chapter 4 the requirements are explained with regard to the feed. Various patterns of feeds that could be used in the final antenna system are shown.

Chapter 6 deals entirely with shaped reflector systems. Analytical expressions and solutions are given. It is pointed out that with shaped reflectors low spillover losses and high aperture efficiencies can be obtained.

In the last chapter a provisional design of an antenna suitable for satellite communications is proposed. It appears that the diameter of the main reflector should be at least 27 metres to meet the specification.

1. Introduction

An antenna for a satellite communication groundstation has to meet very high standards. Apart from the required antenna gain, which can only be realised by apertures of 25 meter diameter or more, the need for low noise is essential as well. Noise is introduced by the microwave receiver itself and further contributions arise from losses in the waveguides, diplexers, etc. Moreover the noise is increased by thermal radiation from the sky and also via side lobes and back radiation from the ground. Especially the contribution due to ground radiation is critical, as the ground can usually be regarded as a thermal source of 290° K, while the sky radiates at an average temperature of only 10° K.

It has bevome common practice in satellite communications to introduce the "figure of merit", which is defined as the ratio of antenna gain G and the system noise temperature T. This G/T ratio therefore depends not only on the reflector system and feed but also on the environment in which the antenna operates, the elevation of the antenna and the noise in the rest of the receiver system.

The remarks above apply not only to the use of the antenna for reception purposes but to some extent also to that af transmitting purposes. As a matter of fact, a high antenna gain is also wanted ih the latter case, while the radiation in unwanted directions must be low, to avoid interference with stations operating on the same frequency. Low side lobes are therefore essential as well. In case the antenna gain is too low for transmission, the transmitter power can be increased to some extent, so that the antenna gain is not so critical for transmission as for reception purposes.

2. Possible approaches for satellite communication ground station antennas

The simplest solution to meet the very high requirements of antenna gain in the frequency band of 4,000 - 6,000 Mc/s is found in paraboloid reflectors with a diameter of 25 meters or more.

A possible arrangement is what is known as front-fed paraboloid with the primary source at the focus. This arrangement was selected for satellite communication in Goonhilly (lit. 1, 2), but the aperture illumination had to he sacrified to low noise operation. Moreover, it is found inconvenient to locate low noise receivers at the focus, and long waveguides have to be used, resulting in losses. These losses form a major contribution to the system noise.

A means of overcoming the difficulties is found in the cassegrain arrangement (lit. 3, 4, 5, 6), where a second focus is introduced near the main dish by a secondary hyperboloid reflector. The primary feed and low noise receiver can thus be placed near the vertex of the dish, keeping the waveguide losses as low as possible. The spillover from the primary feed along the secondary reflector is now mainly directed towards the cold sky, reducing the antenna temperature.

Systems with two reflectors offer various possibilities. Instead of a hyperboloid subreflector an ellipsoid subreflector can be used (gregorian system); other arrangements where slight modifications in the cassegrain principles are introduced, are discussed by several authors (lit. 7, 8, 9).

All these antennas can meet the G/T specifications for satellite communication of 40.7 dB at 4,000 Mc/s. However, great difficulties are being met in the keeping the spillover low along the subreflector and at the same time in obtaining high aperture efficiency.

Better results may be expected by a two reflector system with shaped surfaces. This system is very similar to the cassegrain system but the main reflector and subreflector are no longer true paraboloid and hyperboloid, respectively (lit. 10, 11, 12).

Theoretically the latter modified cassegrain arrangement enables an aperture efficiency of 100% to be obtained as the main reflector is illuminated uniformly. Moreover, it is permissible to have a subreflector edge illumination in excess of -20 dB, thus reducing the noise attended with spillover to a considerable extent. Further details and the electrical properties of existing or planned antennas for ground stations can be found in a recent report (lit. 13).

The antenna design discussed in the present paper is based on the modified cassegrain antenna. Moreover, the report contains several calculations and recommendations which apply to the true as well as to the modified cassegrain system.

3. The classical cassegrain antenna system

3.1. Introduction

In 1672, the french optician Cassegrain invented a telescope consisting of two reflectors. This type of telescope has been used by astronomers for a long time, and even very recently a new telescope was built according to his principle (lit. 14).
The application of the cassegrain system to microwave attennas is, however, of only recent date (lit. 3).

The classical form of the cassegrain system is shown in Fig. 3.1. The system employs a main dish which is a paraboloid and an auxilary reflector, or subdish, with a hyperbolic contour. One of the foci, P_1, is the real focal point of the system and is located near the main dish. The other focus, P_2 is a virtual focal point located at the focus of the paraboloid. When the primary feed is situated at the focus P_1 and the secondary reflector is illuminated, the waves are reflected in accordance with ray optics.

On reaching the main dish, the waves are again reflected in accordance with ray optics, and because of the antenna geometry employed, the rays emerge parallel, with a plane wave front, forming a collimated beam.

At radio frequencies, however, a theoretically analysis of the scattered power from the hyperboloid subreflector may not be carried out using rays optics, because spillover and diffraction effects are unexplained by optical approximations. A further limitation of cassegrain systems is the blocking of the aperture by the subdish and the subdish support legs.

It is the purpose of this chapter to explain and calculate various effects with regard to antenna efficiency (by means of analytical expressions) and to outline the design principles. Moreover, its advantages and limitations will be discussed and compared with front-fed paraboloids.

3.2. Geometrical and optical relations

The equation of the paraboloid (Fig. 3.1) in polar coordinates is

$$\rho_2 = \frac{2F}{1 + \cos \psi_2} = \frac{F}{\cos^2 \frac{1}{2} \psi_2} \quad . \tag{3.1}$$

Also from the geometry of Fig. 3.1.

$$\sin \psi_2 = \frac{r}{\rho_2} \ ,$$

so that Eq. 3.1 con be written as

$$r = 2F \tan \tfrac{1}{2} \psi_2 \quad . \tag{3.2}$$

The equations of the hyperboloid in polar coordinates are

$$\rho 1 = \frac{-f(e^2-1)}{2e\ (-\ e \cos \psi_1 + 1)} \tag{3.3a}$$

and

$$\rho'_1 = \frac{f(e^2-1)}{2e(e \cos \psi_2 + 1)} \quad . \tag{3.3b}$$

Combining Eq. 3.2 with Eqs. 3.3 we obtain

$$r_s = \frac{-f(e^2-1)}{2e(-e \cos \psi_1 + 1)} \sin \psi_1 \tag{3.4a}$$

and

$$r_s = \frac{-f(e^2-1)}{2e(e \cos \psi_2 + 1)} \sin \psi_2 \quad . \tag{3.4b}$$

A well-known relation in a hyperboloid is

$$\tan \tfrac{1}{2} \psi_1 = \frac{e-1}{e+1} \tan \tfrac{1}{2} \psi_2 \ ; \tag{3.5}$$

where e is the hyperboloid eccentricity.

Another relation can be found by combining Eq. 3.4b and Eq. 3.5 and eliminating the eccentricity, giving

$$\cot \Psi_1 + \cot \Psi_2 = \frac{2f}{D_s} \quad , \tag{3.6}$$

where Ψ_1 and Ψ_2 are the maximum angles from the horizontal axis to the rays from the feed and paraboloid focus respectively. Potter (lit. 15) indicates the relationship between the gain function of the primary feed and the hyperboloid gain function

$$G_1(\phi_1) \sin^2 \phi_1 = G_2(\phi_2) \sin^2 \phi_2 \quad , \tag{3.7}$$

where $G_1(\phi_1)$ is the gain function of the primary feed and $G_2(\phi_2)$ the hyperboloid gain function, both functions being circularly symmetrical. Eq. 3.4b, Eq 3.5 and Eq. 3.7 are represented graphically by the figures 3.2, 3.3 and 3.4 respectively.

3.3. The antenna gain

Silver (lit. 16, p.192) has calculated the secondary field pattern of a radiating circular symmetrical aperture obtaining

$$E(\theta) = j\frac{2\pi}{\lambda} \int_0^{\frac{1}{2}D} E(r) \cdot J_o(\frac{2\pi}{\lambda} r \sin \theta)\, r\, dr \quad , \tag{3.8}$$

at unit distance, where E(r) is the aperture illumination and $J_o(\frac{2\pi}{\lambda} r \sin \theta)$ the Bessel function of zero order. This expression is only valid for small angles θ . Afifi (lit. 17) has found that the angle for which Eq. 3.8 holds should not exceed 5^o. The maximum intensity of the main lobe is found by substituting $\theta = 0$ in Eq. 3.8. See also Fig. 3.5 for the coordinate system employed.

To obtain a better insight in the relationship between the secondary field pattern and the gain function of the primary feed, the aperture illumination function E(r) in Eq. 3.8 is replaced by $G_1(\Psi_1)$ or $G_2(\Psi_2)$. It makes no difference which gain function is used as, according to Eq. 3.7, they are interrelated. Silver (lit. 16, p. 419) has found that

$$E(r) = 2\left(\frac{\mu}{\varepsilon}\right)^{\frac{1}{2}} \frac{P_T}{4\pi}^{\frac{1}{2}} \cdot \frac{\{G_2(\psi_2)\}^{\frac{1}{2}}}{\rho_2} , \qquad (3.9)$$

P_T being the total power radiated by the feed. By Eqs. 3.1, 3.5 and 3.7 we obtain

$$E(r) = 2\left(\frac{\mu}{\varepsilon}\right)^{\frac{1}{2}} \frac{P_T}{4\pi}^{\frac{1}{2}} \frac{\{G_2(\psi_2)\}^{\frac{1}{2}}}{F} \cdot \cos^{\frac{1}{2}} \psi_2$$

or

$$E(r) = 2\left(\frac{\mu}{\varepsilon}\right)^{\frac{1}{2}} \frac{P_T}{4\pi}^{\frac{1}{2}} \frac{\{G_1(\psi_1)\}^{\frac{1}{2}}}{F} \cdot \cos^{\frac{1}{2}} \psi_1 \cdot \frac{e-1}{e+1} \cdot \qquad (3.10)$$

From Eq. 3.10 it will be recognised that a cassegrain reflector system can be replaced by a front-fed paraboloid having a focal length of

$$F^* = F \cdot \frac{e+1}{e-1} . \qquad (3.11)$$

Substituting Eqs. 3.2 and 3.10 in Eq. 3.8 this equation becomes

$$E(\theta) = j\left[2\left(\frac{\mu}{\varepsilon}\right)^{\frac{1}{2}} \cdot \frac{P_T}{4\pi}\right]^{\frac{1}{2}} \cdot \frac{\pi D}{\lambda} \cdot \cot\frac{\psi_1}{2} \int_0^{\psi_1} \left[G_1(\psi_1)\right]^{\frac{1}{2}} \cdot J_o\left(\frac{\pi D}{\lambda} \cot\frac{\psi_1}{2} \cdot \tan\frac{\phi_1}{2} \cdot \sin\theta\right) \cdot \tan^{\frac{1}{2}} \psi_1 \, d\psi_1 \cdot \qquad (3.12)$$

The maximum intensity for $\theta = 0$ is now found to be

$$E(0) = j\left[2\left(\frac{\mu}{\varepsilon}\right)^{\frac{1}{2}} \cdot \frac{P_T}{4\pi}\right]^{\frac{1}{2}} \cdot \frac{\pi D}{\lambda} \cot\frac{\psi_1}{2} \int_0^{\psi_1} G_1(\psi_1)^{\frac{1}{2}} \tan^{\frac{1}{2}} \psi_1 d\psi_1 \cdot \qquad (3.13)$$

The power per unit solid angle $P(0,0)$ radiated in the forward direction is now given by

$$P(0,0) = \frac{1}{2}\left(\frac{\varepsilon}{\mu}\right)^{\frac{1}{2}} \left|E(0,0)\right|^2$$

and the antenna gain by

$$G = \frac{4\pi \cdot P(0,0)}{P_T} . \qquad (3.14)$$

An equation for the antenna gain is now found similarly to Silver's calculations (lit. 16,p. 425)

$$G = \left(\frac{\pi D}{\lambda}\right)^2 \cot^2 \frac{\Psi_1}{2} \left| \int_0^{\Psi_1} \left[G_1 (\psi_1)\right]^{\frac{1}{2}} \tan \tfrac{1}{2}\psi_1 \, d\psi_1 \right|^2 . \quad (3.15)$$

The factor $G_o = \left(\frac{\pi D}{\lambda}\right)^2$ is the gain of a uniformly illuminated constant phase aperture; the rest is the antenna efficiciency

$$\eta_o = \cot^2 \frac{\Psi_1}{2} \cdot \left| \int_0^{\Psi_1} \left[G_1(\psi_1)\right]^{\frac{1}{2}} \tan \tfrac{1}{2}\Phi_1 \, d\psi_1 \right|^2 . \quad (3.16)$$

For cassegrain reflector systems Eq. 3.15 has to be modified decreasing the antenna gain and efficiency (Sec. 3.6) .

3.4 Aperture Blocking

3.4.1. Introduction

A limitation of cassegrain systems is the blocking of the aperture by the subdish and support legs. These limitations are less severe in frontfed paraboloids as the feed which causes blocking in this case as well, is mostly much smaller than the subreflector. Moreover, the subreflector support legs can be made much thinner. Usually, the shadows of the obstacles on the aperture are determined by ray optics, not taking into account the effects by diffraction. Corrections due to diffraction are mostly introduced afterwards as they play an important part in determining the antenna temperature.

In a cassegrain system plane and spherical wavefronts are found. It is explained in Sec. 3.4.2. that each of these wavefronts gives a different contribution to the shadow of the obstacles on the aperture. Consequently, these parts of the aperture are not illuminated, resulting in the following effects:

(a) Decrease of the antenna gain; this effect can be expressed by the relative blocking coefficient $\frac{\eta_B}{\eta_o}$, where η_o is the efficiency of the unblocked aperture.

(b) Increase of the side lobe of the antenna pattern.
Different contributions are introduced by the obstacles.
The contribution by the subreflector will be circularly symmetrical, while the contribution by the subreflector support legs is more typical the radiation of a rectangular aperture distribution.
(c) Increase of the noise temperature of the antenna, as energy is spread from the main beam to the side lobes, if these side lobes are directed towards sources with a high noise temperature.

3.4.2. Calculations of aperture blocking

Fig. 3.6 shows a half cross-section of a two reflector system with one support leg. In this figure Ψ_2 is the angular aperture and ρ_2 is the distance, between the focal point of the paraboloid and the edge of the main reflector. Fig. 3.7 is obtained by constructing a tangent plane to a cone formed by main dish and subdish and with the vertex in the focus. The shadow length l on the main dish and the width w of the support legs are small compared with the dimensions of the two dishes.Therefore, the tangent plane will contain bith w and l.

Fig. 3.8a shows shadows on the aperture obtained by projecting the subreflector and support legs on the aperture by a plane wave, perpendicular to the aperture.
The shadow in Fig. 3.8b is formed by projecting the support legs on the aperture by a spherical wave. The fase centre of this spherical wave is the focus P_2. The shadow length l can be found from Figs. 3.6 and 3.7, thus

$$\rho_1' = \frac{D_s}{2 \sin \Psi_2} , \tag{3.17}$$

ρ_1' being the distance between the focal point and the edge of the subreflector. Further,

$$\tan \alpha = \frac{w}{2\rho_1'} = \frac{w}{D_s} \sin \Psi_2 . \tag{3.18}$$

The angle α is also determined by

$$\tan \alpha = \frac{l}{2\rho_2} . \tag{3.19}$$

Combining Eq. 3.18 and Eq. 3.19 we have

$$\frac{1}{2} = \frac{w \cdot \rho_2 \sin \Psi_2}{D_s} \quad . \tag{3.20}$$

Substituting Eq. 3.20 in the equation for the paraboloid, Eq. 3.1, we obtain

$$\frac{1}{2} = \frac{2F \cdot w}{D_s} \cdot \frac{\sin \Psi_2}{1 + \cos \Psi_2},$$

or

$$\frac{1}{2} = \frac{2F \cdot w}{D_s} \cdot \tan \tfrac{1}{2}\Psi_2 \quad . \tag{3.21}$$

Substituting Eq. 3.2 in the preceding relation we obtain finally the working formula

$$1 = w \cdot \frac{D}{D_s} \quad . \tag{3.22}$$

If the support legs are fixed to the main dish at a distance $(1-t)\frac{D}{2}$ from the axis of the cone, the angle β is found in Fig. 3.8c.

$$\tan \tfrac{1}{2} \beta = \frac{w}{t.D} \cdot \left[\frac{D}{D_s} - 1 \right] \quad . \tag{3.23}$$

The projection of the support legs by the spherical wave is very similar to a trapezoid. However, Wested (lit. 21) has found that the non parallel sides are not straight lines but circular arcs. In spite of this very small inaccuracy Wested used the trapezoid approximation, as it simplifies the calculations considerably.

3.4.3. The power balance of the blocked aperture

If there is no spillover around the edge of the subreflector and all the power P_T which is radiated by the feed is intercepted by the subreflector, the power reradiated by the aperture is found by substracting the power blocked P_B by the obstacles from the total power P_T .

Let the coordinates of a point in the aperture be (ξ , η) and the electrical field over the aperture $F(\xi , \eta)$. The total power radiated by the non-blocked aperture is according to Silver (lit. 16, p. 177)

$$P_T = \tfrac{1}{2} \left(\frac{\varepsilon}{\mu}\right)^{\frac{1}{2}} \int_A |F(\xi , \eta)|^2 \, d\xi . d\eta \, . \, (\overline{I_z} . \overline{s}). \quad (3.24)$$

In this equation $\overline{s}$ is the unit vector along a ray and $\overline{I}_z$ the unit vector perpendicular to the aperture, along the z-axis. For $\vartheta = 0$ the rays are parallel to the z-axis so that $(\overline{I}_z . s) = 1$.

If the aperture is blocked by a number of obstacles (Fig. 3.9a and b) totalised by

$$B = \sum_{n=1}^{n=m} B_n \quad , \quad (3.25)$$

the blocked power becomes

$$P_B = \tfrac{1}{2} \left(\frac{\varepsilon}{\mu}\right)^{\frac{1}{2}} \int_B |F(\xi , \eta)|^2 \, . \, d\xi \, . \, d\eta \, . \quad (3.26)$$

This part of the total power P_T is radiated by the primary feed but it cannot be reradiated by the blocked aperture in the proper way, as it will be scattered by the feed support and the feed cone.

The gain function of a lossless antenna is expressed by $G(\theta , \varphi)$, where θ and φ are spherical coordinates illustrated in Fig. 3.5. The gain function must also satisfy the relation

$$\int_{4\pi} G(\theta, \varphi) \, d\Omega = 4\pi \quad , \quad (3.27)$$

$d\Omega$ being the element of solid angle.
If $P(\theta , \varphi)$ is the power radiated by the antenna per unit solid angle in direction θ , φ, and P_T the total power radiated, the gain is defined as

$$G(\theta , \varphi) = 4\pi \, \frac{P(\theta , \varphi)}{P_T} \quad . \quad (3.28)$$

The power reradiated by the aperture less the blocked areas will now not be equal to Eq. 3.24 but to

$$P_T - P_B = \tfrac{1}{2} \left(\frac{\varepsilon}{\mu} \right)^{\frac{1}{2}} \int_{A-B} |F(\xi, \eta)|^2 \, d\xi \cdot d\eta \quad . \quad (3.29)$$

This equation shows that the surface integral extends over the aperture surface A less, the blocked surfaces B. A new gain function $G'(\theta, \varphi) = 4\pi \frac{P'(\theta, \varphi)}{P_T}$ will now be formed depending on the power $P'(\theta, \varphi)$ radiated per unit solid angle whereas

$$\int_{4\pi} P'(\theta, \varphi) \, d\Omega = P_T - P_B \quad . \quad (3.30)$$

Compared with Eq. 3.27, the gain of the antenna where in the production of which the blocked power is not transported to the aperture, is now determined by

$$\int_{4\pi} G'(\theta, \varphi) \, d\Omega \neq 4\pi \quad , \quad (3.31)$$

or

$$\int_{4\pi} G'(\theta, \varphi) \, d\Omega = 4\pi \cdot \left[1 - \frac{P_B}{P_T} \right] \quad ,$$

or

$$\int_{4} G'(\theta, \varphi) \, d\Omega = 4\pi - \frac{2\pi}{P_T} \left(\frac{\varepsilon}{\mu} \right)^{\frac{1}{2}} \int_{B} |F(\xi, \eta)|^2 \, d\xi \, d\eta \quad . \quad (3.32)$$

The power P_B is scattered by the subreflector support legs, feed and feedcone and adds new contributions to the antenna pattern $G'(\theta, \varphi)$ so that the power balance restored. This scattered power radiates in various directions which are difficult to predict. Isotropic scatter seems a practical assumption. Practically no scatter will be found in direction $\theta = 0$ so that the influence on the aperture efficiency can be ignored. The modification of the antenna pattern by the support legs is even more difficult to estimate. Trentini (lit. 8) makes some introductary remarks on this subject, while an experimental study at M.I.T. recently carried out gives some more detailed information (lit. 20) . Also Wested, too, (lit. 21) studied this effect and states the problems clearly.

The antenna pattern $G'(\theta,\varphi)$ with supplementary contributions from the scattered power P_B will increase the noise temperature of the antenna if these contributions are directed towards noise sources at high temperatures. Apparently, the blocked power increases the side-lobe level and the antenna noise temperature as well. This contribution has to be added to the contribution already mentioned in Sec. 3.4.1. Therefore, the total influence of blocking part of the aperture results in a double effect, viz.

(1) a decrease of the antenna efficiency η_B/η_0 and an increase of the side lobe level, with the possibility of higher antenna temperature, as the blocked power P_B is not available for reradition by the non-blocked parts of the aperture;

(2) an increase of the side lobe level and, therefore, higher noise temperature by the scatter of the blocked energy P_B .

3.4.4. The blocking efficiency

Let A be a non-blocked aperture and the coordinates of a point in the aperture be (ξ,η). Let the aperture field be $F(\xi,\eta)$. According to Silver (lit. 16,p. 177) the maximum value of the gain function is found to be

$$G_A = \frac{4\pi}{\lambda^2} \frac{\int_A \left| F(\xi,\eta)\, d\xi\, d\eta \right|^2}{\int_A |F(\xi,\eta)|^2\, d\xi\, d\eta} \quad . \tag{3.33}$$

If the aperture illumination is uniform, $F(\xi,\eta)$ will be a constant. From Eq. (3.33) the gain in that case is

$$G_o = \frac{4\pi A}{\lambda^2} \quad . \tag{3.34}$$

The efficiency η_o of this non-blocked aperture will now be defined by the relation

$$\eta_o = \frac{G_A}{G_o}$$

or

$$\eta_o = \frac{1}{A} \frac{\left| \int_A F(\xi,\eta)\, d\xi\, d\eta \right|^2}{\int_A |F(\xi,\eta)|^2\, d\xi\, d\eta} \quad . \tag{3.35}$$

The integral $\int_A |F(\xi,\eta)|^2 \, d\xi . d\eta$ is a measure for the power radiated by primary feed and intercepted by the main reflector if no spillover is present. The integral $\int_A F(\xi,\eta) \, d\xi \, d\eta$, however, is proportional to the field intensity.

Let the aperture be blocked by a number of obstacles B_1, B_2, B_3.....B_n (Fig. 3.9b) and let G_{AB} be the maximum gain of the aperture A containing the blocking obstacles B. The efficiency η_B of the blocked aperture is now found to be

$$\eta_B = \frac{G_{AB}}{G_o}$$

or

$$\eta_B = \frac{1}{A} \cdot \frac{\left| \int_{A-B} F(\xi,\eta) \, d\xi d\eta \right|^2}{\int_A |F(\xi,\eta)| \, d\xi \, d\eta} \cdot \qquad (3.36)$$

Comparing the efficiency of the blocked and non-blocked apertures we obtain the relative efficiency

$$\frac{\eta B}{\eta_o} = \frac{1}{A} \cdot \frac{\left| \int_{A-B} F(\xi,\eta) d\xi \, d\eta \right|^2}{\int_A |F(\xi,\eta)|^2 \, d\xi \, d\eta} \cdot A \cdot \frac{\int_A |F(\xi,\eta)|^2 \, d\xi d\eta}{\left| \int_A F(\xi,\eta) \, d\xi d\eta \right|^2} \qquad (3.37)$$

or

$$\frac{\eta_B}{\eta_o} = \left| \frac{\int_{A-B} F(\xi,\eta) d\xi d\eta}{\int_A F(\xi,\eta) \, d\xi d\eta} \right|^2 \cdot \qquad (3.38)$$

The integral $\int_{A-B} F(\xi,\eta) d\xi \, d\eta$ is equivalent to

$$\int_A F(\xi,\eta) d\xi \, d\eta - \int_B F(\xi,\eta) d\xi \, d\eta$$

so that

$$\frac{\eta_B}{\eta_o} \equiv \left| 1 - \frac{\int_B F(\xi,\eta) d\xi d\eta}{\int_A F(\xi,\eta) d\xi \, d\eta} \right|^2 \cdot \qquad (3.39)$$

In case of uniform illumination, $F(\xi,\eta)$ is a constant, therefore,

$$\frac{\eta_B}{\eta_o} = \left| 1-\frac{B}{A} \right|^2 \quad . \tag{3.40}$$

In the following sections it will be proved that the blocking efficiency η_B/η_o can be further increased to a maximum of

$$\frac{\eta_B}{\eta_o} = \left| 1- \frac{B}{A} \right| \quad , \tag{3.41}$$

if the aperture is illuminated uniformly.

3.4.5. Optimising the blocking efficiency

In Sec. 3.4.3. it was already found that part of the total power P_T radiated by the feed will not be reradiated by the blocked aperture in the proper way but scattered in all directions by the feed support and feed cone. This chapter will deal with a possible solution to transport the blocked power to the aperture in the correct direction and phase so that it will contribute to an increase of the blocking efficiency.

Let $F(\xi,\eta)$ be the field over the aperture A and $F'(\xi,\eta)$ the field over this aperture after the blocked power is properly spread over the aperture. We want $F'(\xi,\eta)$ and $F(\xi,\eta)$ to be of the same form. Both fields are then related to each other by

$$F'(\xi,\eta) = c.F(\xi,\eta)$$

where c is a constant.

The power P_T radiated by the non-blocked aperture is

$$P_T = \tfrac{1}{2} \left(\frac{\varepsilon}{\mu}\right)^{\frac{1}{2}} \int_A \left| F(\xi,\eta) \right|^2 d\xi\, d\eta \quad . \tag{3.24}$$

This power should be equal to

$$\tfrac{1}{2}\left(\frac{\varepsilon}{\mu}\right)^{\frac{1}{2}} \int_A \left| c\ F(\xi,\eta) \right|^2 d\xi\, d\eta - \tfrac{1}{2}\left(\frac{\varepsilon}{\mu}\right)^{\frac{1}{2}} \int_B \left| c\ F(\xi,\eta) \right|^2 d\xi\, d\eta, \tag{3.42}$$

as the total power radiated by the feed will now be reradiated by the aperture. Eq. 3.42 is not valid in Sec. 3.4.3, as in that case the blocking power P_B was lost by scattering.

The constant c can now be determined by

$$c^2 = \frac{\int_A |F(\xi,\eta)|^2 d\xi d\eta}{\int_A |F(\xi,\eta)|^2 d\xi d\eta - \int_B |F(\xi,\eta)|^2 d\xi d\eta} = \frac{P_T}{P_T - P_B} \qquad (3.43)$$

or

$$c^2 = \frac{\int_A |F(\xi,\eta)|^2 d\xi d\eta}{\int_{A-B} |F(\xi,\eta)|^2 d\xi d\eta}. \qquad (3.44)$$

Since the illumination is now increased by a factor c, Eq. 3.38 can be written for the new blocking coefficient

$$\left(\frac{\eta_B}{\eta_o}\right)_{max} = \left| \frac{\int_{A-B} c.F(\xi,\eta)\, d\xi d\eta}{\int_A F(\xi,\eta) d\xi d\eta} \right|^2 = c^2 \frac{\eta_B}{\eta_o} \qquad (3.45)$$

It will be clear that in the demoninator of Eq. 3.45 the field remains unchanged, otherwise the non-blocked aperture would radiate too much power.

Substituting Eq. 3.44 in Eq. 3.45 we obtain

$$\left(\frac{\eta_B}{\eta_o}\right)_{max} = \left| \frac{\int_{A-B} F(\xi,\eta)\, d\xi d\eta}{\int_A F(\xi,\eta)\, d\xi d\eta} \right|^2 \times \frac{\int_A |F(\xi,\eta)|^2 d\xi d\eta}{\int_{A-B} |F(\xi,\eta)|^2 d\xi d\eta}. \qquad (3.46)$$

Comparison of Eq. 3.46 with Eq. 3.37 shows only a difference in the demoninator. In Eq. 3.46 we find the expression

$$\int_{A-B} |F(\xi,\eta)|^2 d\xi d\eta \qquad (3.47)$$

compared with

$$\int_A |F(\xi,\eta)|^2 d\xi d\eta \qquad (3.48)$$

in Eq. 3.37.

Eq. 3.47 can be explained as being the power radiated by the blocked aperture with the original aperture field $F(\xi,\eta)$. This power is less than the power radiated according Eq. 3.48. This also means that the

blocking efficiency η_B/η_o will increase as compared with the blocking efficiency discussed in Sec. 3.4.4, Eq. 3.38.
In case of uniform illumination, $F(\xi,\eta)$ is a constant.
Hence Eq. 3.46 is written as

$$(\frac{\eta_B}{\eta_o})_{max} = 1 - \frac{B}{A} , \qquad (3.41)$$

which expression was already predicted in Sec. 3.4.4. and which also shows that gain and surface are in proportion to each other.

In Eq. 3.41 the term B can be subdivided in contributions due to spherical and to plane waves. The present study indicates that by proper shaping (lit. 11) of main and subreflector the shadow on the aperture caused by spherical waves can disappear entirely. This idea will be worked out more in detail in chapter 7.

3.4.6. Some calculations of blocking efficiency

3.4.6.1. Uniform illumination

Fig. 3.10 shows a calculation of the blocking efficiency of a cassegrain antenna with uniform illumination. It was proved in chapter 3.4.2. that the relative blocking coefficient η_B/η_o is independent of the angular aperture Ψ_2. It was also proved that the long side of the trapezoid shaped shadow was equal to wD/D_s. All shadows have been determined by geometrical optical relations. The greater part of these shadows is due to the subreflector supports and particularly the trapezoid shaped shadows. The calculated blocking coefficient was 0.91. This figure may be improved upon if the illumination is tapered instead of uniform.

Trentini (lit. 8) has used a different method of calculating the blocking efficiency by introducing an average width of the supports. The disadvantage of this method lies in the fact no clear insight is available as to which part of the shadow is formed by spherical waves and which part by plane waves.

3.4.6.2. Tapered illumination

In dealing with circular aperture problems polar coordinates (r',φ) are often used which are related to the usual coordinates (ξ,η) by

$$\xi = r'\cos\varphi' \text{ , and } \eta = r'\sin\varphi' \text{ ,} \qquad (3.48)$$

r' being normalised to unity so that $r_{max} = 1$. The aperture field distribution is now denoted by $F(r', \varphi')$.
Doidge (lit. 23) has calculated the relative blocking coefficient of a circular symmetrical aperture using the field distribution

$$F(r') = q + (1-q)\,(1-r'^2)^p \quad 0 < q < 1, \qquad (3.49)$$

where q is the edge illumination taper and p a shaping factor of the aperture illumination. Uniform illumination is obtained for $q = 1$. The blocking efficiency is

$$\frac{\eta_B}{\eta_o} = \left[\frac{(1-\Delta)\,\left[q(p+1) + (1-q)\,(1-\Delta^2)\right]^p}{q(p+1)}\right]^2 \text{ ,} \qquad (3.50)$$

where Δ is the ratio D_s/D.

Fig. 3.11 shows the blocking coefficient as a function of the edge illumination, where $\Delta = 0.1$. This figure shows that blocking reaches a minimum when the illumination is uniform. Attention has to be paid to recent work done by Wested (lit. 21). He used an aperture illumination field

$$F(r') = 1 - \alpha_o . r'^2 \text{ ,} \qquad (3.51)$$

where α_o is a tapering constant. He has introduced very useful information by calculating the blocking effects caused by plane and spherical waves, although the projection of the supports by the spherical wave has been approximated by a trapezoid (see also Sec. 3.4.2.).

Gray (lit. 22) too, has carried out calculations on the blocking coefficient; however, Wested (lit.21) has pointed out a few inaccuracies in Gray's work. Finally Gillitzer (lit. 7) should also be mentioned here as his approach is somewhat different from the others. Following his method, calculations were carried out of the blocking effect on the antenna efficiency and sidelobes (Sec. 3.4.7.2.).

3.4.7. The influence on the antenna pattern

3.4.7.1. Calculation by means of aperture functions

If the aperture of a circular symmetrical antenna is illuminated uniformly the secondary pattern becomes

$$g(u) = \frac{\pi D^2}{2} \cdot \frac{J_1(u)}{u} , \qquad (3.52)$$

where D is the diameter of the aperture, $J_1(u)$ a Bessel function of the first order and

$$u = \frac{\pi D}{\lambda} \sin\theta . \qquad (3.53)$$

The angle θ constitutes a part of a spherical coordinate system (Fig. 3.5) and the antenna-axis is found $\theta = 0$.
According to Afifi (lit. 17) this method of pattern calculation is only valid for small angles θ. Afifi (lit. 17, p. 20) has found that the maximum angle θ_{max} at which the aperture method is still valid is determined by

$$2\ \theta_{max} \approx 4 \cdot (\text{width main lobe}) \cdot \sqrt{\frac{2F}{\lambda}} . \qquad (3.54)$$

If for example D = 25 metres, λ = 7.5 cm and F/D = 0.33 the width of the main lobe is 0.2 °, therefore θ_{max} is approx. 6°.
The effect of a blocking obstacle can be regarded as an 180° out of phase field superimposed on the original distribution, to obtain zero illumination over the blocked parts of the aperture. This principle is often called the "zero field concept". See also Silver (lit. 16, p.191).

The pattern of the subreflector can be represented by

$$g(u') = \frac{\pi D_s}{2}^2 \cdot \frac{J_1(u')}{u'} , \qquad (3.55)$$

where

$$u' = \frac{\pi D_s}{\lambda} \sin \theta . \qquad (3.56)$$

The modified pattern is now (Fig. 3.12)

$$g(\theta) = g(u) - g(u') . \qquad (3.57)$$

In this way Potter (lit. 24) has calculated the gain of the blocking aperture as a function of subreflector size and frequency for an 85 ft antenna with an aperture efficiency of 55 percent. The gain of the blocking aperture is also shown. Moreover, a figure is given with the location of the first side lobe maximum, as a function of subreflector diameter. It can be seen from these figures that the first sidelobe of g(u') comes nearer to the mainlobe if the subreflector diameter increases. Noise contributions of the ground can therefore be kept small even at low elevation angles.

It is easily found from Fig. 3.10 that for uniform illumination the intensity of the first sidelobe of the aperture increases according to the following table

intensity ratio	uniform illumination	
First sidelobe of unblocked aperture	0.1318	(-17.6 dB)
Contribution of subreflector	0.0100	
Contribution of supports	0.0350	
First sidelobe of blocked aperture	0.1768	(-15 dB)

The effect of tapering the illumination down towards the edge of the subreflector can also be illustrated by aperture distribution functions. Silver (lit. 16, p.194) has carried out calculations using the following aperture field distributions

$$F(r', \varphi') = (1-r'^2)^p \qquad p = 1,2,3,.... \qquad (3.58)$$

and

$$F(r', \varphi') = 1-r'^2\cos^2 \varphi' \quad .$$

Sciambi (lit.25,26) has carried out calculations with an aperture distribution already mentioned before

$$F(r', \varphi') = q + (1-q)\,(1-r'^2)^p \quad . \qquad (3.49)$$

The results of his work are shown by a great number of very clear graphs. The paper of Doundoulakis (lit. 27) is worth mentioning. He uses a method in which the distribution over the aperture can be characterised by its moments μ_m (Silver lit. 16, p.184). It is found that the gain function of a circular reflector possessing a circular symmetrical field distribution $F(r')$ can be written as

$$g(u) = \frac{\pi D^2}{2}\,\mu_o \sum_{n=o}^{\infty} \frac{(-1)^n}{(u!)^2} \cdot \left(\frac{u}{2}\right)^{2n} \cdot \frac{\mu_n}{\mu_o} \quad . \qquad (3.59)$$

Eq. 3.59 is found by substituting the Bessel function

$$J_o(ur) = \sum_{n=o}^{\infty} \frac{(-1)^n\,(ur')^{2n}}{(u!)^2\;2^{2n}} \qquad (3.60)$$

in the equation

$$g(u) = \frac{\pi D^2}{2} \int_o^1 F(r')\, J_o(ur')\, r'\, dr' \quad , \qquad (3.61)$$

where

$$u = \frac{\pi D}{\lambda} \sin\theta$$

and

$$\mu_n = \int_o^1 F(r')\, r'^{2n+1}\, dr' \quad .$$

A great number of calculations have been carried out by aperture field distributions such as

$$F(r') = (1-r'^2)^q ,$$

$$F(r') = e^{-kr'}$$

and

$$F(r') = e^{-pr'^2} ,$$

where k, p and q are constants describing the order of taper of the aperture illumination.

Afifi (lit. 17, p. 49) has also carried out calculations with the circular rotational symmetrical function

$$F(r') = 1 - a\, r'^n \qquad 0 < a < 1 \qquad (3.63)$$

and for different values of n.

The contribution of the supports to the radiation pattern of the main aperture is different from the circular symmetrical contribution of the subreflector. The supports can be regarded as rectangular radiating apertures so that according to Silver (lit. 16, p. 180), the radiation pattern of the supports at uniform illumination will be

$$g(\theta,\varphi) = A \cdot \left[\frac{\sin\left(\frac{\pi a}{\lambda}\right) \sin\theta \cos\varphi}{\frac{\pi a}{\lambda} \sin\theta \cos\varphi}\right]\left[\frac{\sin \frac{\pi b}{\lambda} \sin\theta \sin\varphi}{\frac{\pi b}{\lambda} \sin\theta \sin\varphi}\right], \qquad (3.64)$$

where A is the aperture and a and b are the dimensions of the aperture . A number of examples are found in Silver (lit. 16, p, 187).

The work of Gray (lit. 22) should also be mentioned here. He approximates the contribution of the supports to the radiation pattern of the antenna.

It has been mentioned before that in addition to the above calculations the contributions of the blocked and scattered power should also be taken into consideration. Very little is known about this phenomenon.

A survey of the effects mentioned above is found in Trentini's work (lit. 8.) . Fig. 3.13 shows these effects. Curve 1 shows the pattern

of an aperture with a tapered edge illumination of -20 dB corresponding to

$$F(r') = 1 - \frac{1}{t+1} r'^2 \quad , \tag{3.65}$$

where t = 0.11. Curve 2 shows the pattern of a uniformly illuminated aperture. The blocking effects of subreflector and supports are found in curve 3, where the edge illumination taper is -20 dB and curve 4 the blocking effects at uniform illumination.
It may be concluded that no purpose is served by tapering as the side-lobe level is mainly determined by the blocking effects.

3.4.7.2. Calculation by means of gain functions

According to the zero field concept already discussed in Sec. 3.4.7.1. the obstacle field should be superimposed on the original field so that over the blocking aperture the illumination is zero. For the subreflector this means that the aperture field between 0 and $\frac{1}{2} D_s$ should be subtracted from the original field.

Apparently all radiation between $0 < \psi_2 < \Psi_B$ (Fig. 3.1) from the feed is blocked and scattered in all directions. Using the same constants as in Sec. 3.2. the pattern to be subtracted from the main pattern is

$$E_B(\theta) = j \cdot \left[2 \left(\frac{\mu}{\varepsilon}\right)^{\frac{1}{2}} \frac{P_T}{4\pi} \right]^{\frac{1}{2}} \cdot \frac{\pi D_s}{\lambda} \cot \frac{\Psi_B}{2} \int_0^{\Psi_B} \left[G_2(\Psi_2) \right]^{\frac{1}{2}} J_0 \left(\frac{\pi D_s}{\lambda} \cot \frac{\Psi_B}{2} \tan \frac{\psi_2}{2} \sin\theta \right) \cdot \tan \frac{\psi_2}{2} \, d\psi_2 \tag{3.66}$$

Generally, D_s is small compared with D, hence $G_2(\psi_2)$ is constant for $0 < \psi_2 < \Psi_B$. Confined to this small region, the angle ψ_2 will be so small that $\tan \frac{1}{2} \psi_2 = \frac{1}{2} \psi_2$.
As

$$\int x J_0(x) \, dx = x J_1(x) \quad , \tag{3.67}$$

Eq. 3.66 can be written as

$$E_B(\theta) = j\left[2\left(\frac{\mu}{\varepsilon}\right)^{\frac{1}{2}} \cdot \frac{P_T}{4\pi} \cdot \left]^{\frac{1}{2}} \frac{\pi D_s}{\lambda} \cot\frac{\Psi_B}{2} \cdot \left[G_2(\phi_2)\right]^{\frac{1}{2}} \frac{J_1\left(\frac{\phi_2}{2}\right) \cdot \frac{\pi D_s}{\lambda} \cot\Psi_B \sin\theta)}{\frac{\pi D_s}{\lambda} \cdot \cot\frac{\Psi_B}{2} \cdot \sin\theta} \cdot \phi_2 \right. \tag{3.68}$$

and after filling in the integration limits

$$E_B(\theta) = j\left[2\left(\frac{\mu}{\varepsilon}\right)^{\frac{1}{2}} \frac{P_T}{4\pi} \cdot \left]^{\frac{1}{2}} \frac{\pi D_s}{\lambda} \tan\frac{\Psi_B}{2} \cdot \left[G_2(\phi_2)\right]^{\frac{1}{2}} \cdot \frac{J_1\left(\frac{\pi D_s}{\lambda} \sin\theta\right)}{\frac{\pi D_s}{\lambda} \sin\theta} \right. . \tag{3.69}$$

Considering that in the region $0 < \Psi_2 < \Psi_B$

$$\left[G_1(0)\right]^{\frac{1}{2}} \tan\tfrac{1}{2}\phi_1 \simeq \left[G_2(0)\right]^{\frac{1}{2}} \tan\tfrac{1}{2}\phi_2 ,$$

and using Eqs. 3.1 and 3.2, Eq. 3.69 becomes

$$E_B(\theta) = j\left[2\left(\frac{\mu}{\varepsilon}\right)^{\frac{1}{2}} \frac{P_T}{4\pi}\right]^{\frac{1}{2}} \cdot \frac{\pi D}{\lambda} \left[G_1(0)\right]^{\frac{1}{2}} \cdot \tan\tfrac{1}{2}\Psi_1 \cdot \left(\frac{D_s}{D}\right)^2 \cdot \frac{2J_1\left(\frac{\pi D_s}{\lambda}\sin\theta\right)}{\frac{\pi D_s}{\lambda}\sin\theta} , \tag{3.70}$$

and for $\theta = 0$

$$E_B(0) = j\left[2\left(\frac{\mu}{\varepsilon}\right)^{\frac{1}{2}} \frac{P_T}{4\pi}\right]^{\frac{1}{2}} \cdot \frac{\pi D}{\lambda} \left[G_1(0)\right]^{\frac{1}{2}} \cdot \tan\tfrac{1}{2}\Psi_1 \cdot \left(\frac{D_s}{D}\right)^2 . \tag{3.71}$$

3.5. Diffraction

3.5.1. Diffraction phenomena introduced by the subreflector

The cassegrain system was originally designed for use at optical frequencies. At radio frequenties, however, the dimensions of the subreflector may often be in the order of a few wavelengths. Diffraction effects will now arise, which cannot be explained by geometrical optics. The diffraction effects play an important part in the determination of antenna noise temperature, so that methods are to be found to calculate this phenomenon. A very good approximation can be obtained by calculating the field by optical methods and adding a correction term found by means of the principle of stationary phase, according to Silver (lit. 16 p. 119). By this method it is found that under certain

circumstances only stationary points yield contributions to the electrical field. The integrals used can be extented to infinity as the effects of a whole surface differ to a negligible extent from the areas about those points on the surface which have a stationary phase. If the domain of the surface is not infinite, one of the variables in the field integrals should not be extended to infinity.

Calculations following this method have been carried out by Gillitzer (lit. 7). It has been found that the field reflected from the subreflector is partly characterised by small oscillations, which are explained by fresnel integrals. Near the edge of the subreflector, however, the field decreases monotonically; this decrease continues even for the region where $\psi_2 > \Psi_2$ (Fig. 3.14). The total field reflected from the subreflector is found from the sum of the variations discussed above and the field found by using geometrical optics according to Eq. 3.7 and Fig. 3.4.

An accurate method determining diffraction effects has been carried out by Rusch (lit. 18). According to Silver (lit. 16, p.149), in this method, which involves very complicated calculations, the field scattered from the subreflector is found from an integration of the induced current over the surface of the subreflector. Comparing the two methods, it appears that the approximation with the stationary phase principle gives very good results if the subreflector diameter $D_s >> \lambda$. The total field $G_2'(\psi_2)$ reflected from the subreflector can now be split into two parts

$$G_2'(\psi_2) = G_2(\psi_2) \text{ for } 0 < \psi_2 < \Psi_D \qquad (3.72)$$

and

$$G_2'(\psi_2) = G_2(\psi_2)\, e^{-2\gamma(\psi_2 - \Psi_D)} \text{ for } \Psi_D < \psi_2 < \Psi_2 \qquad (3.73)$$

The field $G_2(\psi_2)$ is determined by geometrical optics according to Eq. 3.7. The field in Eq. 3.73 expresses the monotonic decrease of the amplitude of the reflected wave near the edge of the subreflector by an exponential term.

From calculations already carried out by Gillitzer (lit. 7) it is easely found that

$$\Psi_D = \Psi_2 - 0{,}65\sqrt{\frac{\lambda \sin \Psi_2}{D_s}} \qquad (3.74)$$

and

$$\gamma = 1{,}07\sqrt{\frac{D_s}{\lambda \sin \Psi_2}} \; . \qquad (3{,}75)$$

In these equations Ψ_D is the angle from where the monotonic decrease of the field scattered from the subreflector begins. This decrease reaches a value of -6 dB at the angular aperture Ψ_2 of the paraboloid (Fig. 3.14). This value is in accordance with the computer results published by Rusch (lit. 18). Also Potter (lit. 19) has found this value by a totally different method. Summerising, the total field $G'(\phi_2)$ is equal to the field found by geometrical optics for $\phi_2 < \Psi_D$ and has to be multiplied by an exponential term between Ψ_D and Ψ_2 resulting in a decrease of -6 dB at $\phi_2 = \Psi_D$.
For values $\phi_2 > \Psi_2$ Eq. 3.73 rapidly becomes very inaccurate compared with the Kirchhoff integration over the subreflector surface such as made by Rusch. If the field for $\phi_2 > \Psi_2$ has to be found, the calculations of Rusch offer very good possibilities.

In connection with Eq. 3.12 the radiation diagram has to be corrected by

$$E_D(\theta) = j\left[2\left(\frac{\mu}{\varepsilon}\right)^{\frac{1}{2}} \frac{P_T}{4\pi}\right]^{\frac{1}{2}} \frac{\pi D}{\lambda} \cot\frac{\Psi_2}{2} \int_{\Psi_D}^{\Psi_2} \left[G_2(\phi_2)\right]^{\frac{1}{2}} \left[1 - e^{-\gamma(\phi_2 - \Psi_D)}\right] \cdot$$

$$\cdot J_o\left(\frac{\pi D}{\lambda} \cot\frac{\Psi_2}{2} \tan\frac{\phi_2}{2} \sin\theta\right) \tan\frac{\phi_2}{2} \, d\phi_2 \; . \qquad (3.76)$$

In the forward direction, where $\theta = 0$, we obtain

$$E_D(0) = j\left[2\left(\frac{\mu}{\varepsilon}\right)^{\frac{1}{2}} \frac{P_T}{4\pi}\right]^{\frac{1}{2}} \frac{\pi D}{\lambda} \cot\frac{\Psi_2}{2} \int_{\Psi_D}^{\Psi_2} \left[G_2(\phi_2)\right]^{\frac{1}{2}} \left[1 - e^{-\gamma(\phi_2 - \Psi_D)}\right] \tan\frac{\phi_2}{2} \, d\phi_2$$

3.5.2. Diffraction and scattering of the subreflector supports

The scatter problems of the subreflector supports have been discussed in principle by Trentini (lit. 8), who, however, used geometrical optical methods. The discussion is completed by some radiation patterns which have been measured including the influence of the supports. Potter (lit. 6) also discusses this matter as being a very important factor in the design of a cassegrain antenna. A short introduction into the problems is found in one of Wested papers (lit. 21), but he could develop no complete theory.
Experimental work on this problem has been carried out at M.I.T. and published by Sheftman (lit. 20). The summary of literature above makes it clear that this problem has the attention of several designers but that a conclusive theory has so far not been found. Apparently, here lies a problem for further study. For the moment we assume that half of the scattered radiation is directed towards the ground the other half towards the sky.

In practice, some measures have been taken to suppress noise contributions due to scattering of the supports. In Goonhilly only 3 supports are used instead of the conventional 4. The supports are situated in such a way that the greater part of the scattering surface of the supports is directed towards the sky if the antenna axis makes a small elevation angle with the horizon. A decrease of noise temperature was found (lit. 1). The design of the antenna in Raisting (lit.8) contains a ring around the main reflector to give protection against noise contributions from the "hot" earth. It seems better, however, to use only a ring for the bottom half of the main reflector, to prevent the top half from introducing scatter directed towards the earth. By omitting the top half, at low elevation angles of the antenna, scatter will be directed towards the sky instead of towards earth.

3.5.3. The diffraction efficiency of the subreflector

Let η_o be the efficiency of an antenna system without blocking and, according to Silver (lit. 16, p. 425), be represented by

$$\eta_o = \cot^2 \frac{\Psi_2}{2} \left| \int_0^{\Psi_2} \left[G_2(\psi_2) \right]^{\frac{1}{2}} \tan \frac{\psi_2}{2} \, d\psi_2 \right|^2 . \qquad (3.16)$$

The relative diffraction efficiency η_D is found from

$$\frac{\eta_D}{\eta_o} = \left| 1 - \frac{E_D(\theta)}{E(\theta)} \right|^2 \qquad \text{for } \theta = 0 \qquad (3.78)$$

where $E_D(\theta)$ is found from Eq. 3.77 and $E(\theta)$ from Eq. 3.13.

As the integration region is limited, Eq. 3.77 can be approximated by the equation

$$\left[G_2(\psi_2) \right]^{\frac{1}{2}} . \tan \frac{\psi_2}{2} = \left[G_2(\Psi_2) \right]^{\frac{1}{2}} . \tan \frac{\Psi_2}{2} . \qquad (3.79)$$

After some calculation Eq. 3.77 can be written

$$E_D(\theta) = 0.18 \, j \left[2 \left(\frac{\mu}{\varepsilon}\right)^{\frac{1}{2}} \frac{P_T}{4\pi} \right]^{\frac{1}{2}} . \frac{\pi D}{\lambda} . \left[G_2(\Psi_2) . \frac{\lambda \sin\Psi}{D_s} \right]^{\frac{1}{2}} \qquad \text{for } \theta = 0 \qquad (3.80)$$

Substituting Eq. 3.16 and Eq. 3.80 in Eq. 3.78 we find

$$\frac{\eta_D}{\eta_o} = (1-\delta)^2 , \qquad (3.81)$$

where

$$\delta = 0{,}18 \left[G_2(\Psi_2) . \frac{\lambda \sin \Psi}{\eta_o . D_s} \right]^{\frac{1}{2}} . \qquad (3.82)$$

3.6. The antenna gain as a function of system parameters

Using the equations 3.13, 3.71 and 3.77 it is possible to obtain in one equation the effects of blocking and diffraction of the subreflector (lit. 52)

$$G_t = \left(\frac{\pi D}{\lambda}\right)^2 . \cot^2 \frac{\Psi_1}{2} \left| \int_0^{\Psi_1} \left[G_1(\psi_1) \right]^{\frac{1}{2}} \tan \frac{\psi_1}{2} d\psi_1 - \left[G_1(0) \right] \tan \frac{\Psi_1}{2} \left(\frac{D_s}{D}\right)^2 - \right.$$
$$\left. - \cot \frac{\Psi_2}{2} \int_{\Psi_D}^{\Psi_2} \left[G_2(\psi_2) \right] \left[1 - e^{-\gamma(\psi_2 - \Psi_D)} \right] \tan \frac{\psi_2}{2} \, d\psi_2 \right|^2 . \qquad (3.83)$$

The factor $(\frac{\pi D}{\lambda})^2$ is the gain for a uniformly illuminated constant phase aperture, the rest is called the antenna efficiency η. This efficiency will always be lower than 1. In Eq. 3.83 a great number of parameters are present influencing the gain of a cassegrain system. Calculations have been carried out to find out the relationship between the antenna efficiency η and

(1) the ratio F/D or angular aperture Ψ_2;

(2) the diameter of the subreflector D_s;

(3) the tapered illumination towards the edge;

(4) the radiation pattern of the primary feed $G_1(\psi_1)$.

The feed patterns considered belong to the class

$$G_1(\psi_1) = 2(n+1)\cos^n\psi_1 \quad 0 < \psi_1 < \tfrac{1}{2}\pi \ .$$

These feed patterns are very similar to the main lobes of most available feeds. The chosen valus of n are 60, 40, 24, 16, 12 and 10; the higher the value of n, the smaller the main lobe of the feed pattern. The edge tapers were -6 dB, -8 dB, -10 dB, -15 dB, -20 dB and the diameters of the subreflector 21λ , 24λ , 27λ , 30λ , 33λ , and 36λ . The diameter of the main reflector was kept constant for all calculations ($D=333\lambda$). These time consuming calculations could only be carried out by a computer. The results of these investigations have been laid down in a number of figures (Fig. 3.15 to 3.18, page 3.33). Some very important conclusions can be drawn from these figures. Using the cosine shaped feed pattern, it is in the first place clear that the maximum antenna efficiency that can be reached is about 74%. Comparing this value with Silver (lit. 16,p. 426) who used similar feed patterns as primary radiators for front-fed paraboloids, the antenna efficiency is about 8% lower. This difference is entirely determined by the influence of the subreflector. Figs. 3.15 and 3.16 answer the question if the antenna efficiency is a function of the ratio F/D (or angular aperture Ψ_2). It is clear from these figures that there is practically no relationship. Using a subreflector diameter of 33λ , it appears that the highest efficiencies are found at F/D = 0.25, the efficiency decreasing very gradually at at increasing F/D. As the curves are very close to each other only curves for F/D = 0.25 and F/D = 0.48 are given.

If the subreflector diameter is changed, it is possible to obtain a slight increase in efficiency. A maximum was found of 74.2% at an F/D ratio 0.25, an edge illumination of -10.5 dB, and a subreflector diameter of 24λ .

The maximum efficiency at an F/D ratio of 0.48 was 73.3% at an edge illumination of -10 dB and a subreflector diameter of 27λ . Although the differences are very small, a low F/D ratio seems slightly favourable. Fig. 3.17 shows the maximum efficiency that can be reached with different primary gain functions. These curves show that the primary feed pattern $G_1(\psi_1)$ is not critical, as for practically all values of n from 10 to 60 in the gain function $G_1(\psi_1) = 2(n+1)\cos^n\psi_1$ an efficiency could be reached of about 74%, although this figure is reached under slightly different circumstances, such as edge illumination and subreflector diameters. In Fig. 3.18 using the primary gain function mentioned above with different values of n as parameter the efficiency is found as a function of the subreflector diameter. It appears that an optimum value of the efficiency can be reached. A maximum may be expected if it realized that the losses due to blocking increase at increasing D_s, while conversely, the losses caused by diffraction decrease if D_s is increased. The maximum in the curves, however, is very flat; therefore, the choice of diameter D_s of the subreflector often depends on other circumstances such as the influence of the noise temperature (see chapter 4).

3.7 Conclusion

If a comparison is made between the front-fed paraboloid and the cassegrain antenna it appears that in the latter the primary feed is much better located. In this way the waveguide connections between feed and low losses in the antenna system.Location of the feed near the vertex and low noise receivers can be kept short introducing only low losses in the antenna system. Location of the feed near the vertex of the paraboloid is found very convenient for service purposes.

The noise properties of the cassegrain antenna can also be expected to be better than those of a front-fed paraboloid, as in the latter case the greater part of the spillover is directed towards the "hot" earth, while the cassegrain system has no such contribution. There is spillover around the edge of the subreflector of cassegrain antennas; however the greater part

of this spillover is directed towards the cold sky. Further, the subreflector blocking causes sidelobes centering around the main lobe. Spillover and blocking sidelobes will therefore only contribute to the antenna noise temperature at very low elevation angles, while the front-fed paraboloid receives radiation from the ground at every elevation angle.

A disadvantage of the cassegrain system is no doubt a decrease in antenna efficiency by blocking and diffraction introduced by the subreflector. Diffraction occurs if the dimensions of the subreflector are no longer much greater than the wavelength. It appears that a decrease of 8% in antenna efficiency caused by these effects may be expected. The investigations carried out so far indicate that the subreflector supports are very important as well. The aperture surface blocked by the supports is even greater than the part blocked by the subreflector.

It has been proved theoretically that blocking results in a double effect. A decrease in antenna efficiency may be expected not only because parts of the aperture are blocked, but also because the blocking power P_B is scattered (Sec. 3.4.3.). Both effects increase the sidelobe level and the antenna noise temperature. The effects of blocking can be decreased by shaping the subreflector surface.

Interesting conclusions can be drawn from calculations carried out by a computer. It appears that by blocking and diffraction of the subreflector the antenna efficiency η_o decreases from 82% to 74%, η_o being the product of aperture efficiency and spillover efficiency. It has also been shown that an efficiency of 74% can be obtained with almost every primary gain function. The calculation on diffraction of the subreflector shows the important contribution of this effect to the noise temperature. Diffraction at the main reflector also contributes to some extent to the noise temperature.

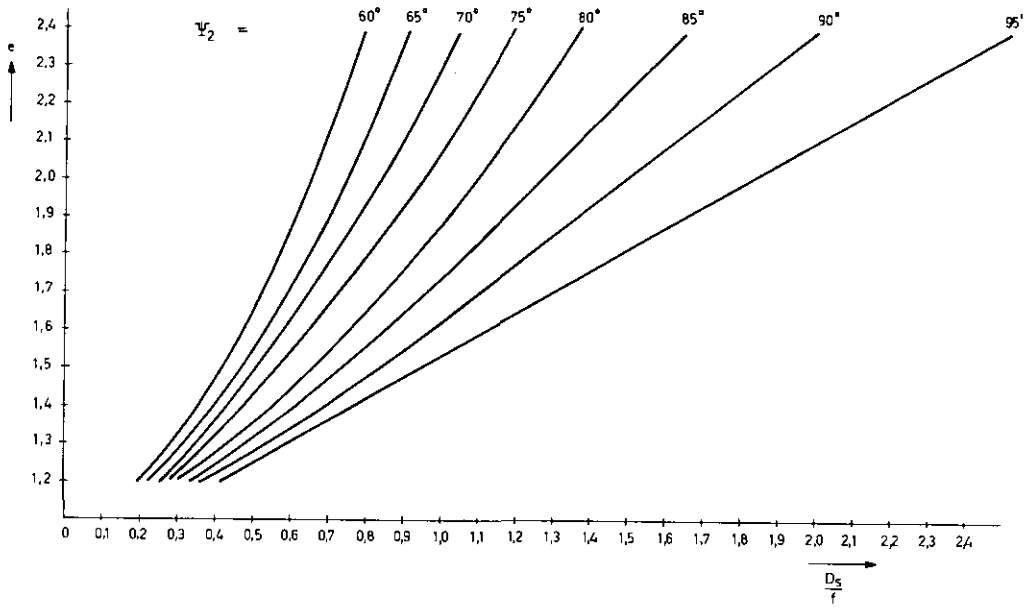

Fig. 3.2. The hyperboloid eccentricity as a function of D_s and f with the angular aperture Ψ_2 as a parameter.

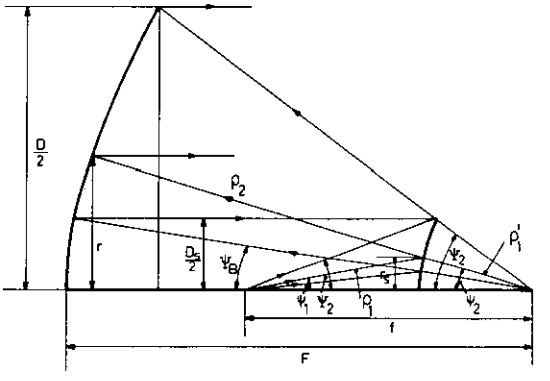

Fig. 3.1. Classical Cassegrain reflector system.

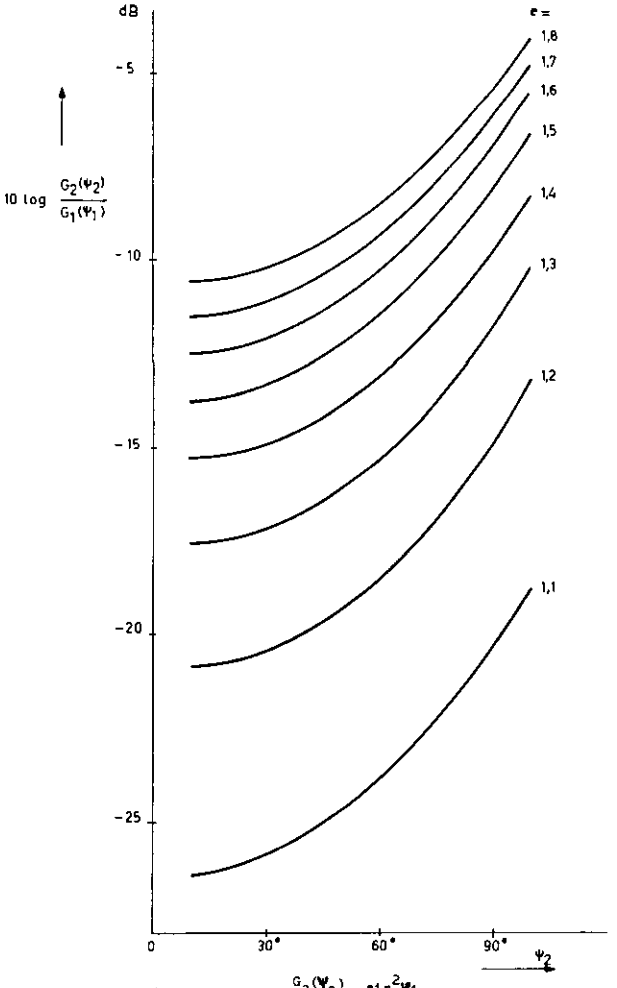

Fig. 3.4. The function $\frac{G_2(\Psi_2)}{G_1(\Psi_1)} = \frac{\sin^2\Psi_1}{\sin^2\Psi_2}$

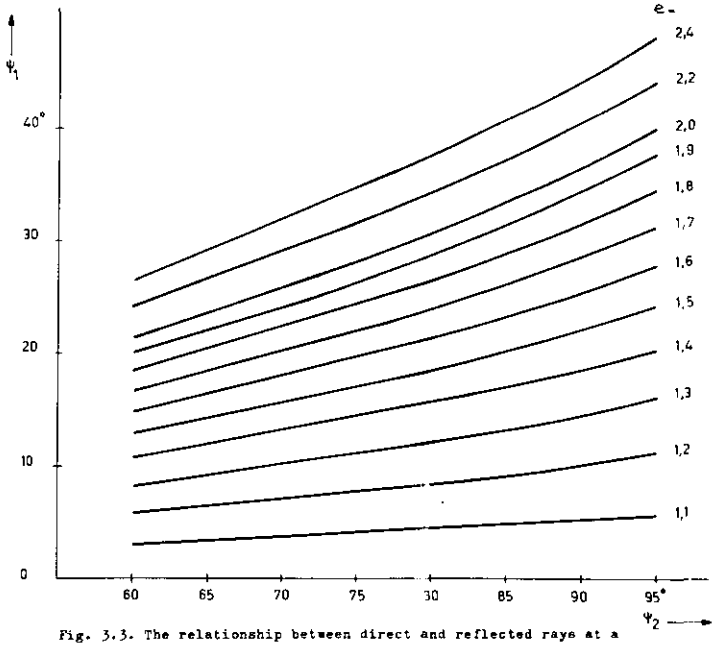

Fig. 3.3. The relationship between direct and reflected rays at a hyperboloid subreflector with the eccentricity as a parameter.

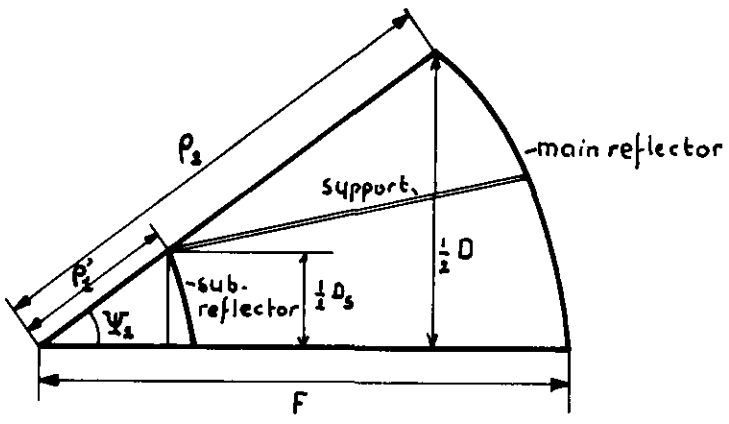

Fig. 3.6. Cross-section of a two reflector system.

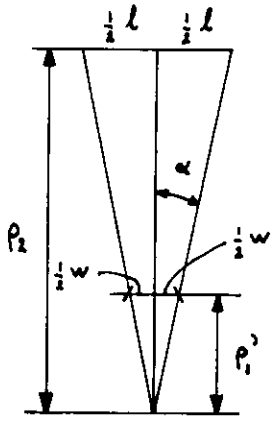

Fig. 3.7. Tangent plane on cone of antenna system.

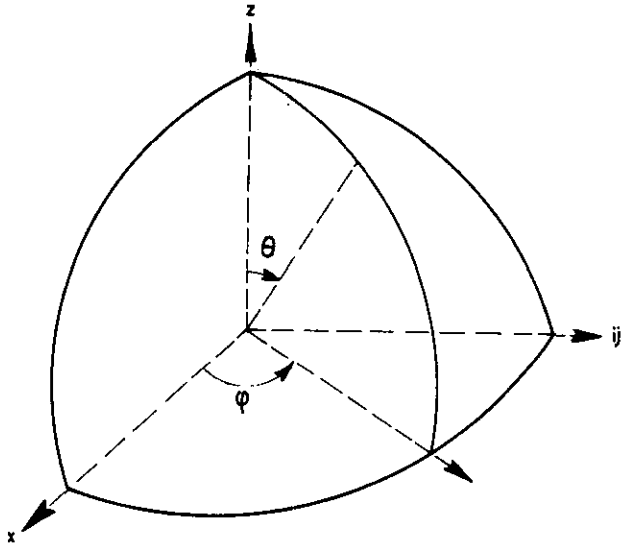

Fig. 3.5 – Spherical coordinates

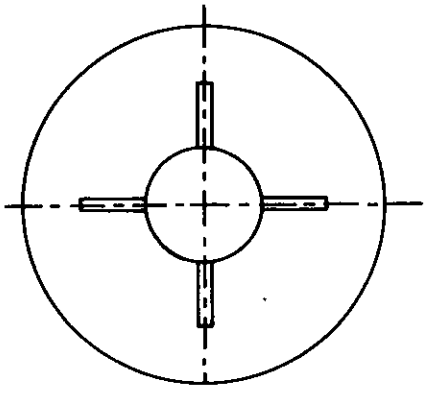

Fig. 3.8a. Shadow by a plane wave.

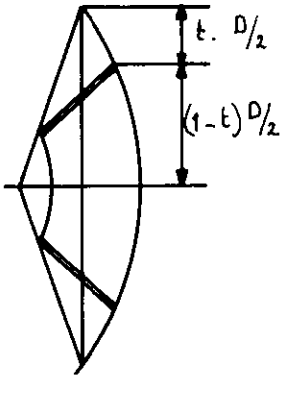

Fig. 3.8b. Geometry of the antenna.

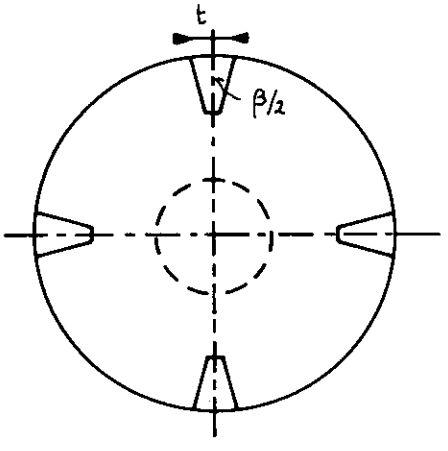

Fig. 3.8c. Shadow by a spherical wave.

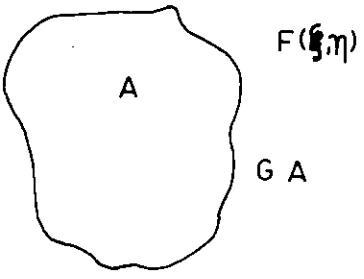

Fig. 3.9a. Aperture A without blocking.

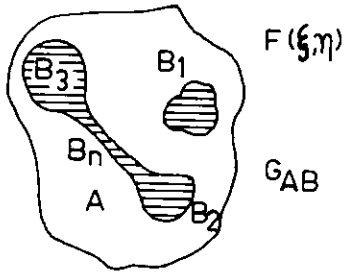

Fig. 3.9b. Aperture A blocked by obstacles B.

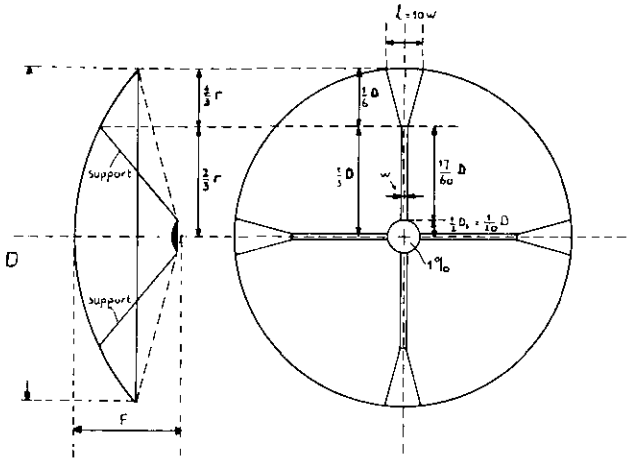

Fig.3.10. Blocking in a cassegrain antenna system at uniform illumination.

Data: $F/D = 0{,}33$; $\frac{D}{D_s} = 10$

$\frac{w}{D} = 0{,}0057$; $\frac{w}{\lambda} = 1{,}9$

4 supports

area one support = $\frac{17}{60}$ w.D

area one trapezoid = $\frac{11}{12}$ w.D $\Big\}$ $A_s = \frac{6}{5}$ w.

4 supports = $4 \cdot A_s = \frac{24}{5}$ w.D

A_{tot} = total aperture area = $\frac{1}{4}\pi D^2$

$\frac{4A_p}{A_{tot}} = \frac{96}{5} \cdot \frac{w}{D} = 6{,}12 \frac{w}{D} =$

$= 6{,}12 \times 0{,}0057 = 0{,}035$

area blocked by subreflector = $0{,}01\ A_{tot}$

Total area blocked = $(0{,}035+0{,}01)A_{tot}$

$= 0{,}045\ A_{tot}$

$\frac{\eta_B}{\eta_o} = (1-0{,}045)^2 = 0{,}91$ or $-0{,}41$ dB.

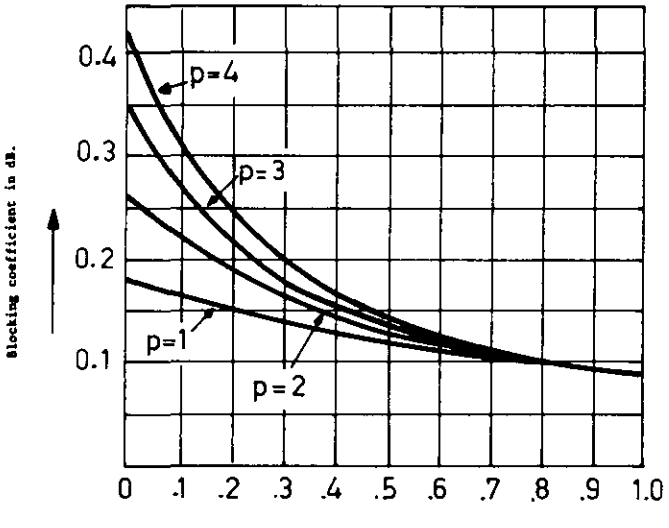

Fig. 3.11. Blocking coefficient of the subreflector.

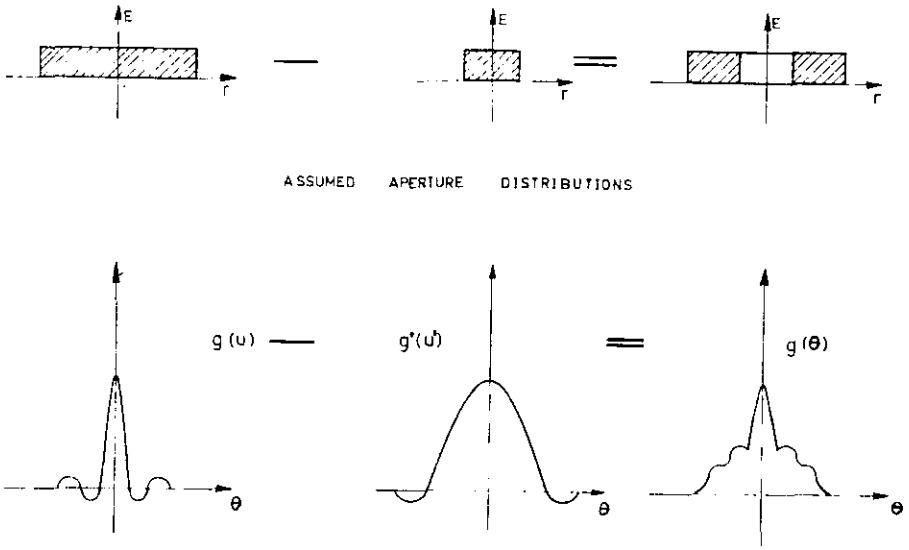

Fig. 3.12. Principle of aperture blockage analysis.

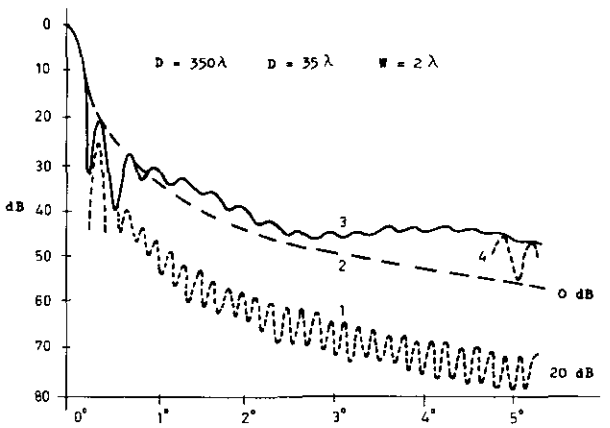

Fig. 3.13. Radiation pattern of a circular aperture, blocked by subreflector and subreflector supports.

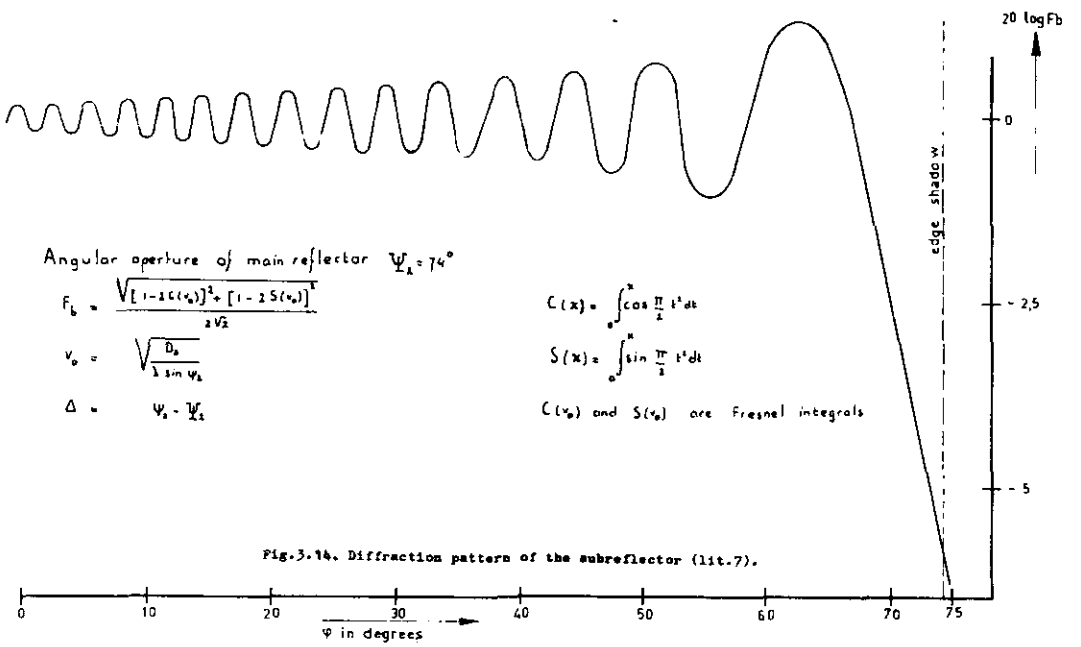

Fig.3.14. Diffraction pattern of the subreflector (lit.7).

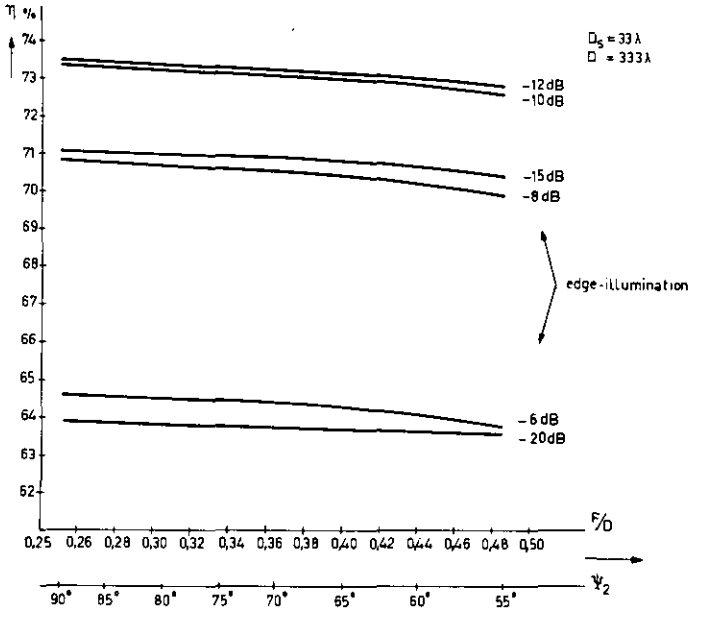

Fig. 3.15. The antenna efficiency η as a function of F/D with the edge illumination of the subreflector as a parameter Gainfunction of the feed: $G(\Psi_1) = 122 \cos^{60}\Psi_1$

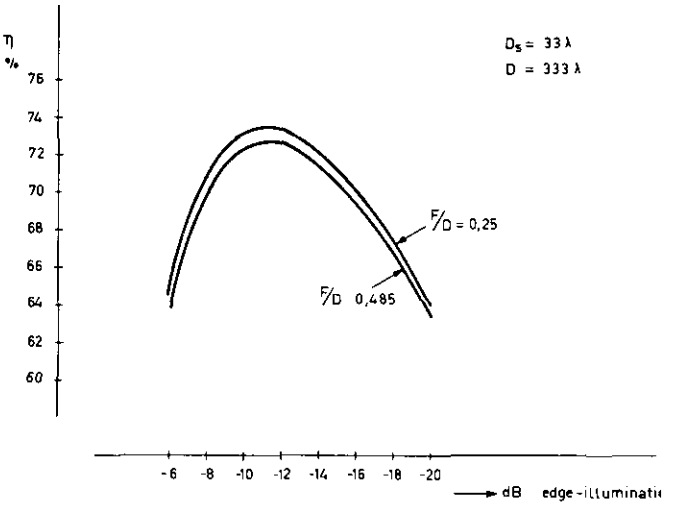

Fig. 3.16. The antenna efficiency η as a function of the edge illumination with the ratio F/D as a parameter.
Gain function $G(\Psi_1) = 122 \cos^{60}\Psi_1$

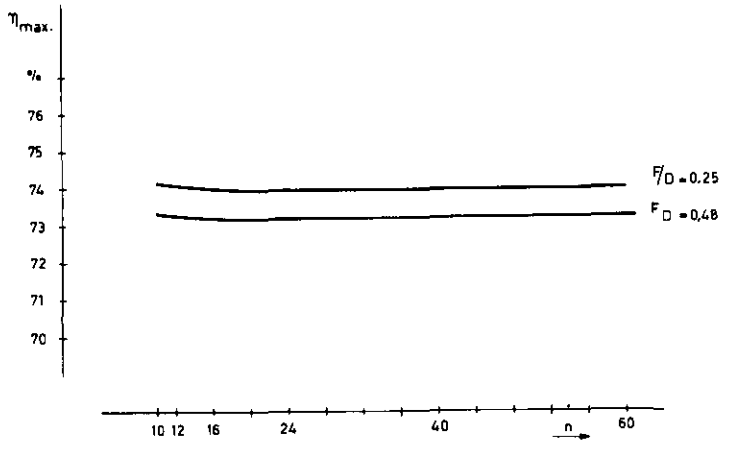

Fig. 3.17. The maximum efficiency as a function of the primary feed pattern
$G(\Psi_1) = 2(n+1) \cos^n\Psi_1$

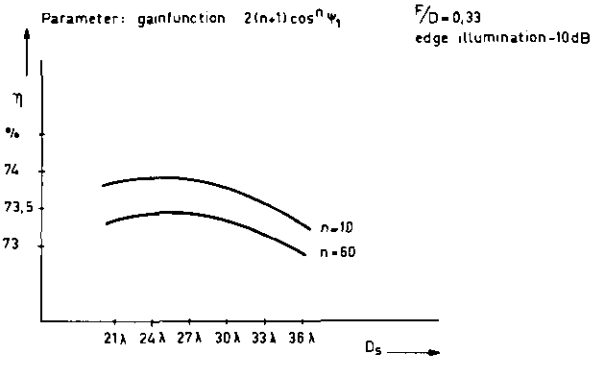

Fig.3.18. The antenna efficiency as a function of the subreflector diameter.

4. On antenna noise temperature

4.1. Introduction

The antenna noise temperature is becoming a very important feature nowadays, owing to the application of antennas for satellite communications. These satellites mostly operate in the frequency band of 4 to 6 GHz. Earlier, the noise temperature of microwave receivers was high compared with the antenna noise temperature. Special components like masers and parametric amplifiers have now reduced the receiver noise temperature in this frequency band to about 5 to 30°K. In designing antennas for satellite communications great care has to be taken to keep the antenna noise temperature on the same level.

This paper pays much attention to the environment of the antenna seeing that the earth acts like a full-absorbing medium as well as a partially reflecting surface.

The antenna temperature is calculated for the case that the radiation pattern $G(\theta,\varphi)$ is known either analytically or by measurement or by calculation. Detailed computations have been carried out for an isotropic antenna, an antenna radiating isotropically in one hemisphere, and a cassegrain antenna system with a pattern known by measurement. A theory is developed for the calculation of the noise temperature in case the antenna radiation pattern $G(\theta,\varphi)$ is not known precisely. It appears that the noise temperature can be found by adding a great number of small contributions. In a two-reflector system these contributions can be: spillover along the subreflector, diffraction at the subreflector edge, back radiation of the feed, etc.

The influence of the reflection losses and ohmic losses of the antenna system have also been examined, and the surface inaccuracies of the main reflector and the corresponding noise contribution have been studied as well.

Finally, the figure of merit of the antenna G/T_s is discussed together with the part played by the system components not belonging to the antenna.

4.2. Physical background

An antenna receiving a signal in a frequency band with a bandwidth of B Hertz will also receive noise power in that frequency band in accordance with the relation

$$W = k \cdot T_A \cdot B \quad , \qquad (4.1)$$

where k = Boltzmann's constant = $1.38.10^{-23}$ Joule/^{o} K, and T_A = the antenna temperature.

Therefore, the noise power delivered to the antenna terminals is characterised by a number T_A in degrees Kelvin. Apparently the antenna noise power is calculated in the same way as the noise power of a resistor at a temperature of T^{o} K.

The bandwidth B is mostly kept small, so that the antenna temperature is kept constant within the frequency band. In satellite comminications, however, the antenna temperature should be known over a wide frequency range (3700-4200 Mc/s).

Noise power received by an antenna may be radiated by any hot body at all frequencies. The distribution of this energy as a function of the frequency for an ideal black body is given by the Planck's radiation law and the approximation of Rayleigh-Jeans which holds reasonably well at microwave frequencies. To derive an expression for the antenna temperature discrete thermal sources are replaced by equivalent black bodies everywhere in the field of view of the antenna (lit. 33). A single discrete source radiates thermal energy according to the Rayleigh-Jeans law through a small cone of solid angle at all parts of the antenna. An integration has to be carried out over the whole antenna to find the total power available at its terminals from the single discrete source. A second integration has to be carried out over the entire antenna pattern to add the contributions from all the discrete sources to the power at the antenna terminals. When the derivation is completed the equation for the noise temperature is:

$$T_A = \frac{1}{4\pi} \int_{\theta=o}^{\pi} \int_{\varphi=o}^{2\pi} G(\theta, \varphi).T(\theta,\varphi) \sin\theta \; d\varphi \; d\theta \quad , \qquad (4.2)$$

where

$T(\theta,\varphi)$ = distribution of the temperature over all angles about the antenna;

θ,φ = spherical coordinates according to Fig. 4.1

and $G(\theta,\varphi)$ = the gain function of the antenna defined by

$$G(\theta,\varphi) = 4\pi \frac{P(\theta,\varphi)}{P_T} \quad , \qquad (4.3)$$

where $P(\theta,\varphi)$ = the power radiated per unit solid angle in the direction (θ, φ),

and P_T the total power delivered to the lossless antenna.

It is convenient to write $P(\theta,\varphi)$ as the sum of two orthogonal completely decoupled components (lit. 16 p. 90)

$$P(\theta,\varphi) = P_p(\theta,\varphi) + P_c(\theta,\varphi) \quad , \qquad (4.4)$$

P_p being the principle and P_c the cross polarised component.

We now introduce the normalised gain function

$$G_n(\theta,\varphi) = \frac{P(\theta,\varphi)}{P(0,0)} = \frac{G(\theta,\varphi)}{G(0,0)} \qquad (4.5)$$

where P(0,0) is the power per unit solid angle in the direction (0,0),

and G(0,0) the maximum gain of the antenna.
Therefore

$$G_n(\theta,\varphi) = G_{np}(\theta,\varphi) + G_{nc}(\theta,\varphi) \; . \qquad (4.6)$$

The gain function of an antenna is thus split into two orthogonal components defined by

$$G_{np}(\theta,\varphi) = \frac{P_p(\theta,\varphi)}{P_p(0,0)+P_c(0,0)} \tag{4.7}$$

and

$$G_{nc}(\theta,\varphi) = \frac{P_c(\theta,\varphi)}{P_p(0,0)+P_c(0,0)} \tag{4.8}$$

We assume that in the far field the antenna is surrounded by a sphere with an absorption coefficient of 1 and temperatures $T_p(\theta,\varphi)$ and $T_c(\theta,\varphi)$ on the sphere. Moreover, vacuum exists within the sphere so that there is no atmospheric influence.
We can now write Eq. 4.2

$$T_A = \frac{G(0,0)}{4\pi} \cdot \int_{\theta=0}^{\pi} \int_{\varphi=0}^{2\pi} \left[T_p(\theta,\varphi) G_{np}(\theta,\varphi) + T_c(\theta,\varphi) G_{nc}(\theta,\varphi) \right] \cdot \sin\theta \, d\varphi \, d\theta \, . \tag{4.9}$$

This expression is useful for radio astronomy where the radio sources are not always randomly polarised.
For the determination of the noise temperature in a satellite communication system it is sufficient to assume that the noise temperature of the sources is indepedent of the polarisation so that

$$T_p(\theta,\varphi) = T_c(\theta,\varphi) = T(\theta,\varphi). \tag{4.10}$$

Eq. 4.9 is now written

$$T_A = \frac{G(0,0)}{4\pi} \int_{\theta=0}^{\pi} \int_{\varphi=0}^{2\pi} T(\theta,\varphi) \cdot \left[G_{np}(\theta,\varphi) + G_{nc}(\theta,\varphi) \right] \sin\theta \, d\varphi \, d\theta \, . \tag{4.11}$$

An antenna design usually contains very low cross polarisation components, but if these components are present, they must be taken into consideration, because the total noise temperature mostly consists of a great number of very small contributions. If the cross polarisation component can be neglected, Eq. 4.11 can be written as Eq. 4.2. Now Eq. 4.2 can also be written

$$T_A = \frac{1}{4\pi} \iint_{4\pi} T(\theta,\varphi) \frac{P(\theta,\varphi)}{\frac{1}{4\pi} \cdot P_T} \, d\Omega$$

or

$$T_A = \iint_{4\pi} T(\theta,\varphi) \cdot P_n(\theta,\varphi)\, d\Omega \quad , \tag{4.12}$$

where

$$P_n(\theta,\varphi) = \frac{P(\theta,\varphi)}{P_T} \quad . \tag{4.13}$$

Calculating the antenna temperature it is often possible to indicate a solid angle $\Delta\Omega$ in the direction (θ,φ), where the temperature is a constant. If the power $P(\theta,\varphi)$ radiated within that solid angle is also constant the contribution to the antenna noise temperature of that solid angle can be written

$$T(\theta,\varphi) \cdot P_n(\theta,\varphi) \cdot \Delta\Omega \quad . \tag{4.14}$$

If the power $P(\theta,\varphi)$ is not a constant, it is often possible to substitute in Eq. 4.14 the average normalised power $\overline{P_n(\theta,\varphi)}$ instead of $P_n(\theta,\varphi)$. The term $P_n(\theta,\varphi) \cdot \Delta\Omega$ can also be explained as being the total relative power radiated within the solid angle $\Delta\Omega$ in the direction (θ,φ) and presented as the coefficient β_i. If the total "antenna volume", 4π, is divided into a number of solid angles having an average temperature of T_i, the antenna temperature will be

$$T_A = \sum_{i=1}^{n} \beta_i \cdot T_i \tag{4.15}$$

where

$$\sum_{i=1}^{n} \beta_i = 1. \tag{4.16}$$

If, for example, 1% of the power of the antenna is radiated in the direction of a full absorbing medium with a physical temperature of 300° K, the contribution of this quantity to the total noise temperature of the antenna will be $0.01 \times 300 = 3^\circ$ K.

4.3. The antenna noise temperature and the atmosphere

Let us consider a theoretical antenna radiating all the power into a small solid angle $\Delta\Omega$ where the temperature $T(\theta,\varphi)$ is a constant. Eq. 4.15 now becomes

$$T_A = T(\theta,\varphi) , \qquad (4.17)$$

Since in Eq. 4.15 $\beta_i = 1$ and $n = 1$. Apparently there is only one contribution to the noise temperature. As long as the temperature $T(\theta,\varphi)$ is constant within the solid angle $\Delta\Omega$, the antenna temperature T_A will also be constant and independent of the antenna gain.
If this theoretical antenna model is located in vacuum, the atmosphere will have no influence on the antenna temperature. Only galactic noise will be received now (lit. 30,37), resulting in an antenna temperature which depends on the frequency (Fig. 4.2). Work carried out by Dicke (lit. 38) has shown that the galactic contributions of Fig. 4.2 should be increased by 3.5° K. This increase is caused by cosmic blackbody radiation finding its origin in the expending universe.

If the theoretical antenna model is now located in the atmosphere, absorption takes place by oxygen and watervapour. Therefore, the atmosphere acts like an attenuator with a certain physical temperature and will have its contribution to the noise temperature T_A. The atmosphere should be described near the location of the antenna. For calculating purposes, however, mostly standard pressure and temperature conditions are taken from the "International Model Atmosphere". Fig. 4.3 shows the dependence of temperature, pressure and water vapour as functions of the height, where the normalised radio radius of the earth is 8500 km. No significant differences are found comparing the standard atmosphere with the real atmosphere (lit. 32).

Oxygen has magnetic dipole resonance at 60 GHz (lit. 39). This effect causes absorption within the frequency band of 1 - 10 GHz, which is nearly independent of the frequency but strongly dependent on the antenna elevation (lit. 30).

The water vapour causes two different absorption phenomena; first, there is electrical dipole resonance at 22.5 GHz and secondly the absorption of the water vapour in the infrared region has its influence also in the frequency band 1 - 10 GHz. If the total absorption coefficient $\alpha = \alpha_o + \alpha_w$ is known (lit. 35, 40) the antenna temperature can be calculated (lit. 41)

$$T_A = \int_o^\infty \alpha \cdot T(r) \exp\left(-\int_o^r \alpha dr\right) dr, \qquad (4.18)$$

where α = total absorption coefficient,
α_o = absorption coefficient of oxygen,
α_w = absorption coefficient of water vapour,
$T(r)$ = the temperature at any point in the atmosphere at a distance r from the antenna.

Calculated curves of T_A are found in Fig. 4.2 carried out by Hogg (lit. 30) He also made several calculations with different concentrations of water vapour in the atmosphere. A great number of investigators have measured the atmospheric noise temperature. A graphical survey of the results at 4 GHz is given in Fig. 4.4.

Analytical approximations of the average atmospheric noise temperature can now be made as follows

$$T_A = \left(\frac{2,2}{\cos\theta} + 0,8\right)\ ^oK \quad \text{for } 0 < \theta < 87.5^o$$

$$T_A = 290 - (90-\theta)\times 95,5\ ^oK \quad 87.5 < \theta < 90^o$$

$$T_A = 290^o\ K \quad 90 < \theta < 180^o \qquad (4.19)$$

4.4. The antenna temperature and its environment

The discussion has so far been limited to a theoretical antenna radiating all its power in a small beam $\Delta\Omega$ surrounded by an absorbing medium. In practice, however, the earth will partly reflect the incident energy. The earth will therefore not act as a black body radiator at a

temperature of 290° K but its contribution will depend on the Fresnel reflection coefficient, assuming the earth acts as a smooth surface. The Fresnel coefficient should be known for both horizontal and vertical polarisations. If the earth acts as a rough surface its scattering behaviour is predominantly diffuse and cannot be prescribed by one reflection coefficient. In this case a number of scatter coefficients have to be defined (lit. 42). Various calculations and measurements are found in the literature (lit. 42,43). It appears that the noise temperature depends on the polarisation and the roughness of the terrain, but only to a very small extent. For calculation purposes, therefore, the earth is often considered not to reflect so that in practice the antenna temperature, after inspection the terrain, will always be somewhat lower.

An expression for the antenna temperature T_A is found below for the assumption that the earth is a smooth reflector with a reflection coefficient R (lit. 42). Let us consider the antenna shown in Fig. 4.5. This antenna has a very narrow beam $\Delta\Omega$. Further, the antenna is assumed to be lossless and mounted at a height h above the ground. Beamed at various angles θ with respect to zenith this antenna sees the true brightness temperature $T(\theta)$, independent of φ because the location is circularly symmetrical. The sky noise from the angle $\pi-\theta_o$ is reflected at point P according to the reflection coefficient of the earth at P. The antenna located in O will therefore see a temperature $|R^2| . T(\theta)$. Between O and P noise due to loss in the atmosphere also contributes to the antenna temperature. The atmosphere can be characterised by the loss factor

$$L(h) = \exp(-0{,}2303 \cdot \alpha \cdot h \cdot \sec\theta_o) \qquad (4.20)$$

where h = height of the antenna,

α = attenuation per km; at 4 GHz, α = 0.0058 dB/km.

The reflection of the sky noise due to absorption between P and O will contribute to the total noise temperature an amount of

$$T_A' = |R|^2 \cdot T_\theta \cdot L(h). \qquad (4.21)$$

The earth also generates noise that enters the antenna directly and will contribute to the antenna temperature in O, this contribution being attenuated as well, namely

$$T_A'' = \{ 1 - |R|^2 \} T_o L(h) + \{1-L(h)\} T_s , \qquad (4.22)$$

where T_o is the temperature of the earth, assumed to be 290° K, and T_s the temperature of the sky.

The total antenna temperature measured in O is therefore

$$T_A = |R|^2 \cdot L(h) \cdot T_\theta + \{1- |R|^2 \} T_o L(h) + \{1-L(h)\} T_s . \qquad (4.23)$$

4.5. Noise temperature calculations

4.5.1. Calculation procedure if the gain function of the antenna is known

In Sec. 4.2 an equation was found to calculate the antenna noise temperature

$$T_A = \frac{1}{4\pi} \int\int_{4\pi} G(\theta, \varphi) \cdot T(\theta, \varphi) \, d\Omega \qquad (4.2)$$

This equation can be used if the functions $G(\theta, \varphi)$ and $T(\theta, \varphi)$ are known. Another expression has been derived for the antenna temperature being

$$T_A = \sum_{i=1}^{n} \beta_i \cdot T_i \quad . \qquad (4.15)$$

Eq. 4.15 can be used succesfully when it is known to what solid angle the various parts of the total power of the antenna are radiated. It should be kept in mind, however, that Eq. 4.16 still holds. In all subsequent calculations in this paper the function $T(\theta, \varphi)$ is chosen according to the three analytical expressions in Eq. 4.19 found in Sec. 4.3.

We shall first consider an isotropic radiator where $G(\theta, \varphi)=1$. Therefore, Eq. 4.12 is written

$$T_A = \frac{1}{4\pi} \int_{\theta=0}^{\pi} \int_{\varphi=0}^{2\pi} T(\theta, \varphi) \cdot \sin\theta \, d\varphi \, d\theta$$

or

$$T_A = \tfrac{1}{2} \int_{0}^{\pi} T(\theta) \sin\theta \, d\theta \, . \qquad (4.24)$$

Substituting Eq. 4.19 in 4.24 and carrying out the integration it is found that the antenna temperature of an isotropic radiator at 4 GHz is

$$T_A = 150^{\circ} \text{ K} \, .$$

4.5.2. <u>The temperature of an isotropic antenna radiating in one hemisphere</u>

We will consider an antenna radiating isotropically in one hemisphere. The antenna is located in the origin of a threedimensional coordinate system x,y,z, where θ and φ are spherical coordinates (Fig. 4.1). The antenna gain is now only defined right of the xz plane and will be zero left of the xz plane. The gain of the antenna is $G(\theta, \varphi) = 2$ for $0 < \varphi < \pi$ and $0 < \theta < \pi$. The temperature of this antenna can be easely calculated if the antenna axis points along the y-axis, where $\theta = \varphi = \frac{\pi}{2}$. The procedure is similar to that carried out in Sec. 4.5.1. Indeed, the antenna gain is 2, but φ is only integrated over π rad. It is therefore no suprise that the antenna temperature is here 150° K as well.

If the antenna axis points to zenith, where $\theta=0$, and the integration is carried out, it is found that

$$T_A = \frac{1}{4\pi} \int_{\varphi=0}^{2\pi} \int_{\theta=0}^{\pi/2} 2.T(\theta, \varphi) \sin\theta \, d\varphi \, d\theta = 10^{\circ} \text{ K.}$$

If the antenna axis is directed to θ_o , Φ_o(Fig.4.6) the antenna temperature is a function of Θ_o and Φ_o therefore

$$T_A = \frac{1}{4\pi} \iint T(\theta,\varphi) \cdot G(\theta-\theta_o, \varphi-\Phi_o)\, d\Omega \quad . \qquad (4.25)$$

Using the expression for an antenna radiating isotropically in one hemisphere we find

$$T_A(\theta_o, \Phi_o) = \int_{\theta_o}^{\theta - \pi/2} \int_{\Phi'}^{\pi/2} 2T(\theta,\varphi)\, d\Omega. \qquad (4.26)$$

By means of spherical trigonometry it is found (lit. 36) that

$$\Phi' = \arcsin(\cot\theta \cdot \operatorname{tg}\theta_o) \quad . \qquad (4.27)$$

A calculated curve of T_A as a function of θ_o is found in Fig. 4.7.

4.5.3. The temperature of an antenna with a measured pattern $G(\theta,\varphi)$

If the radiation pattern of an antenna is known by measurement it can be found what part β_i of the total power is radiated by the antenna in any solid angle. Therefore

$$\beta_i = \frac{\frac{1}{4\pi} \int_{\varphi 1}^{\varphi 2} \int_{\theta 1}^{\theta 2} G(\theta,\varphi) \sin\theta \, d\varphi \, d\theta}{\frac{1}{4\pi} \int_{0}^{2\pi} \int_{0}^{\pi} G(\theta,\varphi) \sin\theta \, d\varphi \, d\theta} \quad . \qquad (4.28)$$

The solid angle is defined by $\varphi_2 - \varphi_1$ and $\theta_2 - \theta_1$ while it is easely found that the denominator of Eq. 4.28 is equal to 1. As most radiation patterns show circular symmetry the integration over φ may be carried out from $0 \rightarrow 2\pi$. Eq. 4.28 becomes

$$\beta_i = \frac{1}{2} \int_{\theta_i}^{\theta_{i+1}} G(\theta) \cdot \sin\theta \cdot d\theta \quad . \qquad (4.29)$$

Mostly the measured antenna patterns are very erratic so that β_i cannot be found analytically. The problem can still be solved by

graphical integration using a planimeter. In that case the θ axis has to be weighted according to $\Delta'\theta = \sin\theta \cdot \Delta\theta$.

Fig. A.1 of the appendix shows the radiation pattern of a conical horn antenna. Figs. A.2 and A.3 also show the radiation patterns but now for the weighted θ axis. An example of calculation is given to find the quantity of the total power radiated between the -10 dB points of the main lobe.

Reed (lit. 44) divides the antenna pattern in seven portions: main lobe, first order sidelobes, near sidelobes, forward spillover in cassegrain systems, far sidelobes, rear spillover, and blacklobes. In all these portions the relative power content β_i has to be calculated or estimated keeping in mind that

$$\sum_{i=1}^{7} \beta_i = 1.$$

Although Reed does not indicate how to choose the seven different solid angles the tendency of his work is clear. If the relative powers are known by numerical integration or by the planimeter method, the contribution to the antenna temperature of each portion is found by

$$\Delta T_A = \beta_i \cdot T_i \qquad (4.30)$$

and the total antenna temperature

$$T_A = \sum_{i=1}^{7} \beta_i \cdot T_i \quad . \qquad (4.31)$$

For his 4 GHz cassegrain antenna Reed found the following power contents and antenna temperatures for elevation angles 5°, 20°, and 45° .

	relative power content in %	temperature contributions ^{o}K elevation angle		
		5^{o}	20^{o}	45^{o}
1. Mainlobe	80	23.8	6.2	2.7
2. First order side lobes	5	1.4	0.4	0.2
3. Near sidelobes	1	0.7	0.1	-
4. Hyperbolic spillover	10	10.5	1.2	0.3
5. Far sidelobes	2	2.8	2.6	2.0
6. Parabolic spillover	1.5	2.2	2.4	3.0
7. Back lobes	0.5	0.7	1.0	1.3
Total antenna temperature		42.1	13.9	9.5

4.5.4. Temperature of an antenna with an unknown radiation pattern

4.5.4.1. Introduction

It is often required to calculate or estimate the antenna temperature of an antenna without knowing the exact radiation pattern. Calculation of the radiation pattern of complicated antennas is often not possible. In this case however, it is still possible to calculate the power radiated in some solid angles. The solid angle Ω_i, however, is not defined by one coefficient β_i (Eq. 4.28); we assume therefore, the coefficient β_i to consist of a number of contributions $\gamma_{1_i} + \gamma_{2_i} + \ldots \gamma_{m_i}$ so that Eq. 4.15 can now be written as

$$T_A = \sum_{i=1}^{n} T_i \cdot \sum_{j=1}^{m} \gamma_{ji} \cdot \qquad (4.32)$$

The coefficients γ can be explained by realising that the antenna will radiate in one solid angle power contributions caused by subreflector spillover, subreflector diffraction and scatter owing to the blocking effects. It is therefore, convenient to write Eq. 4.32

$$T_A = \sum_{i=1}^{n} T_i \cdot \gamma_{1i} + \sum_{i=1}^{n} T_i \cdot \gamma_{2i} + \ldots \sum_{i=1}^{n} T_i \cdot \gamma_{mi} \qquad (4.33)$$

or

$$T_A = \sum_{j=1}^{m} \sum_{i=1}^{n} T_i \cdot \gamma_{ji} \cdot \qquad (4.34)$$

Thus the noise contribution from a solid angle is determined first by one particular cause (e.g. spillover) after which all these contributions are added over all solid angles. In this way it is possible to estimate the noise contribution from several causes.

We shall now calculate the antenna temperature from a practical example of a two-reflector system shown in Fig. 4.8.
The radiators in the double reflectorsystem (lit. 34) of this figure are:

1. The primary feed and feed pattern $G_f(\theta, \varphi)$. It is possible to distinguish between a theoretical feed pattern and a feed pattern measured from an existing feed.

2. The main reflector feed system comprising the subreflector and feed $G_s(\theta, \varphi)$. In general, the shape of the subreflector need not be defined and may be hyperbolical, elliptical or may have a special shape.

3. The pattern of the complete antenna $G(\theta, \varphi)$. This comprises the patterns of feed, subreflector and main reflector.

4.5.4.2. The primary feed pattern

Fig. 4.9 shows the primary feed pattern combined with the subreflector. It is found convenient to coincide the origin of the coordinate system of Fig. 4.1 with the phase centre of the primary feed. If the gain function of the feed is $G_f(\theta,\varphi)$, the relative power radiated into a solid angle $\Delta\Omega$ is

$$P_n(\theta,\varphi) = \frac{1}{4\pi} \int_{\theta_1}^{\theta_2} \int_{\varphi_1}^{\varphi_2} G_f(\theta,\varphi) \cdot \sin\theta \; d\varphi \; d\theta \quad . \tag{4.35}$$

This integration can be carried out numerically or graphically (Appendix). We shall now divide the radiation pattern of the feed into 5 circularly symmetrical solid angles, assuming the pattern to be circularly as well. Therefore, in the equations below the integration over φ has already been carried out.

1. The relative power lost owing to blocking of the subreflector and the supports, is scattered in various directions. Its value is

$$P_{n1} = \tfrac{1}{2} \int_{0}^{\theta_B} G_f(\theta) \sin\theta \; d\theta \quad . \tag{4.36}$$

2. The relative power radiated to the subreflector and reflected to the main reflector by optical laws.

$$P_{n2} = \tfrac{1}{2} \int_{\theta_B}^{\Theta} G_f(\theta) \sin\theta \; d\theta \quad . \tag{4.37}$$

3. The relative power lost by spillover along the subreflector.

$$P_{n3} = \tfrac{1}{2} \int_{\Theta}^{\pi/2} G_f(\theta) \sin\theta \; d\theta \quad . \tag{4.38}$$

4. The relative power which is radiated backward.

$$P_{n4} = \tfrac{1}{2} \int_{\pi/2}^{\pi} G_f(\theta) \sin\theta \; d\theta \quad . \tag{4.39}$$

5. The relative power radiated by the cross polarisation component of the feed pattern.

$$P_{n5} = \frac{1}{4\pi} \int_{\theta=0}^{\pi} \int_{\varphi=0}^{2\pi} G_c(\theta,\varphi) \sin\theta \, d\varphi \, d\theta \quad , \tag{4.40}$$

where $G_c(\theta,\varphi)$ is the cross polarisation gain pattern.

If a theoretical feed pattern is used, e.g.,

$$G_f(\theta) = 2(n+1) \cos^n \theta \quad , \tag{4.41}$$

and substituted in Eqs. 4.36 to 4.39, the integration over θ leads to

$$P_n = \cos^{n+1} \theta_1 - \cos^{n+1} \theta_2 , \tag{4.42}$$

where θ_1 is the lower integration limit and θ_2 the upper integration limit used in the Eqs. 4.36 to 4.39.

In the Figs. 4.10 and 4.11 calculated curves are given showing the percentages spillover of the theoretical feed as a function of n and the edge illumination. The spillover from a measured feed pattern can be determined using the methods in the Appendix. Fig. 4.12 shows the angle θ_1 subtending the subreflector as a function of the edge illumination.

4.5.4.3. <u>The main reflector feed system</u>

Fig. 4.13 shows an arrangement of a feed and subreflector. The field radiated by the feed is constant within the solid angle subtended by the hyperboloid and zero elsewhere (lit. 18). A calculated radiation pattern is represented in the same figure. According to optical laws all power radiated by the feed should be captured and reradiated by the subreflector. If this pattern is integrated numerically, it appears that only 79% of the total power is captured by the main reflector and that 21% is lost by diffraction effects along the edge of the subreflector. Rusch' method has the drawback that complicated computer programmes have to be used.

The diffraction effects can also be prescribed using the principle of stationary phase (lit. 5) (see also chapter 3). Using this it is also possible to approximate the relative power lost by diffraction. Using the arrangement shown in Fig. 4.9 the power lost by diffraction, assuming circular symmetry is,

$$P_n\text{diff} = P'_n - P''_n , \tag{4.43}$$

where

$$P'_n = \tfrac{1}{2} \int_{\Theta_D}^{\Theta_2} G(\theta_2) \sin \theta_2 \, d\theta_2 \tag{4.44}$$

and

$$P''_n = \tfrac{1}{2} \int_{\Theta_D}^{\Theta_2} G(\theta_2)\, e^{-2\gamma(\theta_2 - \Theta_D)} \sin \theta_2 \, d\theta_2 , \tag{4.45}$$

with

$$\Theta_D = \Theta_2 - 0.65 \sqrt{\frac{\lambda \sin \Theta_2}{D_s}} \tag{4.46}$$

$$\gamma = 1.07 \sqrt{\frac{D_s}{\lambda \sin \Theta_2}} , \tag{4.47}$$

and

$$G_f(\theta_1) \sin^2 \theta_1 = G_2(\theta_2) \sin^2 \theta_2 . \tag{4.48}$$

With the aid of a computer the relative power lost by blocking could also be calculated. The results are shown in Fig. 4.14 as a function of the edge illumination. A theoretical feed pattern $G_f(\theta_1) = 122 \cos^{60} \theta_1$ was used, in accordance to the relation $G_f(\theta_1) \sin^2 \theta_1 = G_2(\theta_2) \sin^2 \theta_2$, the angular aperture Θ_2 or the F/D ratio being a parameter. This method has the drawback that it is possible to say in what directions the diffracted power is scattered. From the results of Rusch (lit. 18) and the measurements carried out in Chapter 6, however, it is expected that more information will be ready soon for publication.

If only a measured pattern of the feed system including the subreflector is available, the ideal pattern discussed before has to be completed by back radiation and spillover of the primary feed. The same procedure as discussed in Sec. 4.5.4.1. is now followed, i.e., the contributions of back radiation, diffraction, spillover, and cross polarisation are added in any solid angle in order to find the antenna noise temperature.

From the calculations carried out so far it can be concluded that low losses due to spillover, blocking, and diffraction form the most important features reducing ground noise. This is one of the reasons for the good results obtained by the Raisting antenna, where the edge illumination is only - 20 dB. The power lost by diffraction and spillover is still 5% (lit. 6). The aperture efficiency, however, is low. Possibilities to increase the aperture efficiency combined with a low edge illumination taper are obtained by shaping main and subreflector (Chapter 8).

4.5.4.4. The main reflector

The main reflector is illuminated by the available power within the angular aperture Θ_2 (Fig. 5.15). By means of the current integration method (lit. 47) it is possible to calculate the radiation pattern of the main reflector without considering the blocking effects. The pattern near the main lobe can also be found by means of the aperture method. The power distribution over several solid angles can be calculated with both methods (lit. 25,26).

If the aperture is illuminated uniformly it appears that 95% of the power intercepted by the main reflector is reradiated within the main lobe and the near sidelobes within 0.5° of the antenna axis. According to the methods discussed in Sec. 4.5.4.3 the relative power lost by diffraction at the edge of the main reflector can be calculated. Computer programmes based on the current distribution methods will give more information on the relative power radiated into various solid angles.

If the aperture of the main reflector is blocked by some obstacle, the power supplied to the main reflector is decreased (Chapter 3). Power from the main lobe is now spread to the sidelobes (lit. 24). If the size of the subreflector is increased, the sidelobes caused by this blocking will come nearer the main lobe and have little effect on the antenna temperature. The noise contribution, however, from the scattered blocking power can be significant (Sec. 3.4.5). This contribution can be made much smaller if the blocked power is supplied to the aperture by shaping main and subreflectors. Davidson (lit. 1) gives an equation for the increase in noise temperature caused by scattering at the subreflector supports.

Losses can also be expected by surface deviations of the paraboloid reflector from an ideal reflector. Shin (lit. 46) has shown that at a reduction of gain of 0.2 dB, 4.5% of the powercontent of the main lobe will be spread to the near sidelobes of the radiation pattern. The increase in antenna temperature is, the refore, very small. Some information on the average sidelobe level caused by surface deviations is given by Dragone and Hogg (lit. 45).

4.5.4.5. Survey of noise temperature calculation

The previous section has shown the possibility of calculating the antenna noise temperature by adding the following contributions:

1. Contributions from the feed

$$\Delta T_{feed} = \Delta T_{c_1} + \Delta T_b + \Delta T_{sp} , \qquad (4.49)$$

where

ΔT_{c_1} = contribution by cross polarisation,

ΔT_b = contribution by black radiation,

ΔT_{sp} = contribution by spillover.

2. Contributions by the subreflector

$$\Delta T_{sub} = \Delta T_{D_1} + \Delta T_{B_1} + \Delta T_{B_2} + \Delta T_{C_2} , \qquad (4.50)$$

where ΔT_{D_1} = contribution by diffraction on the subreflector,

ΔT_{B_1} = contribution by the scattering of the subreflector blocking power against the feed support,

ΔT_{B_2} = contribution by the scattering of power against the subreflector supports,

ΔT_{C_2} = contribution of cross polarisation effects introduced by the subreflector.

The above may be further explained by mentioning that the power lost by subreflector diffraction is calculated according to the Eqs. in Sec. 4.5.4.3. It is assumed that the diffracted power is radiated isotropically in one hemisphere. The blocking power is also assumed to scatter isotropically in one hemisphere as well as the backradiation . The calculation is simplest if the antenna axis points to the horizon. If the antenna noise temperature has to be specified at any elevation, Fig. 4.7 can be used.

3. Contributions by the main reflector

$$\Delta T_m = \Delta T_{m1} + \Delta T_{D_2} + \Delta T_{C_3} \quad , \tag{4.51}$$

where ΔT_{m1} = contribution of the main lobe with near sidelobes (Sec. 4.5.4.4.). This contribution is found by calculating the relative power contained in this part of the pattern. The latter part also contains distributions caused by surface inaccuracies and blocking, where power from the main lobe is spread to the near sidelobes (Sec.4.5.4.4). In literature it is mostly assumed that the antenna radiates its power within a small solid angle so that the antenna temperature only depends on the antenna elevation angle (Fig. 4.4).

ΔT_{D_2} = contribution by diffraction effects. This contribution can be calculated in the same way as done for the subreflector. (Sec. 4.5.4.3).

ΔT_{C_3} = contribution by cross polarisation at the main reflector.

If the antenna is assumed to have no ohmic losses, the antenna

temperature is found from

$$T_A = \Delta T_{feed} + \Delta T_{sub} + \Delta T_{m.} \qquad (4.52)$$

4.5.5. The antenna temperature and the reflection coefficient of the primary feed

If accurate calculation of the antenna temperature is required allowance must be made for the reflection coefficient of the primary feed. If the V.S.W.R. amounts 1.22, 1% of the power supplied to the feed will be reflected. If we study Fig. 4.16, it is found that the noise power received in reference plane II will be

$$W_{II} = k.T_A.B. \qquad (4.1)$$

If the voltage reflection coefficient ρ_1 is introduced we shall receive in plane I only part of this noise power viz. $k\ T_A\ B(1-|\rho_1|^2)$. The feed is adapted by a line ℓ to the receiver. The physical temperature, however, of this receiver is not 0° K; therefore, the part of the noise power emitted by the receiver and reflected in plane II has also be taken into consideration. If the noise temperature of the receiver is T_R, the part reflected will be $|\rho_1|^2\ k\ T_R\ B$. The total antenna temperature which we shall find in plane II now becomes

$$T_A = (1-|\rho_1|^2)\ T_A + |\rho_1|^2\ T_R\ , \qquad (4.53)$$

so that the increase in antenna temperature caused by the reflection coefficient will be

$$\Delta T_A = -|\rho_1|^2\ T_A + |\rho_1|^2\ T_R\ . \qquad (4.54)$$

If the total system temperature has to be calculated, the reflection coefficient of the amplifier should also be to considered as well as the length of line ℓ (lit. 48).

4.5.6. Ohmic losses within the antenna system

The antenna system will contain several ohmic losses viz,

(1) losses in the primary feed,
(2) losses in the melinex window which protects the feed opening against influence of the weather,
(3) losses in main and subreflector.

We assume that all the power radiated is attenuated by these effects. The increase in antenna temperature is therefore, assuming $\frac{T_A}{T_o} << 1$,

$$\Delta T_A = (1-g_1)\, T_o + (1-g_2)\, T_o + (1-g_3)\, T_o,$$

where g_1, g_2 and g_3 are attenuations caused by feed, window and reflectors, all calculated at the temperature $T_o = 290^\circ$ K. A useful approximation is the rule to increase the noise temperature by 7° K for each 0.1 dB attenuation. Davidson (lit. 1) presents a calculation of the increase of antenna temperature due to absorption by the reflectors. Painting the reflector usually increases the noise temperature.

4.5.7. Noise caused by sun and weather

Observed from the earth, the sun is subtended by angle of 0.5°. If an ideal antenna of the same beamwidth points to the sun, the noise temperature measured will be (lit. 31)

$$T_{sun} = \frac{290 \times 675}{f}, \qquad (4.54)$$

where f is the frequency in GHz. This equation is an approximation of the sun's noise temperature. More accurate relations are shown by Hcgg (lit. 31) and Salomonowich (lit. 35). According to Potter (lit.24) the contribution of the sun to the antenna temperature is given by

$$\Delta T_A = \frac{S}{2k} \cdot A_s = \frac{\lambda^2 S\, G_s}{8\pi\, k}, \qquad (4.55)$$

where S = solar flux density in W/m^2 . Hz.,
λ = wavelength,
A_s = the average effective aperture,
$G_s = \frac{1}{\Delta\Omega} \int_{\Delta\Omega} G(\theta,\varphi)\, d\Omega$, where $\Delta\Omega = 0.5^\circ$.
k = Boltzmann's constant = $1.38 \cdot 10^{-23}$ Joules $/^\circ$ K.

It appears that the contribution by the sun will be 2° K at a

frequency of 4 GHz and an average sidelobe level of + 10 dB above isotropic. Hogg and Semplak (lit. 32) have carried out experiments to determine the influence of clouds and rain on the antenna noise temperature.
A clear increase of the antenna temperature at recent antenna measurements at 8.6 GHz in the Dutch radio station Kootwijk was demonstrated during periods of rain and increasing clouds. The I.C.S.C. requirements for satellite communications are specified at dry, bright weather so that they can be left out of consideration for the time being.

4.6. The figure of merit G/T_s

4.6.1. Introduction

The figure of merit is the ratio of the antenna gain G, measured at the terminals of the noiseless receiver, to the system noise temperature T_s of the system.
Figure of merit is 10 log $G/T_s = G_{(dB)} - T_{s(dB)}$.

The requirements of the I.C.S.C. demand a figure of merit of 40.7 dB or more for an antenna for satellite communications operating at 4 GHz at elevation angles at which the satellite is seen in dry bright weather. This specification is graphically shown in Fig. 4.17, where the maximum permissible antenna noise temperature is shown as a function of the antenna diameter, the antenna efficiency being a parameter. Figures of merit of various existing and planned satellite groundstations are found in a recently published report (lit. 13).

To find optimum ratios G/T_s it is necessary to derive an analytical expression containing this ratio. Davidson (lit. 1) has found such an optimum for a front fed paraboloid using the theoretical gain function

$$G(\theta) = G_o \cos^2 m\theta \quad . \quad (-\tfrac{\pi}{2} < m\theta < \tfrac{\pi}{2}) \quad .$$

Similar work is now carried out at Eindhoven for cassegrain systems. For shaped reflectors as discussed in Chapter 8, it appears that noise temperature and antenna gain are practically independent of each other so that each of them can be optimised separately.

4.6.2. The figure of merit and the system components.

As explained in the previous section it should be mentioned in which reference plane all the quantities are to be calculated or to which reference plane all the quantities should be reduced. The I.C.S.C. clearly specifies that the reference plane should be found at the input terminals of the parametric amplifier. In detailed computations the influence of reflection at these terminals has to be considered as well, therefore, the reference plane in the following will be defined to be situated at the input terminals of the parametric amplifier after reflection has taken place.

The entire antenna system (Fig. 4.18) can be devided into the following components:

(1) the feed and reflectors. Reference plane I is situated in such a way that the feed is separated from the waveguide components. It is assumed that the reflection coefficient in plane I is equal to ρ_1 and that the antenna noise temperature inclusive the contribution of the feed, attenuated by G_1, is equal to T_A in reference plane I before reflection takes place.

(2) the receiver, located to the right of reference plane II with reflection coefficient ρ_2 and consisting of a parametric amplifier P.A. with a noise temperature of T_{PA} and a gain of G_{PA}, arranged in series with a tunneldiode amplifier T.D. (noise temperature T_{TD} and gain G_{TD}) and a travelling wave tube T.W.T. (noise temperature T_{TWT} and gain G_{TWT}).

(3) the connection between feed and receiver, comprising all components between the reference planes I and II. It is further assumed that ρ_1 and ρ_2 are the only reflection coefficients. Several components like duplexer, circulator, tracking coupling device and cross guide directional coupler are located between the two reference planes, with a total attenuation of G_2 at a physical temperature of $T_o=290^o$ K.

The tracking system contributes to the total system temperature an amount of T_{track} and the cross guide directional coupler T_o/g_3, g_3 being the coupling ratio. ($G_3 = 10 \log g_3$)

The antenna gain left of reference plane I (before reflection) is equal to G_o. Reflection will take place at the two planes with an attenuation of G_2. The antenna gain G_o at the input terminals of the parametric amplifier has therefore to be modified according to

$$g_o' = g_o(1 - |\rho_1|^2)(1 - |\rho_2|^2)\, g_2 \quad . \tag{4.56}$$

As the reflection coefficients are nearly equal to unity, the effect of multiple reflections can be neglected.

The total system noise temperature consists of contributions of several noise sources not being correlated, therefore, they may simply be added together. In one single case there may be some correlation such as the noise from multiple reflections introduced by the reflection coefficients ρ_1 and ρ_2, but this fact can only be taken into consideration if the electrical length between plane I and II is know exactly.

The system temperature T_s now found to the right of plane II appears to be a function of a great number of sources modified by the system parameters:

$$T_s = f\,(T_A, T_o, T_{PA}, T_{TD}, T_{TWT}, T_{track}; \rho_1, \rho_2, G_2, G_3, G_{PA}, G_{TD}, G_{TWT}) . \tag{4.57}$$

Expression 4.57 can be split up into a number of interrelated terms

$$T_s = f_1(T_A; \rho_1, \rho_2, G_2) + f_2(T_o; \rho_1, \rho_2, G_2) + f_3(T_{PA}; \rho_1, \rho_2, G_2) +$$

$$+ T_{PA} + \frac{T_{TD}}{g_{PA}} + \frac{T_{TWT}}{g_{PA} \cdot g_{TD}} + f_4(T_o + T_{track}; \rho_1, \rho_2, G_2, G_3) \quad . \tag{4.58}$$

In Eq. 4.58 $f_1(T_A; \rho_1, \rho_2, G_2)$ represents the contribution to the system noise temperature of source T_A modified by the system parameters ρ_1, ρ_2 and G_2 at the input terminals of the parametric amplifier shown to the right of reference plane II in Fig. 4.18 or

$$f_1(T_A; \rho_1, \rho_2, G_2) = T_A(1-|\rho_1|^2)\,(1-|\rho_2|^2)\, g_2 \quad . \tag{4.59}$$

The function f_2 is the contribution of the source T_o (ohmic losses) modified by the system parameters ρ_1, ρ_2 and G_2 to the right of plane II or

$$f_2(T_o;\rho_1,\rho_2,G_2,G_3) = \{(1-g_2)T_o\}\{1-|\rho_2|^2\} + \{(1-g_2)T_o\}\{1-|\rho_2|^2\}.|\rho_1|^2.g_2 , \tag{4.60}$$

suggesting that a noise power flow is available at the reference planes I and II caused by T_o and equal to $(1-g_2)T_o$.

The noise source T_{PA} contributes according to

$$f_3(T_{PA};\rho_1,\rho_2,G_2) = T_{PA}.|\rho_1|^2.\ g_2^2\ \{1-|\rho_2|^2\}^2 . \tag{4.61}$$

This contribution is essential as the feed is not matched ideally to the duplexer.

Finally, function $f_4(T_o+T_{track};\rho_1,\rho_2,G_2,G_3)$ is equal to

$$f_4=(T_o/g_3+T_{track})\ .\ g_2(1-|\rho_2|^2)+(T_o/g_3+T_{track}).|\rho_1|^2.g_2(1-|\rho_2|^2)$$

or

$$f_4 = (T_o/g_3+T_{track})\ .\ g_2(1-|\rho_2|^2)\ (1+|\rho_1|^2) , \tag{4.62}$$

being the contributions from cross coupling and tracking, suggesting that these components are located immediately behind the feed.

The total system temperature T_s expressed in the noise sources and parameters discussed is, therefore, neglecting multiple reflections and correlation of noise

$$\begin{aligned} T_s = {} & T_A(1-|\rho_1|^2)(1-|\rho_2|^2)g_2 + \\ & + (1-g_2).T_o.(1-|\rho_2|^2)(1+|\rho_1|^2g_2)+T_{PA}|\rho_1|^2.g_2^2(1-|\rho_2|^2)^2 + \\ & + T_{PA} + T_{TD}/g_{PA} + T_{TWT}/(g_{PA}\cdot g_{TD}) + \\ & + (T_o/g_3 + T_{track})(1-|\rho_2|^2)(1+|\rho_1|^2)\ g_2. \end{aligned} \tag{4.63}$$

The table below shows a worked out example where

$|\rho_1|^2 = 0.99$ [V.S.W.R. = 1.2]

$|\rho_2|^2 = 0.96$ [V.S.W.R. = 1.5]

$T_{track} = 0.7^\circ$ K; $T_o = 290^\circ$ K; $T_{PA} = 16^\circ$ K; $T_{TD} = 627^\circ$ K(5 dB), $T_{TWT} = 1164^\circ$ K(7 dB), G_1 = (neglected), G_2 = 0,2 dB; G_{PA} = 25 dB; G_{TWT} = 35 dB; G_3 = - 23 dB; G_{TD} = 15 dB.

Table:

Characteristics	decrease of eff.		Increase of noise temp. $^\circ$K
	dB	η	
1. Noise temp. paramp. + receiver $T_{PA}+T_{TD}/g_{PA}+T_{TWT}/(g_{PA}-g_{TD})=16+2.1^\circ$K	-	-	18.1
2. Reflection loss paramp. (V.S.W.R.=1.5) Paramp.noise by reflection of feed(f_3)	0.15	0.960	0.14
3. Ohmic losses 0.2 dB (f_2)	0.20	0.955	12.65
4. Losses by mode conversion	-	-	-
5. Noise by cross coupler (23dB) and tracking system (f_4)	0.01	0.995 0.998	2.16
6. Ellipticity losses	0.056	0.987	-
	Totals		33.05°K

4.7. Conclusion

(1) It is possible to determine an analytical expression for the noise temperature of the environment $T(\theta,\varphi)$. This expression can be investigated in practice by an antenna concentrating all its radiated power in an infinite simal solid angle $d\Omega$.

(2) Knowing $T(\theta,\varphi)$ analytically, it is fairly siple to calculate the noise temperature of an antenna with a radiation pattern $G(\theta,\varphi)$. The calculation of the noise temperature of an isotropic antenna radiating in a hemisphere is very important. The same method can be applied to the calculation of the antenna noise temperature in case the radiation pattern is not known.

(3) It appears to be possible to divide the radiated power into parts, such as spillover, backradiation, diffraction,blocking power, and the power contained within the main lobe. Since antennas obey the reciprocity theorem it is possible, the noise in case the antenna is used for reception purposes, to calculate from the power flow within the antenna system used for transmitting purposes.

(4) Detailed information is given about the influence of imperfections of various components on the noise temperature such as reflection losses, ohmic losses, surface inaccuracies, etc.

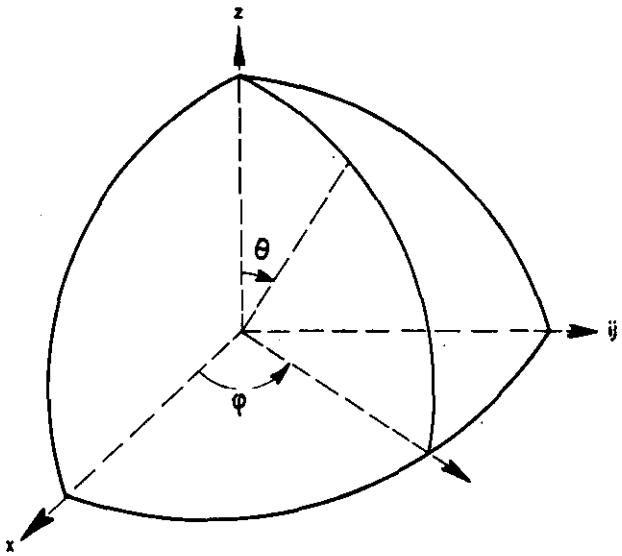

Fig. 4.1. Spherical coordinates.

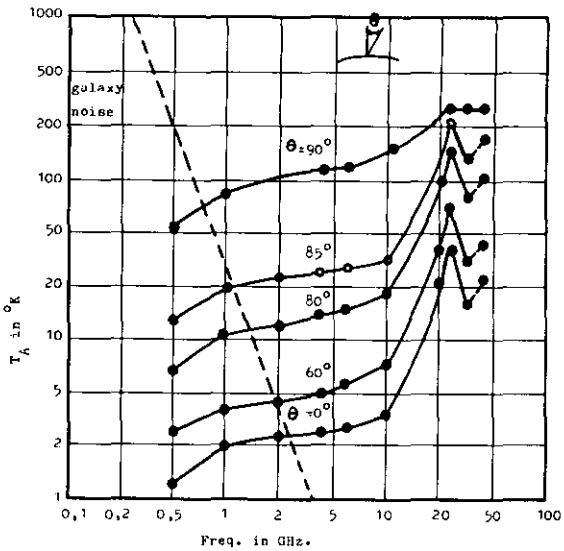

Fig.4.2. Antenna noise temperature by galaxy and atmosphere (lit. 30).

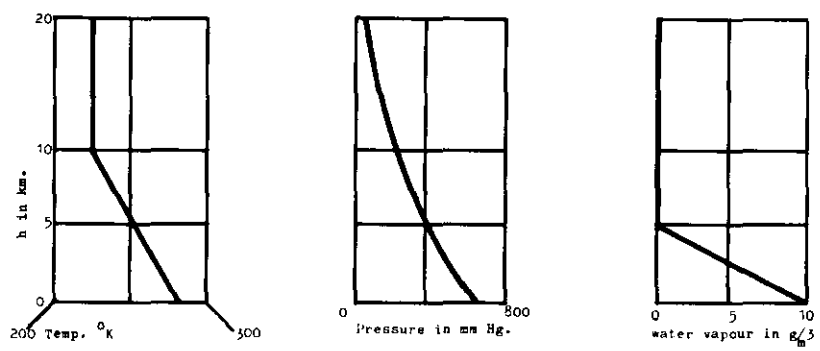

Fig. 4.3. Parameters of standard atmosphere.

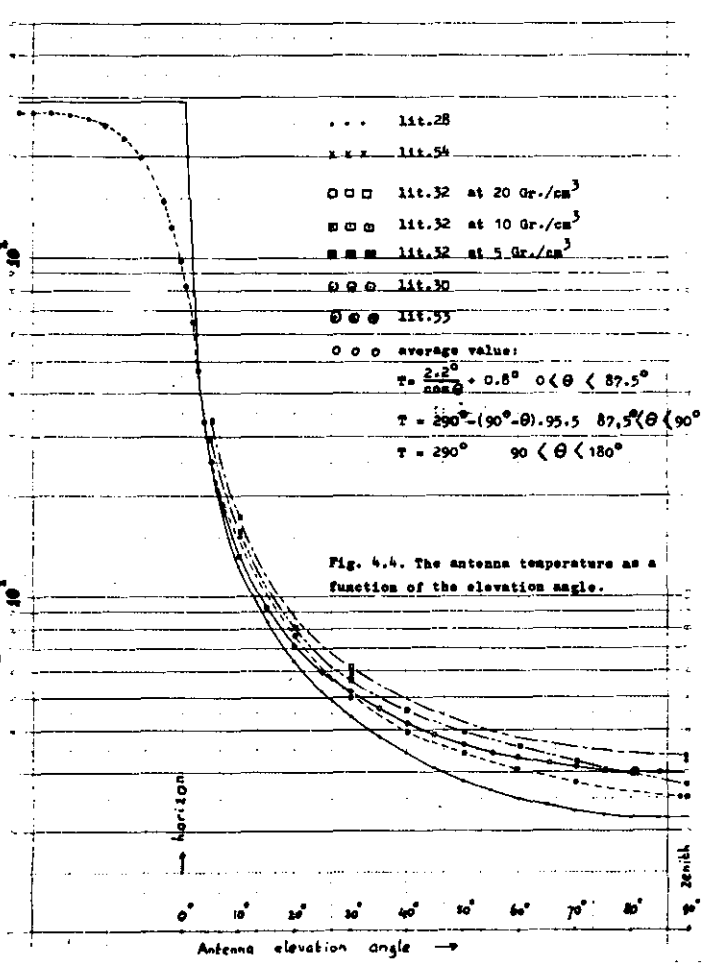

Fig. 4.4. The antenna temperature as a function of the elevation angle.

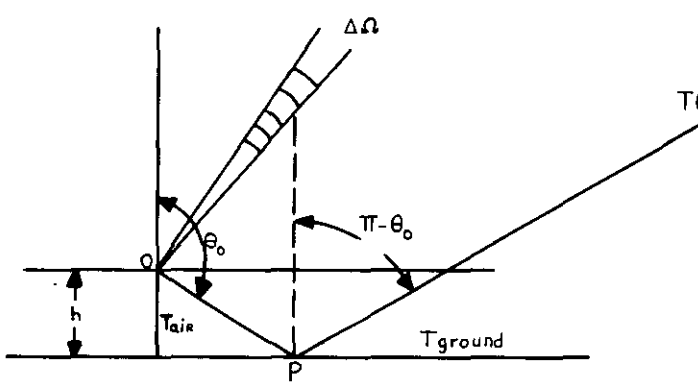

Fig. 4.5. The antenna located above reflecting surface.

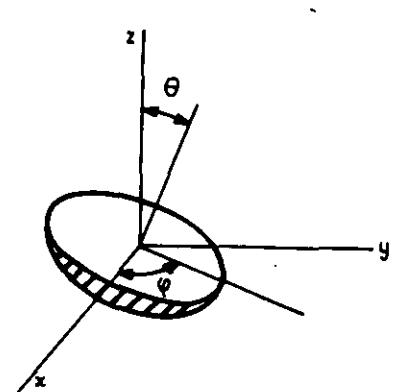

Fig. 4.6. Aperture radiating in one hemisphere in direction (θ,φ).

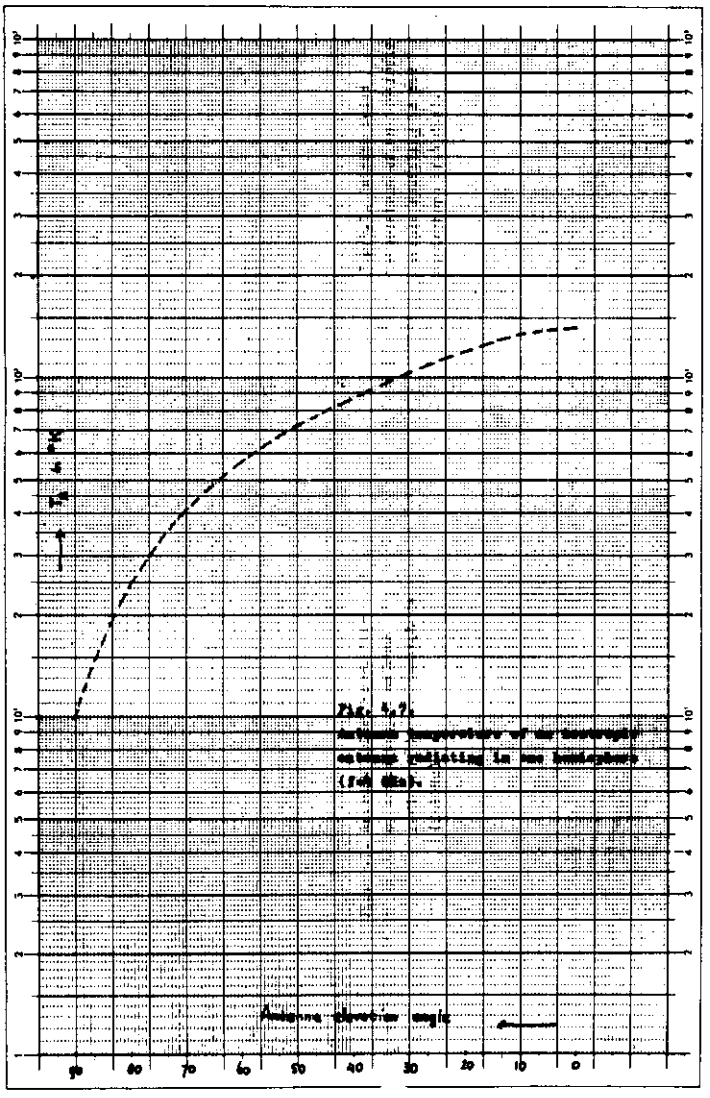

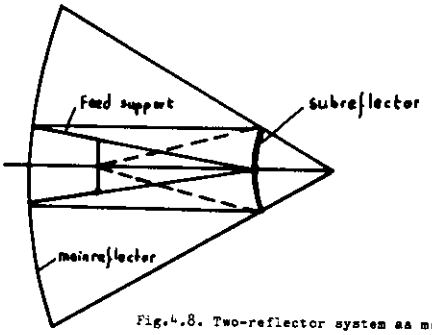

Fig.4.8. Two-reflector system as model for antenna noise temperature calculations.

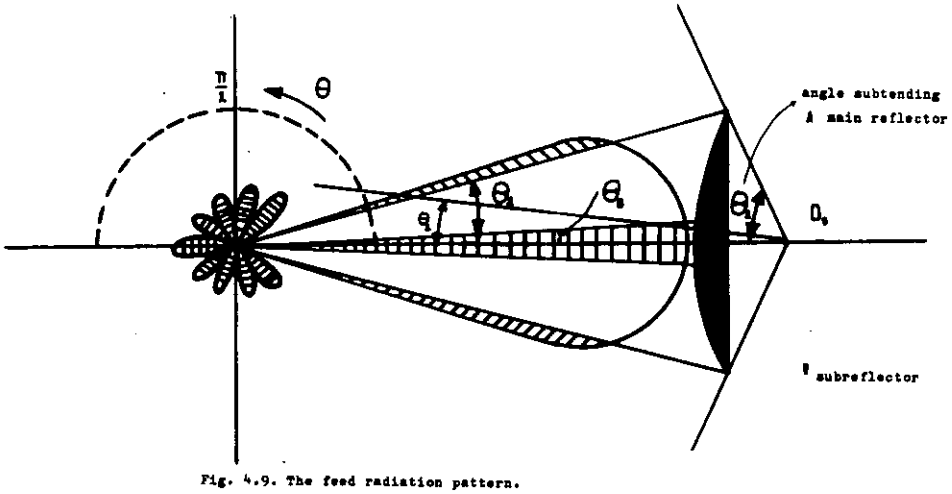

Fig. 4.9. The feed radiation pattern.

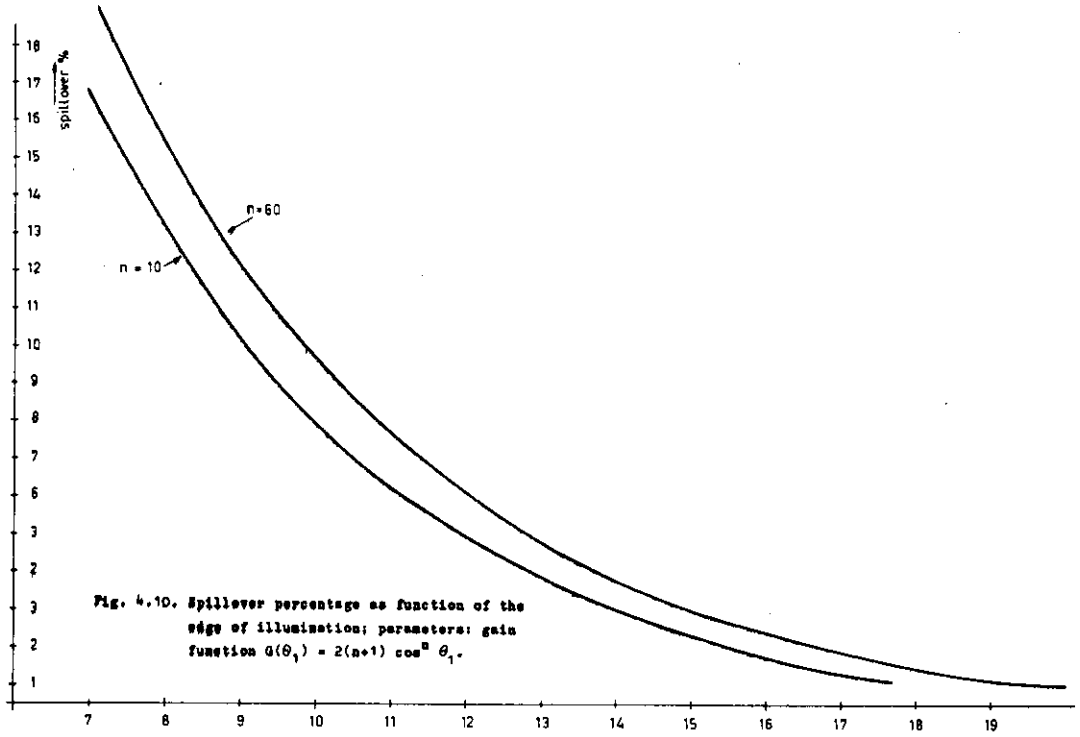

Fig. 4.10. Spillover percentage as function of the edge of illumination; parameters: gain function $G(\theta_1) = 2(n+1)\cos^n \theta_1$.

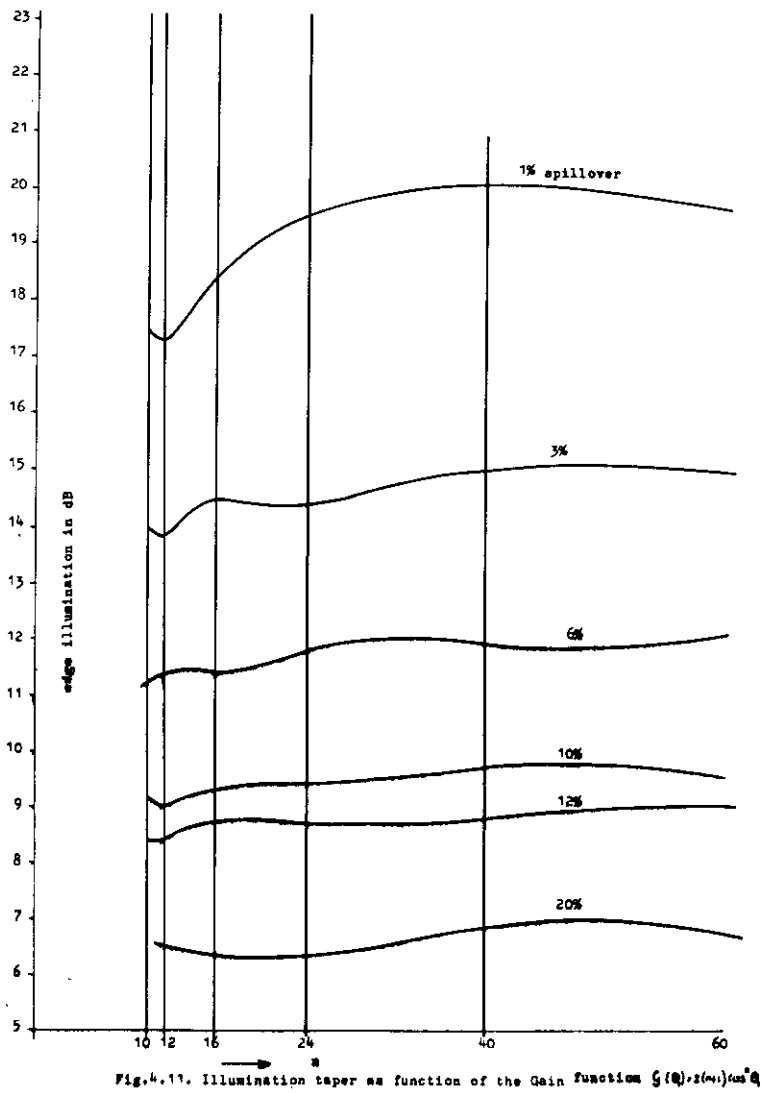

Fig.4.11. Illumination taper as function of the Gain function $G(\theta) = 2(n+1)\cos^n\theta$

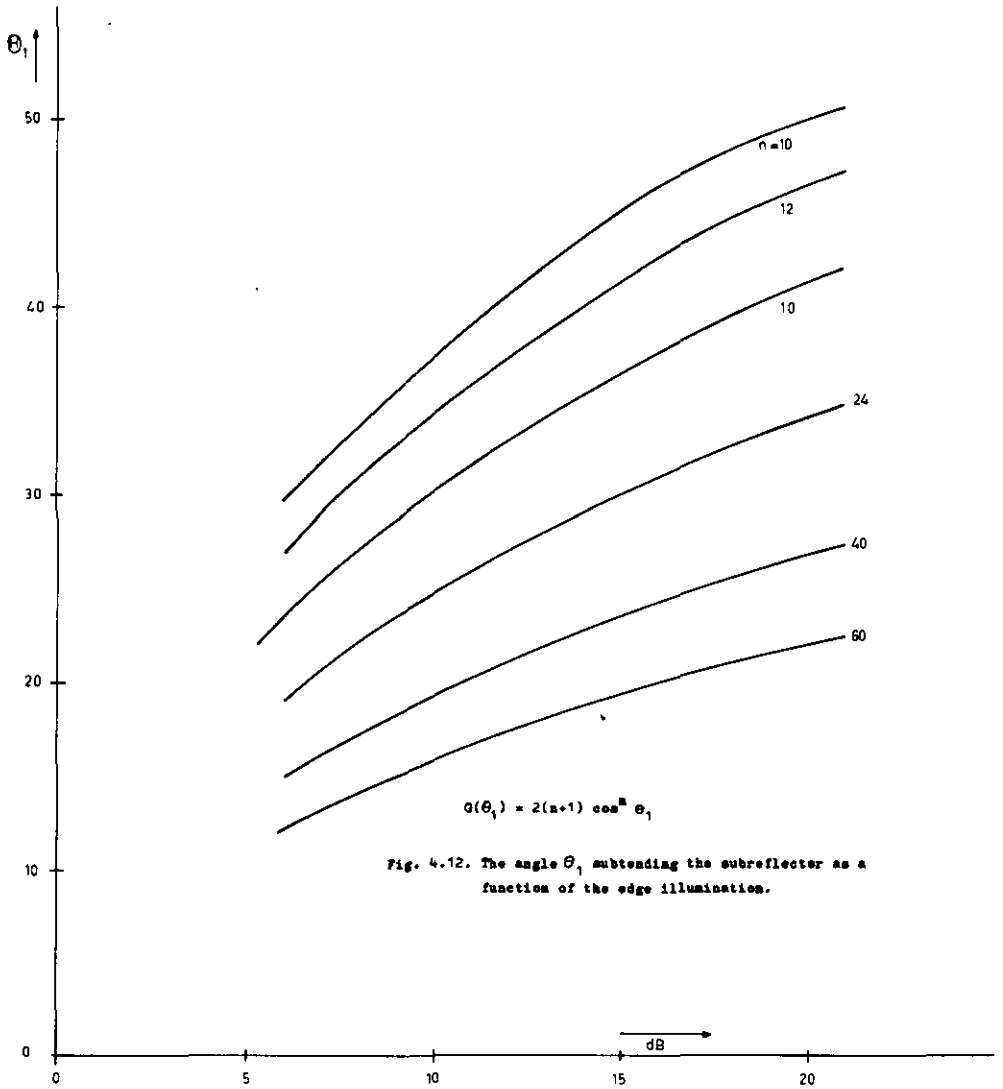

Fig. 4.12. The angle θ_1 subtending the subreflector as a function of the edge illumination.

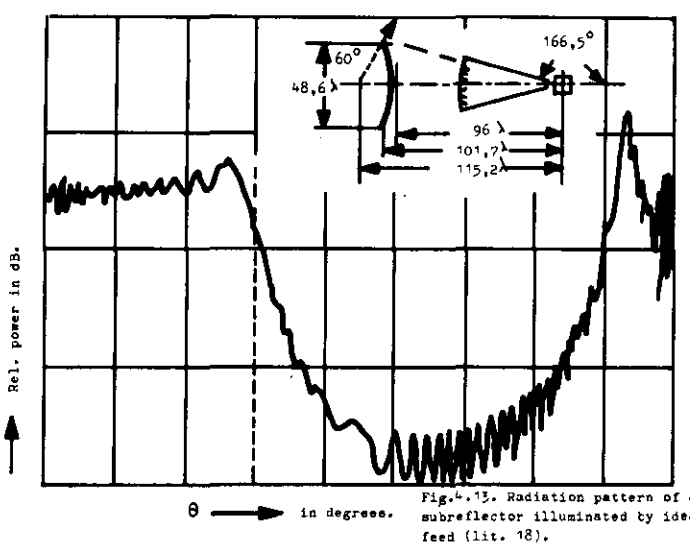

Fig.4.13. Radiation pattern of a subreflector illuminated by ideal feed (lit. 18).

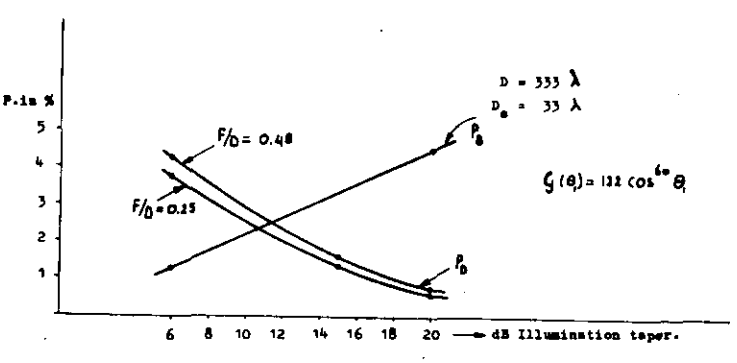

Fig.4.14. Power lost by blocking and diffraction as function of the illumination taper.

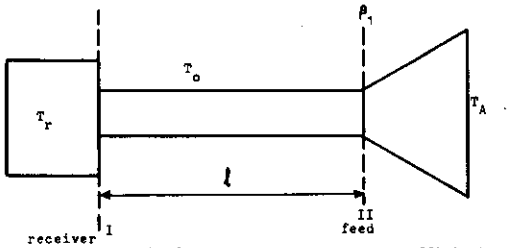

Fig. 4.16. The feed's reflection coefficient and the antenna temperature.

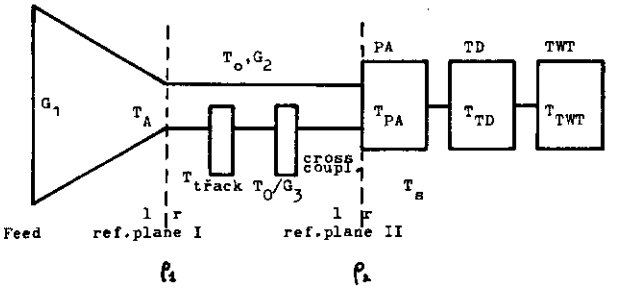

Fig. 4.18. The antenna feed and components for satellite communications.

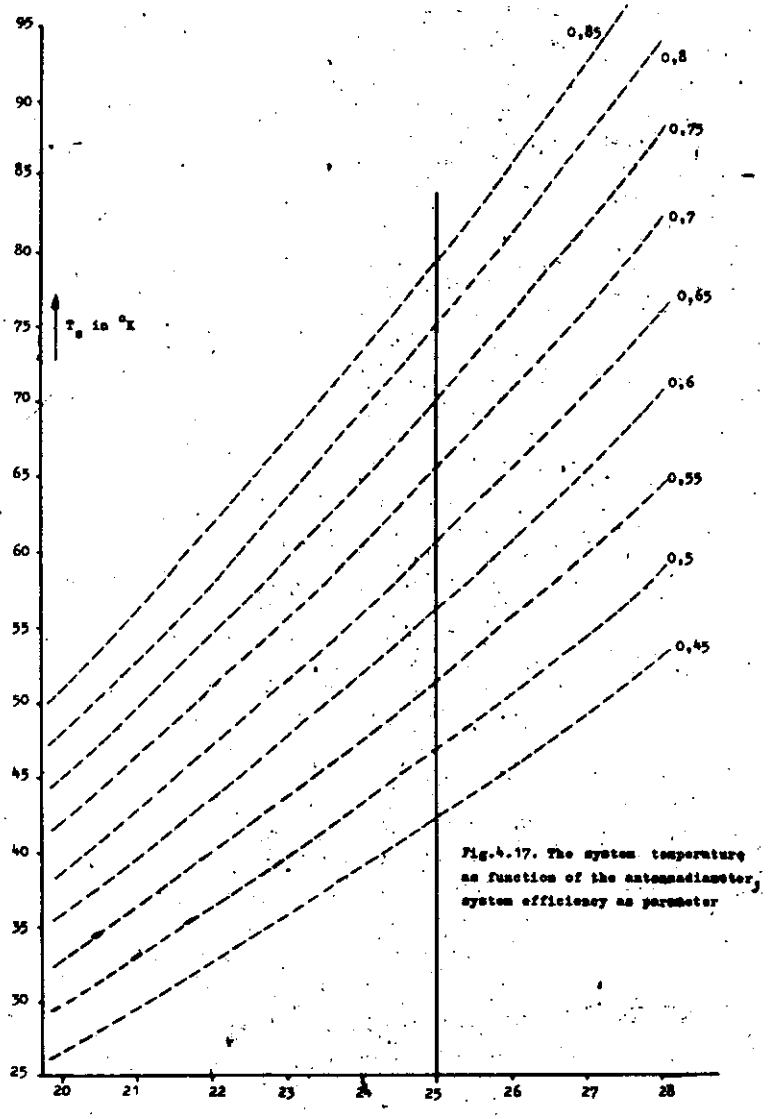

Fig.4.17. The system temperature as function of the antennadiameter, system efficiency as parameter

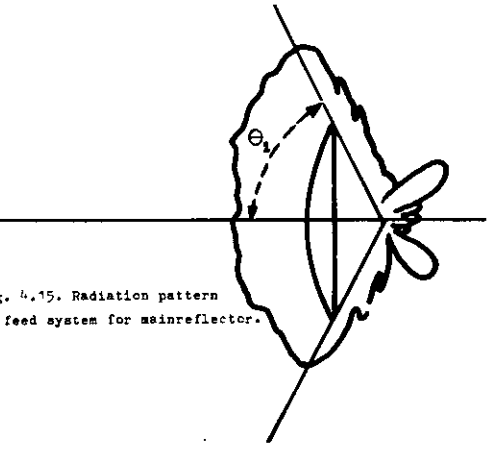

Fig. 4.15. Radiation pattern of feed system for mainreflector.

5.The feed

5.1. Feed requirements

In classical cassegrain systems it is always assumed that the subreflector is illuminated by a point source. The equiphase planes of such a point source are spherical. It is shown in Fig. 5.1.1.

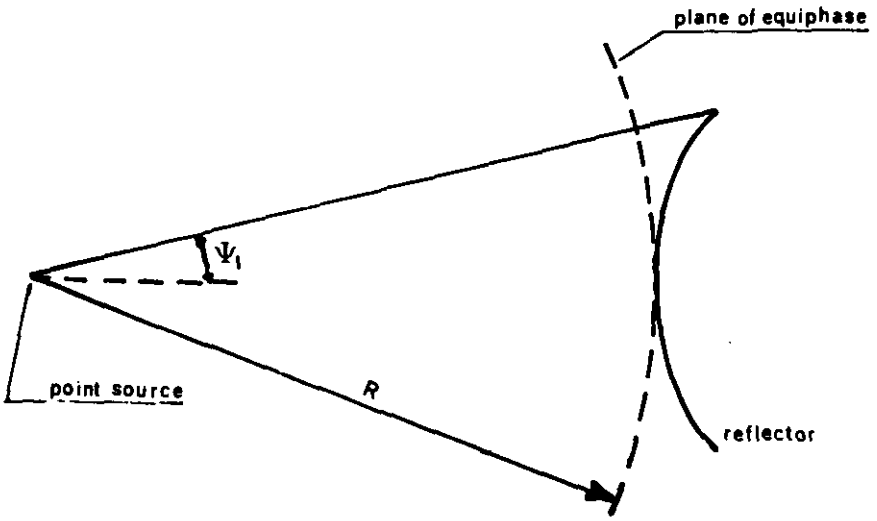

Fig. 5.1.1.

that spherical wavefronts propagate towards the subreflector. Point sources cannot be applied in actual practice since mostly horn antennas are available only. At large distances from the feed, in the far zone, the equiphase planes are spherical, which makes the horn antenna very suitable as a feed system for the subreflector. The far zone is found at distances $R \gg \frac{2d^2}{\lambda}$, where d is the aperture diameter of the feed. The centre of curvature of the equiphase planes in the far field is called the phase centre. This point is found somewhere within the horn feed. The subreflector will be better illuminated if the pattern of the feed is circularly symmetrical.

In classical systems it is advisable to illuminate the centre of the subreflector as uniformly as possible to increase the antenna efficiency. The illumination of the edge should be low so as to decrease spillover and diffraction losses. The pattern of the feed in this case should be in accordance with Fig. 5.1.2.

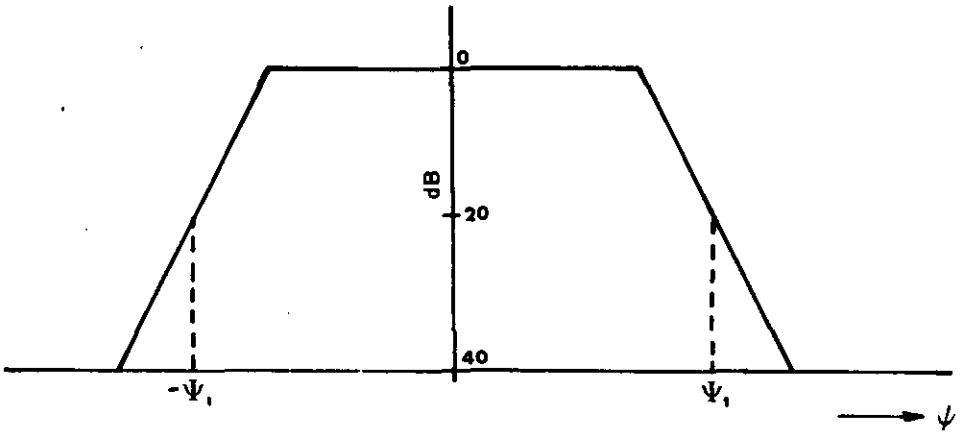

Fig. 5.1.2.

Losses by spillover and diffraction should be limited as much as possible as otherwise the antenna noise temperature will be to high.

The feed has to be used in the frequency bands of 3,700-4,200 MHz and 5,900-6,400 MHz. It will be shown further in this paper that these bandwidths are obtainable by a horn feed with $d \approx 6\lambda$ (Sec. 5.4). To fulfil the far zone requirements it will be clear that the distance R from the phase centre of the feed to the subreflector should be now

$R \gg \frac{2d^2}{\lambda}$, where λ = 8.1 cm, therefore, $R \gg$ 5.83 metres.

Therefore, the distance between feed and subreflector will be fairly large. This large distance has some advantages:

(1) The cone on which the feed is mounted can be made small.

(2) The first stage of the low-noise pre-amplifier can be fitted within te cone. The amplifier can then easily be reached in case of service or repair.

(3) Extra blocking of the feed can now be avoided in accordance with the relation $\frac{D_S}{F} > \frac{d}{f}$; see also Fig. 5.1.3.

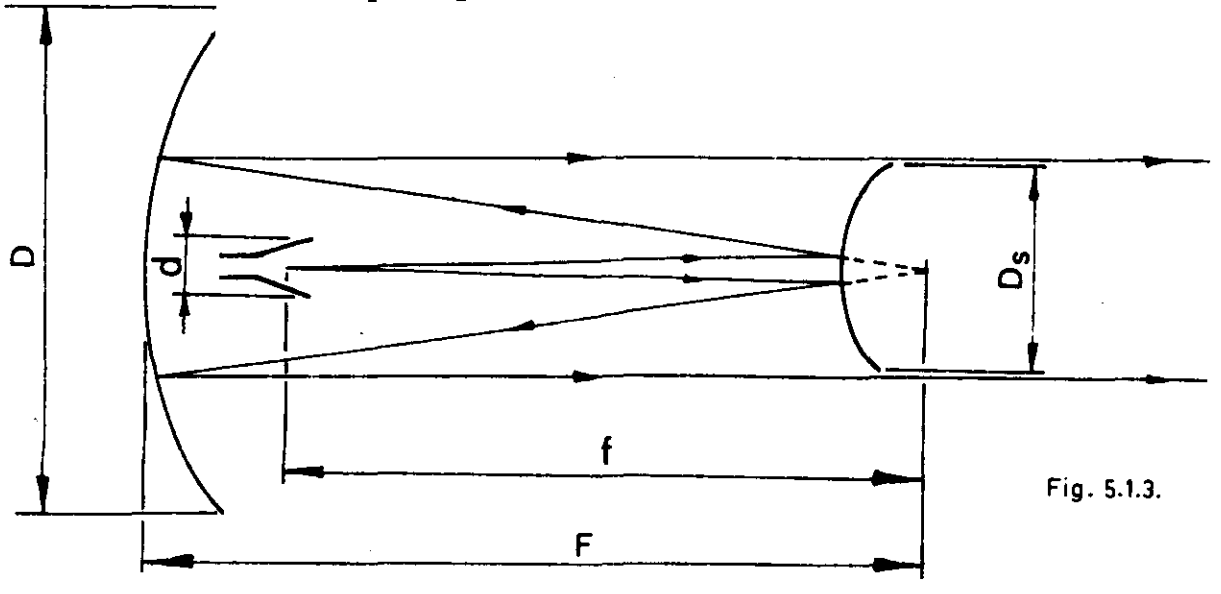

Fig. 5.1.3.

The requirements for the main beam of the feed pattern and the distance phase centre to subreflector hold for the whole frequency band.

A classical cassegrain system is shown in Fig. 5.1.4.

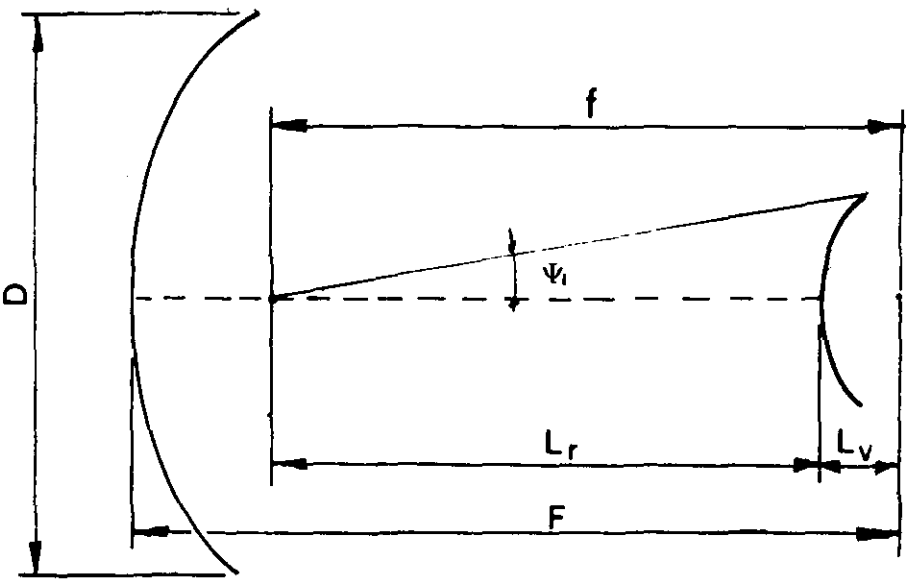

Fig. 5.1.4.

If we assume the following geometry - F/D = 0.33, D = 25 m., D_s = 2.5 m., $\Psi_1 = 15^\circ$, we find that L_r = 4.17 m., L_v = 0.85 m., and the hyperboloid eccentricity e = 1.425.

It is easily seen that the subreflector is not located in the far zone of the feed. However, it is evident that the phase errors will still be very small and tolerable. Also, a choice of $\Psi_1 = 15^\circ$ will lead to an acceptable geometry. In a final design the true angle Ψ_1 may deviate a few degrees from 15°. This difference is easily compensated by a subreflector with a different eccentricity.

Summarising the feed should meet the following requirements:

(a) The feed should have a main beam corresponding to Fig. 5.1.2., although this requirement does not hold for shaped reflector systems (chapter 7).

(b) The energy of that part of the main beam intercepted by the subreflector should be at least 98% of the total power radiated by the feed.

(c) The feed should be suitable to receive and transmit circularly polarised waves.

(d) The mean beam of the feed pattern should be equal in E and H plane (Fig. 5.2).

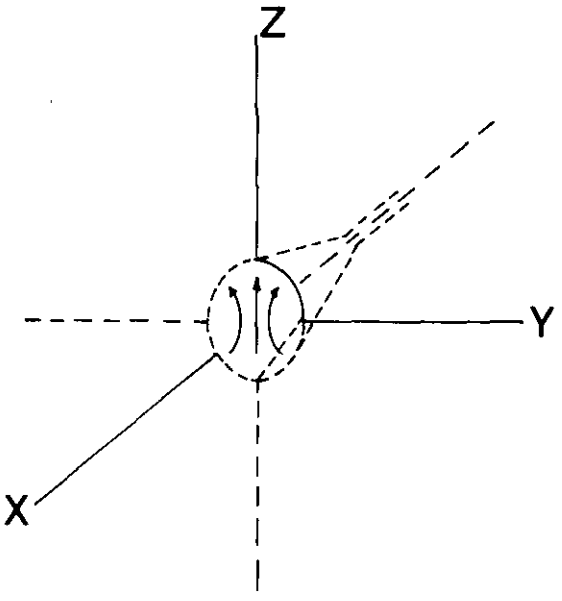

xy plane – H plane

xz plane – E plane

Fig. 5.2.

(e) The phase centres of E and H plane patterns should be the same point.

(f) The cross polarisation energy should be smaller than 1% of the total power radiated by the feed.

(g) The feed must be used for the frequency bands 3,700-4,200 MHz and 5,900-6,400 MHz; the phase centre and beam shape should be independent of the frequency within the frequency bands.

(h) The feed should be well matched: VSWR $\lesssim$ 1.2 over the frequency bands mentioned under (g).

5.2. Short survey of the properties of a conical horn antenna

The feed should receive and transmit circularly polarised radiation. This can be realised in the simplest way by a conical horn antenna. Using a horn already available some measurements were carried at the frequencies 7.6 GHz and 11.4 GHz. The choice of these frequencies is motivated in Sec. 5.4. The dimensions of this feed are found in Fig. 5.3.

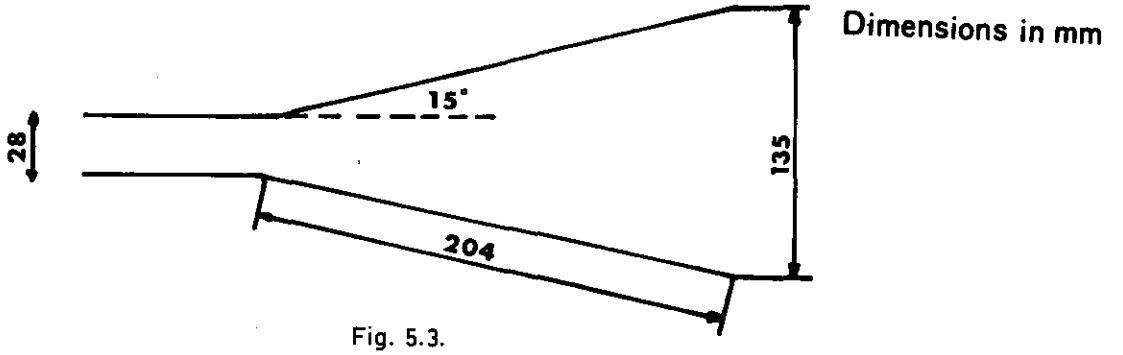

Fig. 5.3.

The choice of the diameter of the diameter of the waveguide coupled to the horn antenna should be such that apart from the TE_{11} mode the TM_{01} mode can propagate as well. In that case the TM_{01} mode can be used for tracking purposes. The measured patterns are found in the Figs. 5.4 to 5.7. From these figures we may conclude that

(1) the radiation pattern in the E plane does not correspond with the radiation pattern of Fig. 5.1.2.
(2) the beamwidth depends on the frequency. The same conclusions may be drawn from other horn antennas. Therefore, these kind of horn antennas cannot be used as primary feeds.

5.3. Possibilities of realising the requirements

5.3.1. Multimode horn antennas

The radiation pattern of a conical horn can be improved by applying two modes. Somewhere in the feed the TM_{11} mode is generated, apart from the TE_{11} mode (Fig. 5.8).

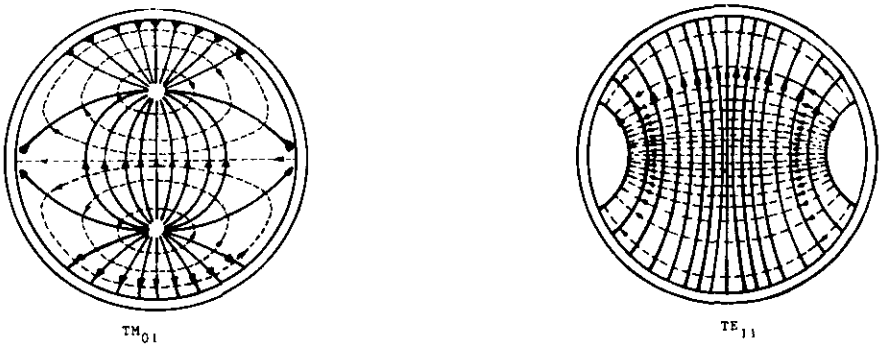

Fig. 5.8.

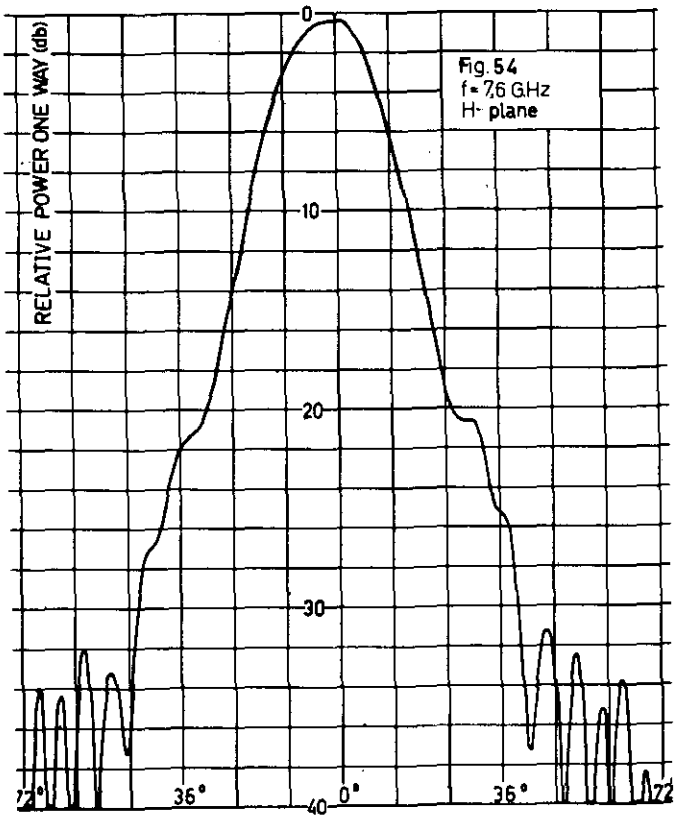

Fig. 5.4
f = 7,6 GHz
H- plane

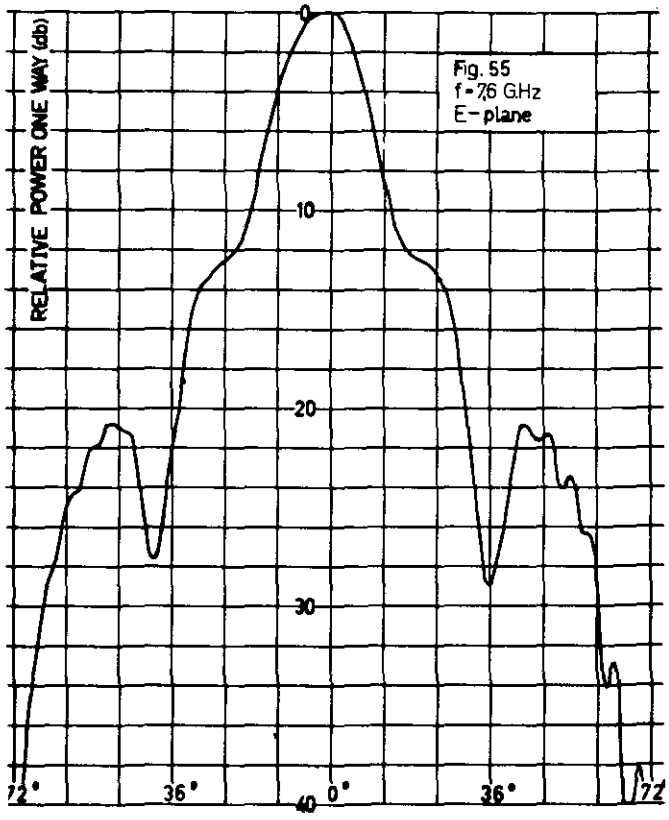

Fig. 5.5
f = 7,6 GHz
E-plane

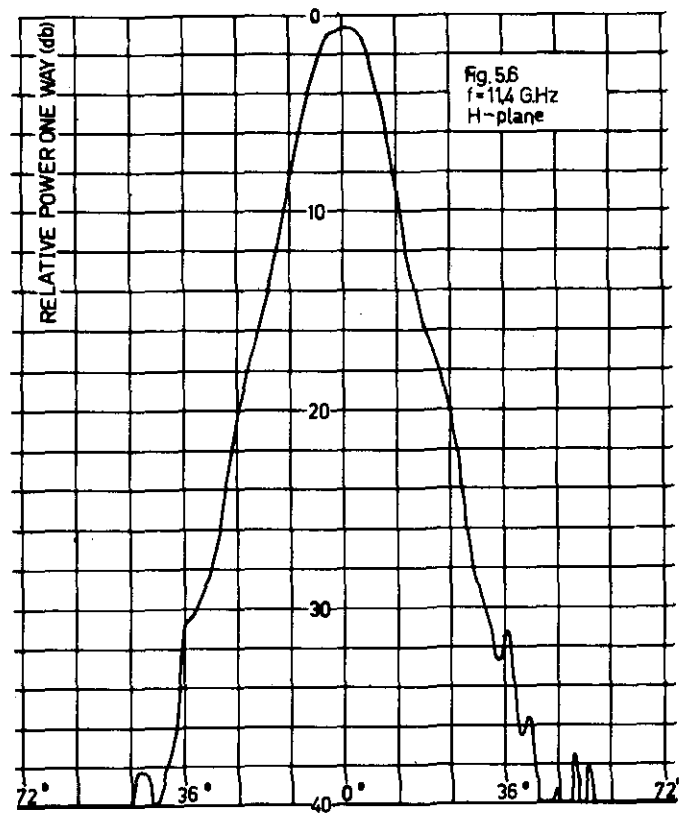

Fig. 5.6
f = 11,4 GHz
H-plane

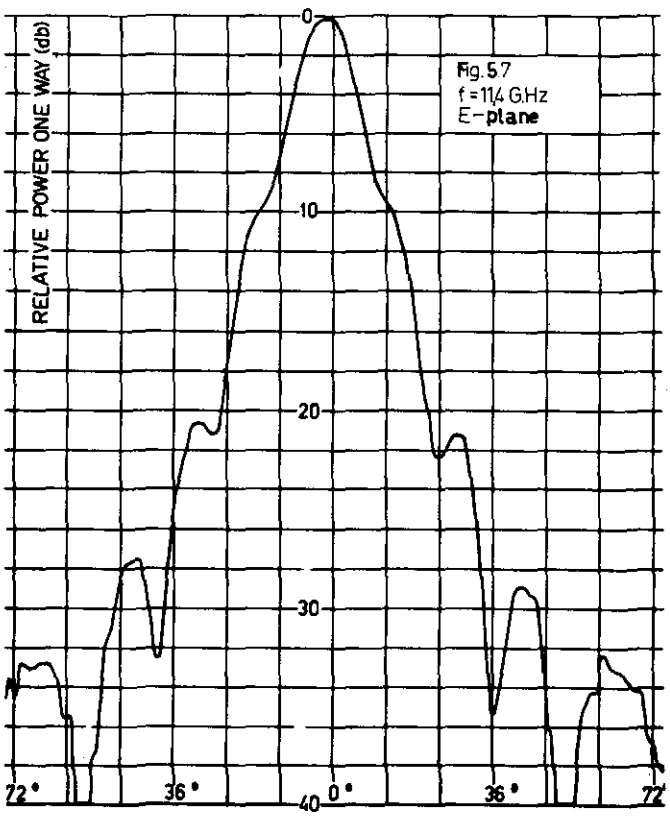

Fig. 5.7
f = 11,4 GHz
E-plane

The improvements can be obtained by seeing to it that the two modes have the correct amplitude and phase relations. The two modes in waveguide 3 (and also in the horn antenna) have different phase velocities.

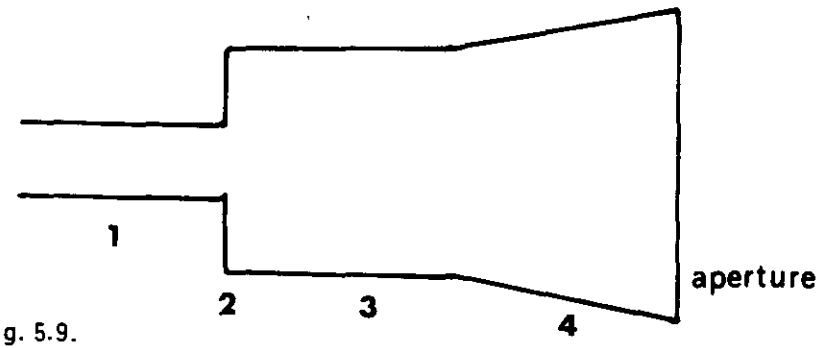

Fig. 5.9.

1: circular waveguide for TE_{11} mode.
2: transition.
3: circular waveguide for TE_{11} and TM_{11} mode.
4: conical horn.

Therefore, the bandwidth of such a system is only 5%, and does not meet the requirements.

Foldes (lit. 49) has found another solution for this problem by using a multimode-multihorn system. Using special broadband components, the system can be made suitable for a feed in an antenna for satellite communication. The feed system has been developed by the "hit and miss" method, and is very complicated. The present knowledge of feeds, however, offers the possibility of a simpler solution (Sec. 5.3.2.).

5.3.2. Modified conical horn antenna

If the field distribution in the aperture of a conical horn antenna is similar in the X-Z plane and the X-Y plane it may be expected that the beamwidth in H- and E-plane will be equal. Moreover, the phase centre for the E- and H-plane will be the same. Applying the TE_{11} mode and TM_{11} mode (or other modes) such a field distribution in the aperture can be realised.

This goal can also be reached by modifying the inside of the horn antenna in such a way that other boundary conditions than the usual ones, have to be introduced (corrigated surface). Moreover, the black radiation can be kept low. Such a horn antenna will henceforth be called the modified conical horn antenna. An objection still exists as for the present moment the radiation pattern cannot be found by calculation.

The bandwidth problem can be solved by a correct choice of the antenna geometry (Fig. 5.10). An experimental investigation has proved that a conical horn antenna, in which $\Delta > \frac{1}{4}\lambda$, possesses a beamwidth almost independent of the frequency over a frequency band of 1:1.7.. This means that the aperture will be no equiphase plane. Combining the two principles above mentioned it appears possible to design a feed which meets the requirements of Sec. 5.1. If such a feed cannot be designed by calculation, all the necessary information has to be collected by experiments on models. A great number of measurements have been carried out to see whether the principles mentioned can be utilised. To decrease cost all measurements have been carried out with small-scale models. A survey of the results is found in Sed. 5.4.

5.4. Modified conical horn antenna measurements

An antenna for satellite communication with stationary satellites must be suitable for the frequency bands of 3.7 - 4.2 GHz and 5.9 - 6.4 GHz. To keep the model dimensions within reasonable limits the measurements have been carried out in the X-band. The table below shows the frequencies in the above mentioned S-band and the corresponding frequency in the X-band.

receiving		transmitting	
S band	X band	S band	X band
3.7	7.0	5.9	11.16
3.8	7.19	6.0	11.35
3.9	7.38	6.1	11.54
4.0	7.56	6.2	11.73
4.1	7,75	6.3	11.92
4.2	7.94	6.4	12.10

Various models have been investigated. Every model has been given a distinguishing letter. The results obtained with some models will now be discussed. The models A and B already proved useless at the beginning of the research. The bandwidth theory was tested on model B (Fig. 5.11). The 10 dB points of the main beam are represented as a function of the frequency in Fig. 5.12. It appears that the beamwidth in the H-plane is more or less independent of the frequency. The beamwidth in the E-plane, however, depends strongly on the frequency. Model A and B have similar dimensions. However, special boundary conditions have been introduced. The 10 dB points of the main beam as a function of the frequency are found in Fig. 5.13. The main conclusion which can be drawn is that the 10 dB points of the E and H plane are less far separated. Moreover. some frequency independence can be observed. However, the beamwidth is still too large.

The next step is an attempt to reduce the beamwidth. Model E was constructed for this purpose, with special boundary conditions and the following dimensions: a = 28 mm, l = 67mm, d = 113 mm, $\theta_o = 40^o$. The results are collected in Fig. 5.14. The frequency dependence is like that of model A. The beamwidth of the 10 dB points, however, appeared to be smaller. Further reduction of the beamwidth was realised with model F, also containing special boundary conditions, and the following dimensions: a = 28 mm, l==150 mm, d = 105 mm, $\theta_o = 15^o$. The results of model F in Fig. 5.15 show a 10 dB beamwidth which is equal in its E- and H-planes. There is, however, a strong dependence of the frequency. The dimensions of the conical horn antenna discussed in Sec. 5.2 are nearly the same as the demensions of model F, measured at two frequencies both in E- and H-plane. Comparison with Figs. 5.4 to 5.7 shows not only that the 10 dB points in the E- and H-planes are equal but also that the main beam in the E- and H-planes are of the same shape.

Beyond the region -72^o to $+ 72^o$ the radiation is at least 40 dB lower than the radiation in the main direction. This is not so when using the common conical horn antenna of Sec. 5.2.

The following attempt concerned the design of an antenna with a 10 dB beamwidth of about 30^o and independent of the frequency (conventional

boundary conditions). The aperture diameter is 6 λ for the lowest frequency and 10 λ for the highest. Some results can be found in Fig. 5.16; moreover, Figs. 5.17 to 5.20 illustrate some radiation patterns. The results are very promising. If special boundary conditions are introduced, it is expected that the E-plane pattern can be further improved.

An important question is where the far zone of model H begins. Starting from the relation $R \gg \frac{2d^2}{\lambda}$ the table below can be calculated

frequency	d	R
3.7 GHz	6 λ	72 λ = 5.83 metres
6.4 GHz	10 λ	100 λ = 4.68 metres

It may be further expected that it is possible to design a conical horn antenna combining the desired properties of models F and H and which is very suitable as a feed in an antenna for satellite communication. Discussing the properties of various models, so far attention has only been paid to the similarity of the beams in the E- and H-planes and the independence of the frequency. Many other measurements indicate that the other requirements mentioned in Sec. 5.1 can be met as well.

5.5. Conclusions

(1) All present descriptions of feeds used in antennas for satellite communication with stationary satellites are very concise.
(2) Designers of such ground station antennas should design and measure the feeds themselves.
(3) To meet the requirements of Sec. 5.1 a modified conical horn antenna will be applied.
(4) The measurements described in Sec. 5.4 show that such a modified conical horn antenna can meet the requirements of Sec. 5.1.

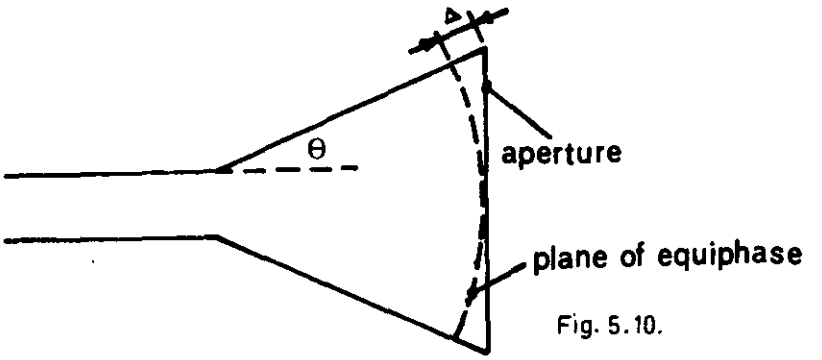

Fig. 5.10.

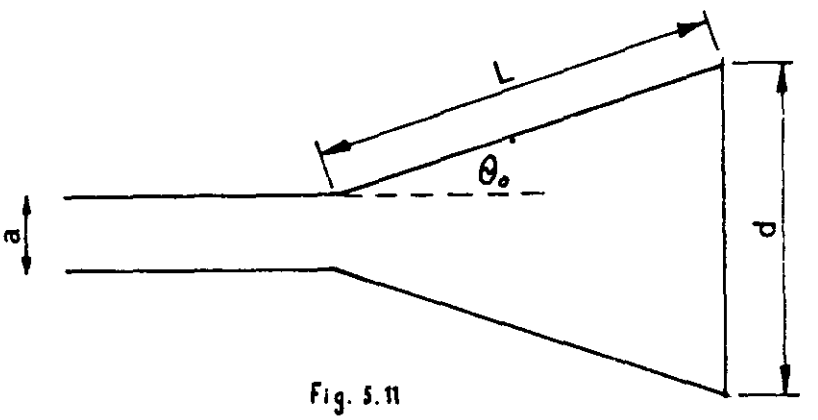

Fig. 5.11

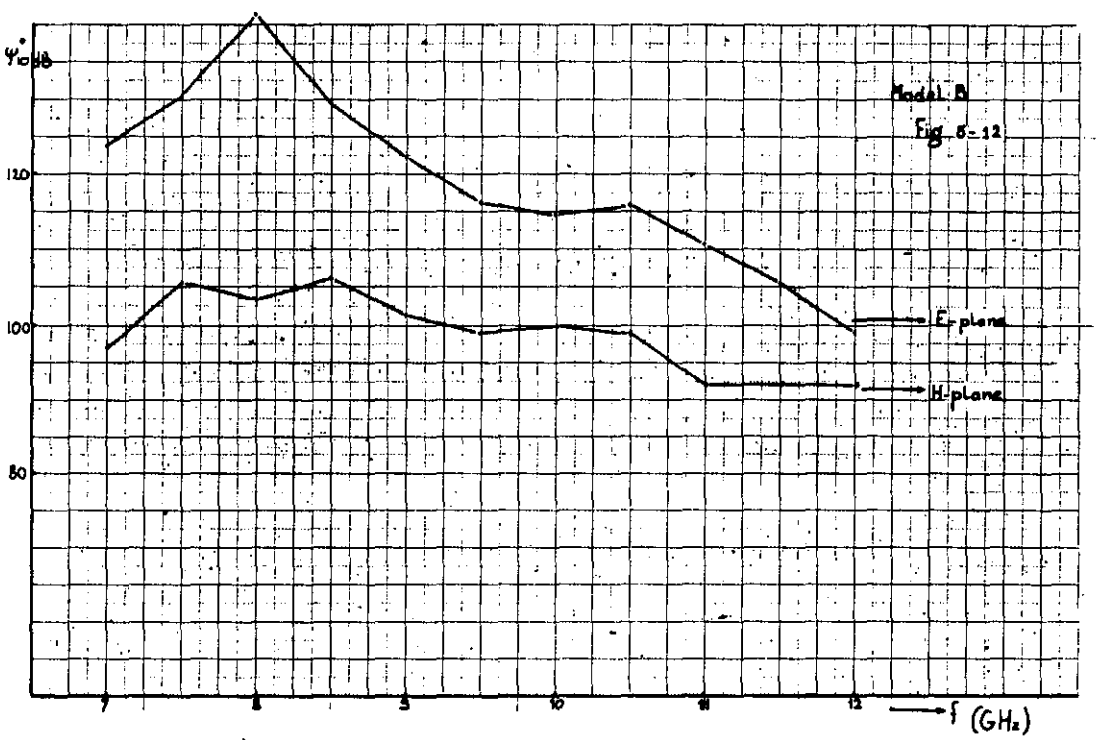

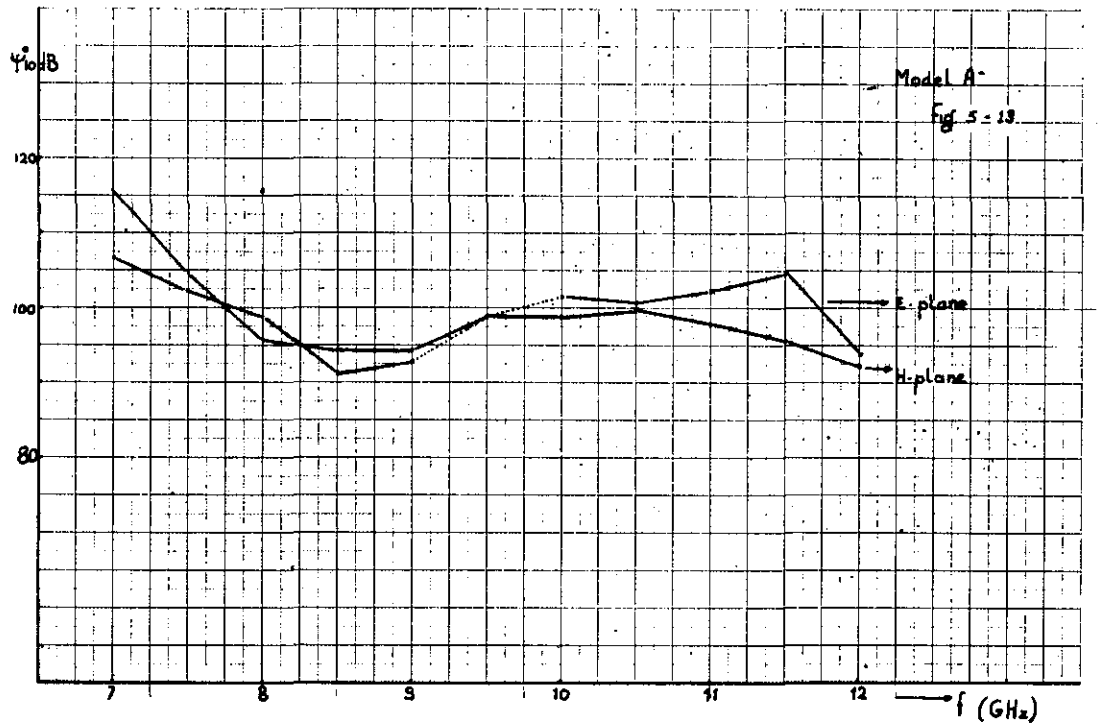
Model A
Fig. 5 - 13
ψ°_{10dB}
120
100
80
E-plane
H-plane
7
8
9
10
11
12
f (GHz)

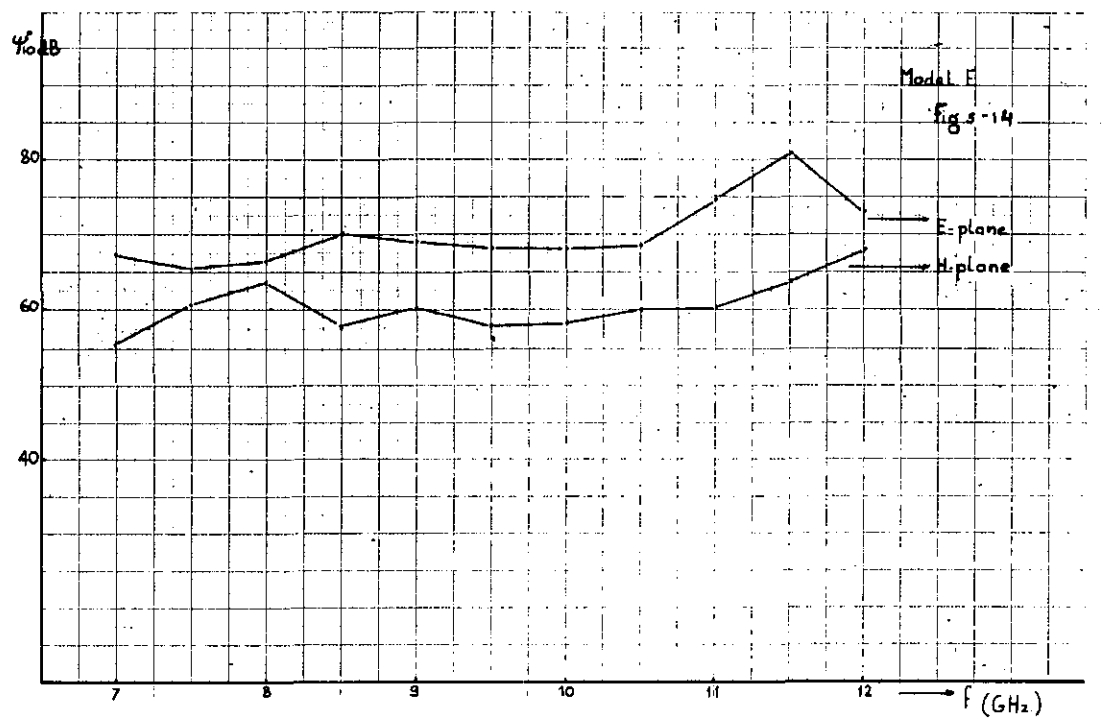
Model E
Fig. 5 - 14
ψ°_{10dB}
80
60
40
E-plane
H-plane
7
8
9
10
11
12
f (GHz)

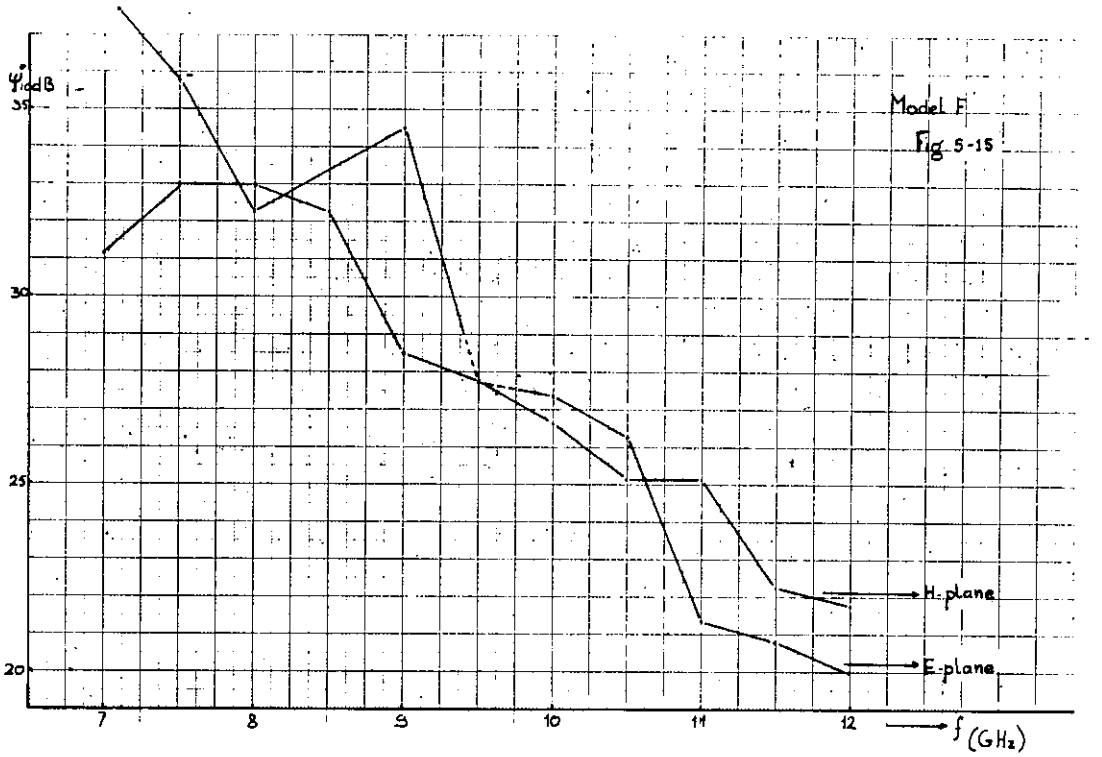
Model F
Fig. 5-15
H-plane
E-plane
35
30
25
20
7
8
9
10
11
12
f (GHz)

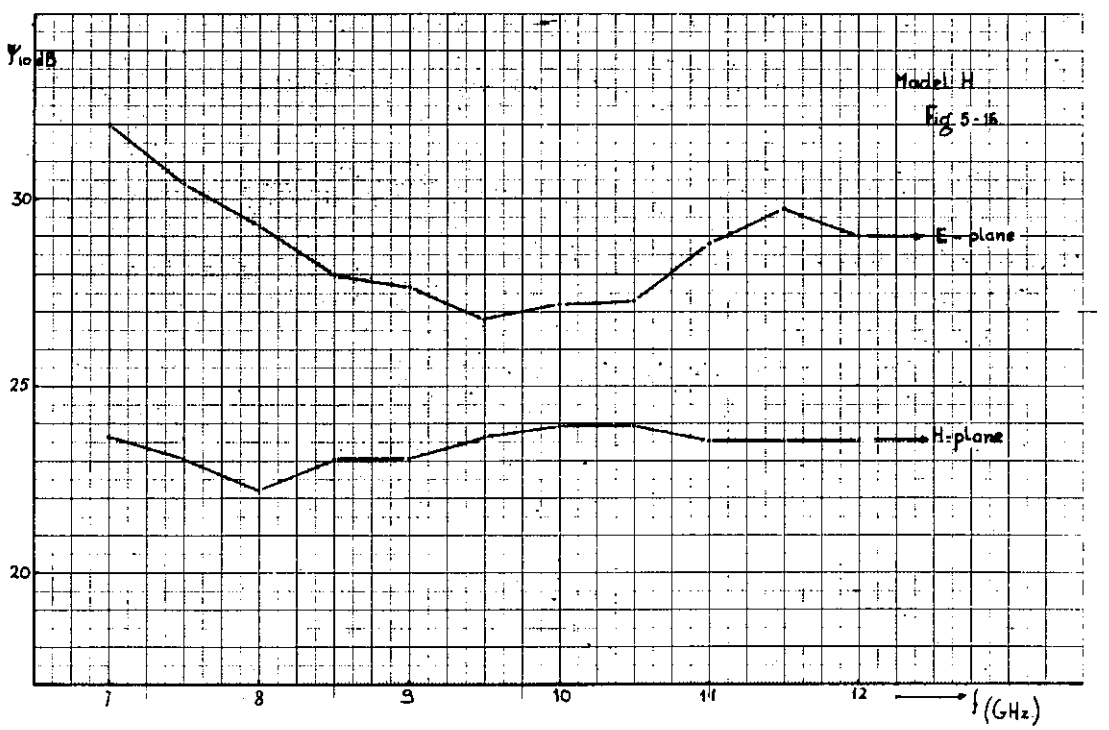
Model H
Fig. 5-16
E-plane
H-plane
30
25
20
7
8
9
10
11
12
f (GHz)

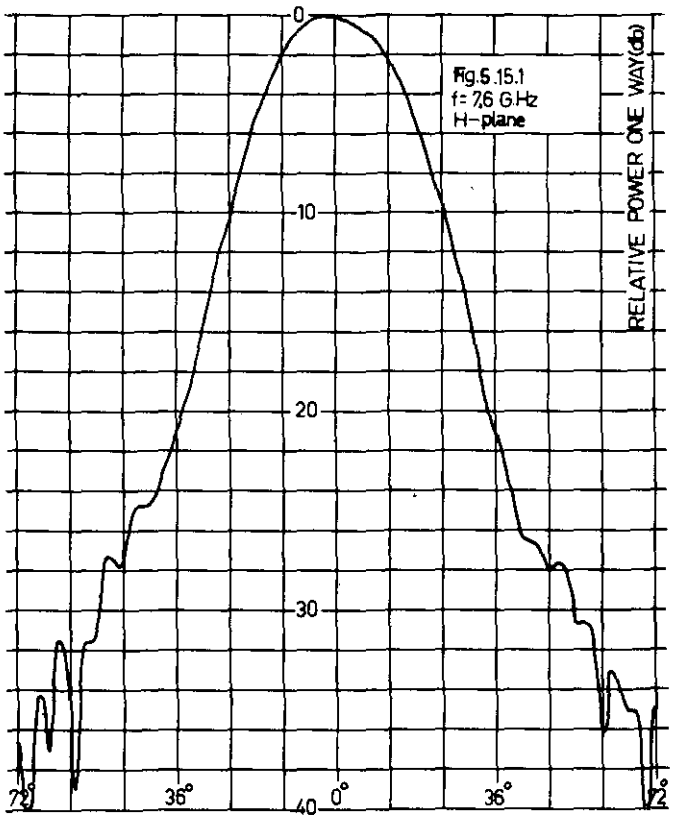
Fig.5.15.1
f= 7,6 GHz
H-plane
RELATIVE POWER ONE WAY(db)
0
10
20
30
40
72°
36°
0°
36°
72°

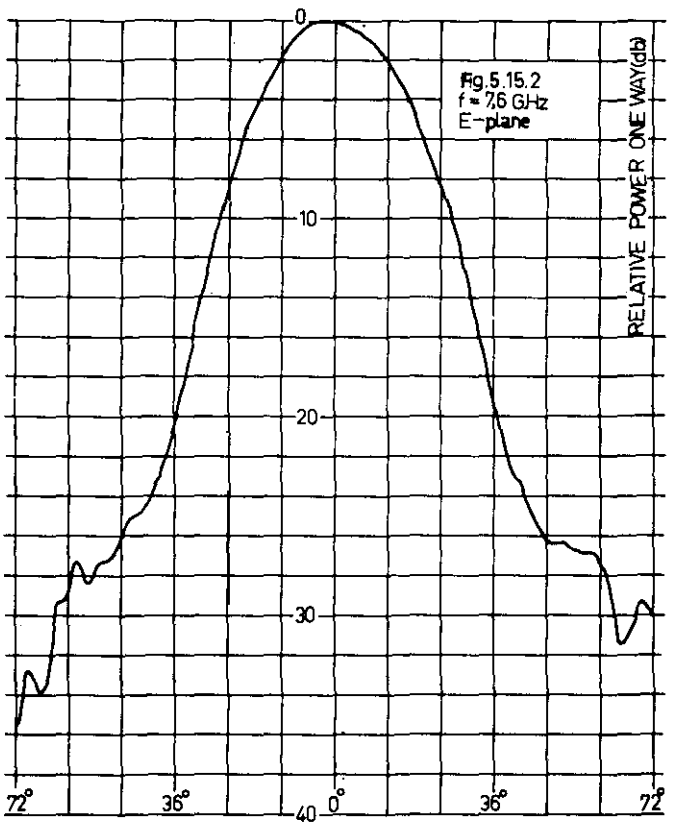
Fig.5.15.2
f = 7,6 GHz
E-plane
RELATIVE POWER ONE WAY(db)
0
10
20
30
40
72°
36°
0°
36°
72°

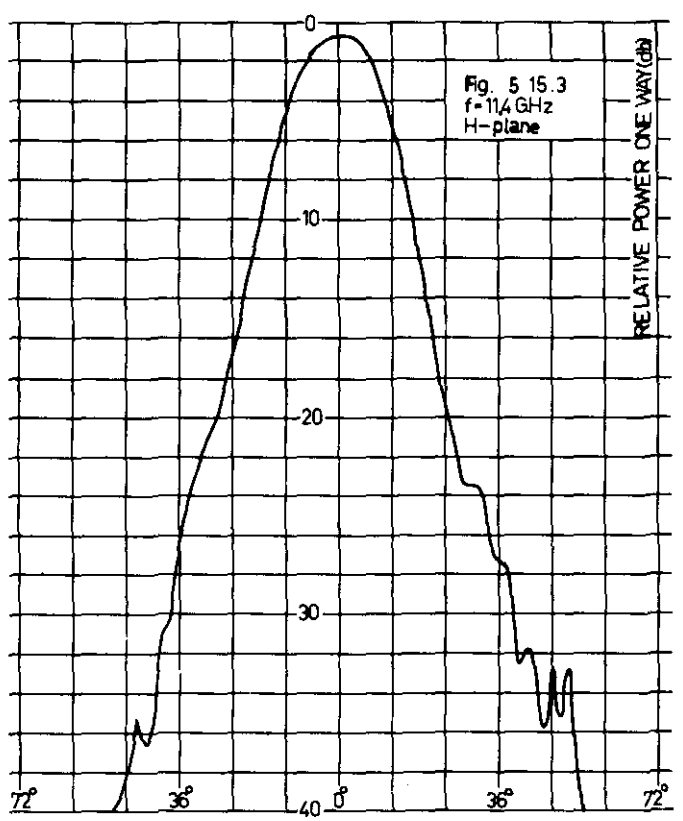
Fig. 5 15.3
f=11,4 GHz
H-plane
RELATIVE POWER ONE WAY(db)
0
10
20
30
40
72°
36°
0°
36°
72°

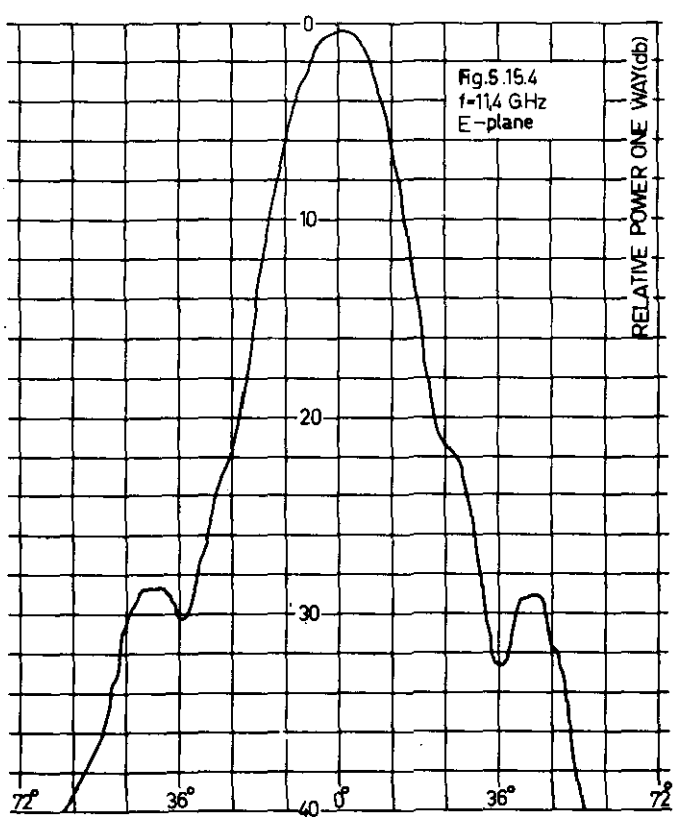
Fig.5.15.4
f=11,4 GHz
E-plane
RELATIVE POWER ONE WAY(db)
0
10
20
30
40
72°
36°
0°
36°
72°

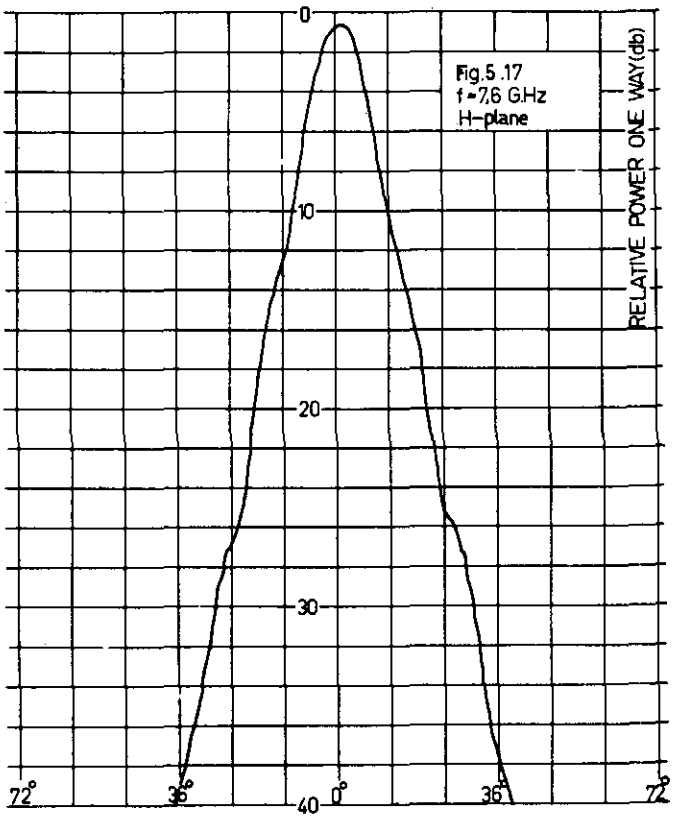
Fig.5.17
f=7,6 GHz
H-plane
RELATIVE POWER ONE WAY(db)
0
10
20
30
40
72°
36°
0°
36°
72°

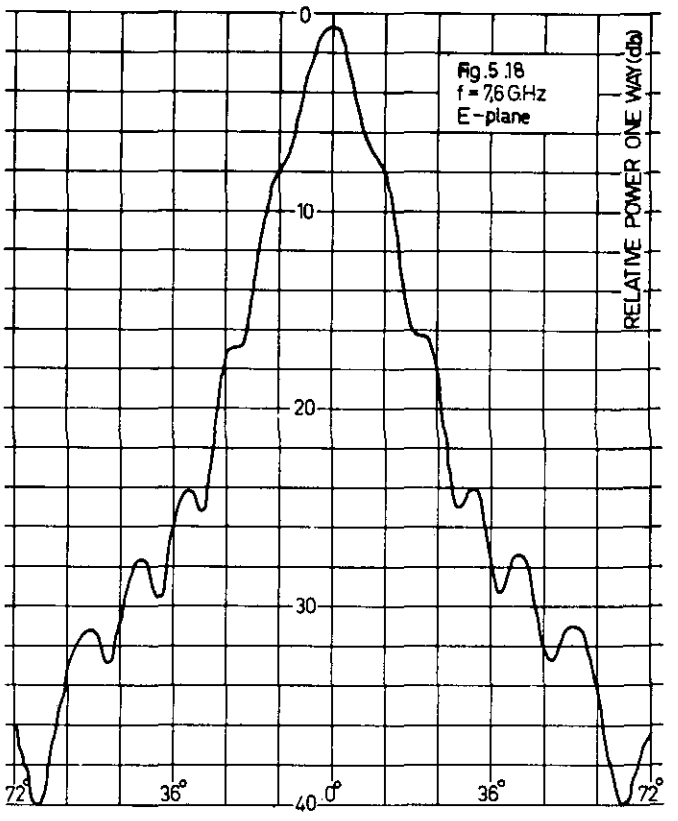
Fig.5.18
f=7,6 GHz
E-plane
RELATIVE POWER ONE WAY(db)
0
10
20
30
40
72°
36°
0°
36°
72°

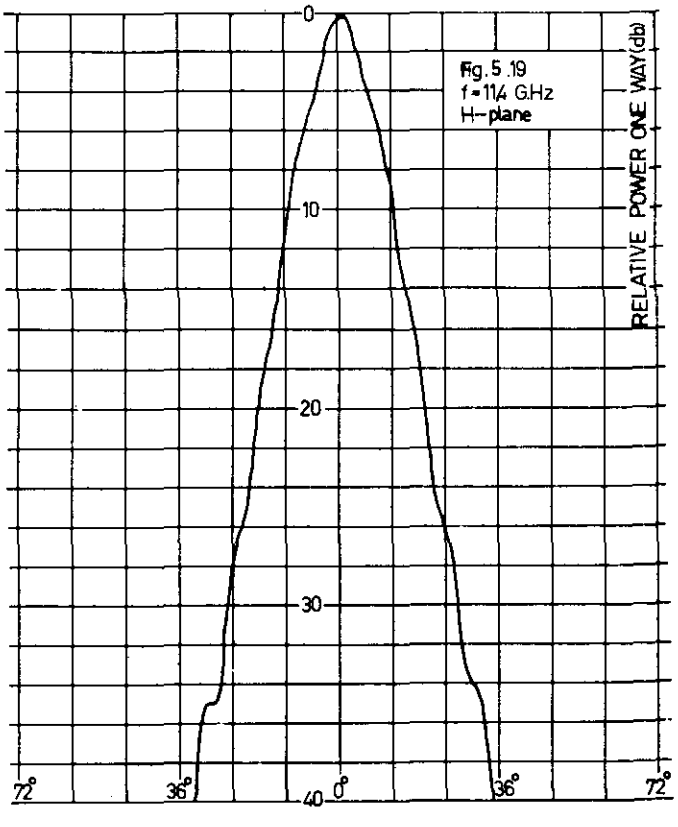
Fig.5.19
f=11,4 GHz
H-plane
RELATIVE POWER ONE WAY(db)
0
10
20
30
40
72°
36°
0°
36°
72°

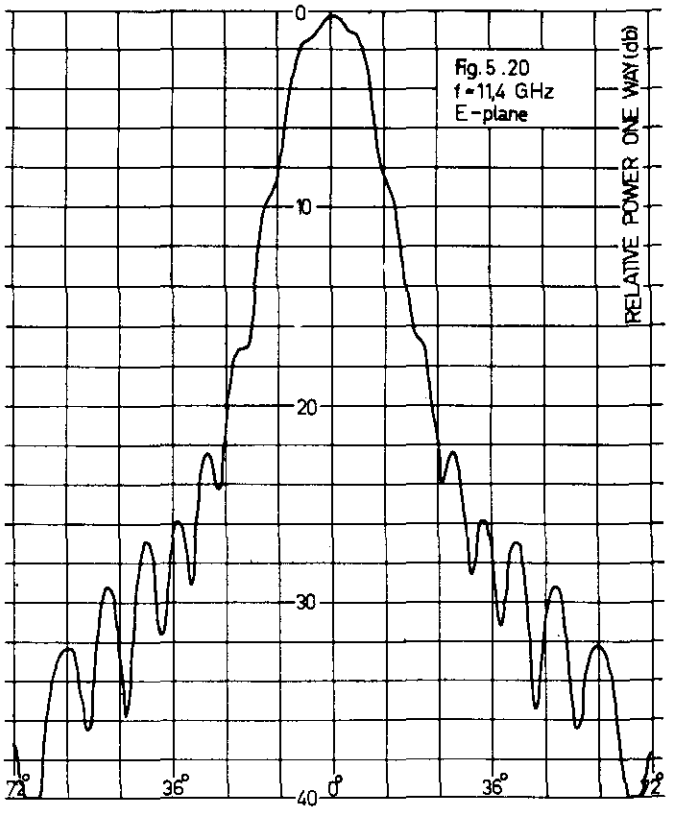
Fig.5.20
f=11,4 GHz
E-plane
RELATIVE POWER ONE WAY(db)
0
10
20
30
40
72°
36°
0°
36°
72°

6. The measurement of scattered radiation from a hyperboloid subreflector

6.1. Measurement

If a subreflector is illuminated by a horn antenna only part of this energy will be intercepted by the subreflector and reflected towards the main reflector, in accordance with optical laws.
Part of the energy intercepted by the subreflector is not radiated towards the main reflector but scattered in all directions by diffraction of the subreflector edge.

Fig. 6.1. shows the measuring arrangements. The combination of horn antenna and subreflector is rotated with the rotation centre in B. At the same time this system will be illuminated from a fixed direction by a plane wave. A photograph on the next page gives more details of the measuring arrangement.

The pattern which is measured in this way is also the pattern by which the main reflector is illuminated. The measuring frequency is 9500 MHz. The subreflector was made of synthetic material and plastered with aluminium foil.

The subreflector dimensions are found by calculation, the following date being known.
(1) F/D = 0.33
(2) The width of the main beam between the dB points is 30°.
(3) The edge illumination is -10 dB.

The further geometry is found in Fig. 6.2. Model F, discussed in the previous chapter, is taken as illuminator for the subreflector. The beamwidth of this model between the -10 dB points of the main beam is about 30°, while at 9500 MHz the beamwidths of E and H-plane main beam are equal. Measurements are now carried out at edge illuminations of -7, -13, -17 and -20 dB, by moving the feed towards the subreflector.

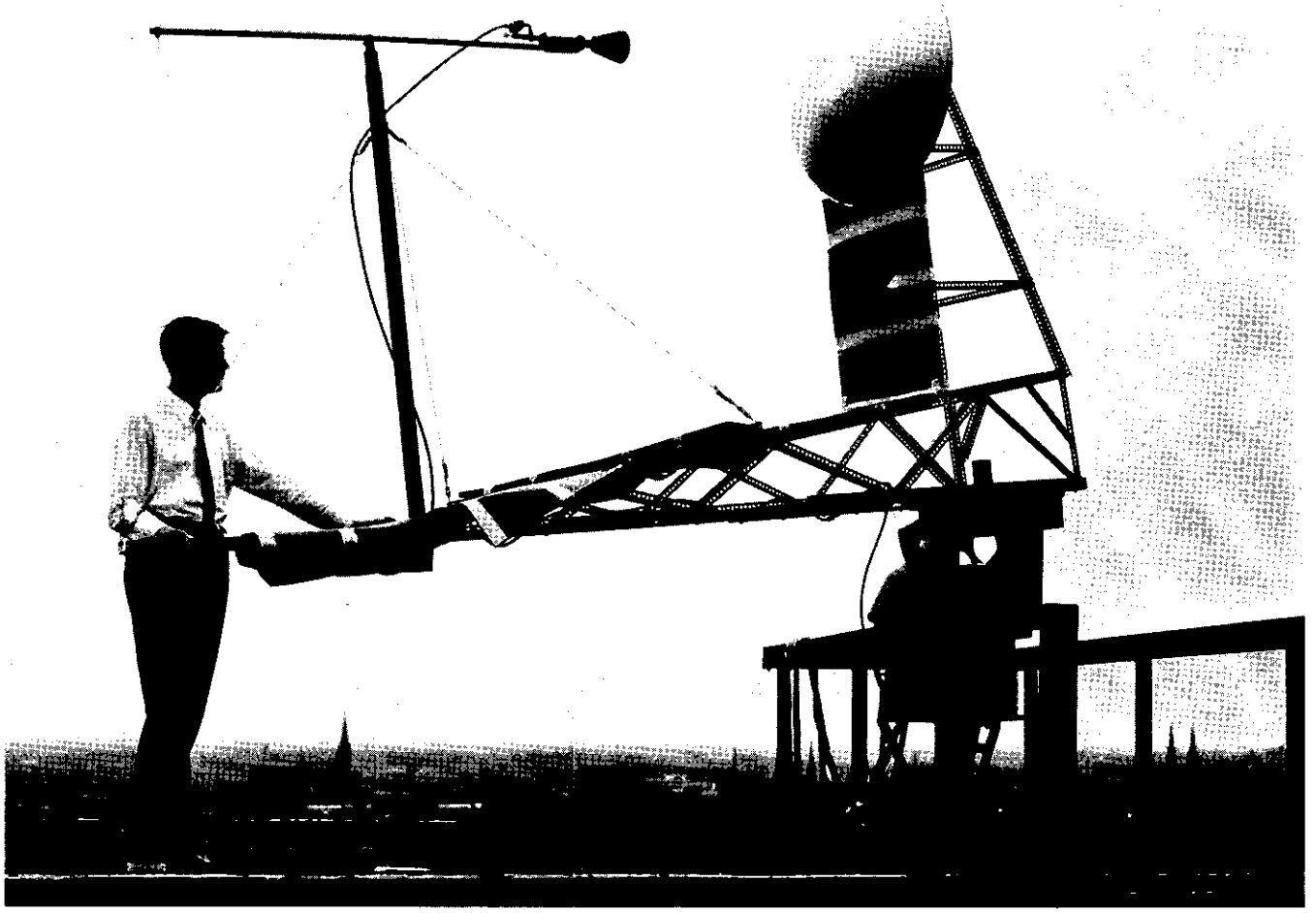

Measuring arrangement of subreflector and feed

Exact measurements could only be expected by using subreflectors with eccentricities adapted to the edge illumination. To reduce costs, only one subreflector was used; therefore, the measurements are only of quantative value. Some valuable conclusions may, however, be drawn. By graphical integration it was found which part of the energy radiated by the feed is intercepted by the subreflector (Table 6.1).

Table 6.1	edge illumination	percentage of intercepted power
	- 7 dB	79.3 %
	- 13 dB	87.9 %
	- 17 dB	92.7 %
	- 20 dB	97.4 %

If the total radiation by the subreflector is measured it can be found in accordance with Fig. 6.3, which part of this power is lost by forward radiation and side radiation, and is, therefore, not intercepted by the main reflector.
The results are collected in Table 6.2.

Table 6.2.		radiation between - Ψ and + Ψ	side radiation	forward radiation
- 7 dB	74°	68.73 %	2.66 %	28.61 %
- 13 dB	$81^{\circ}.40'$	89.80 %	1.08 %	9.12 %
- 17 dB	$85^{\circ}.40'$	93.85 %	0.62 %	5.53 %
- 20 dB	$89^{\circ}.50'$	97.23 %	0.01 %	2.76 %

6.2. Conclusions

(1) At a -7 dB edge illumination the power lost by forward radiation and side radiation is inadmissibly high.

(2) At an edge illumination of -20 dB the side and forward power loss is only a few per cent of the total power radiated and will contribute only slightly to the noise temperature at low elevation angles.

(3) It is not possible to interpret clearly the measurements at -13 dB and -17 dB .

1 feedhorn.

2 hyperboloid subreflector.

A, B hyperboloid foci.

Fig. 6.1.

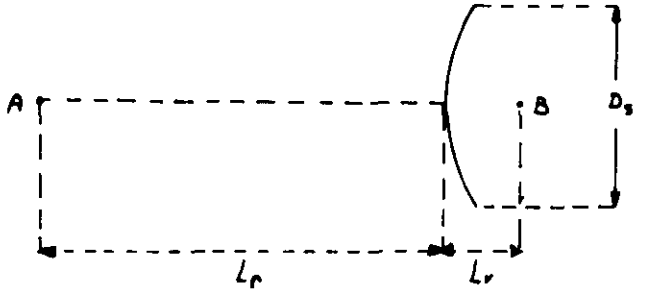

$D_s = 32,1\ \lambda$

$L_r = 50,5\ \lambda$

$L_v = 8,7\ \lambda$

Fig. 6.2.

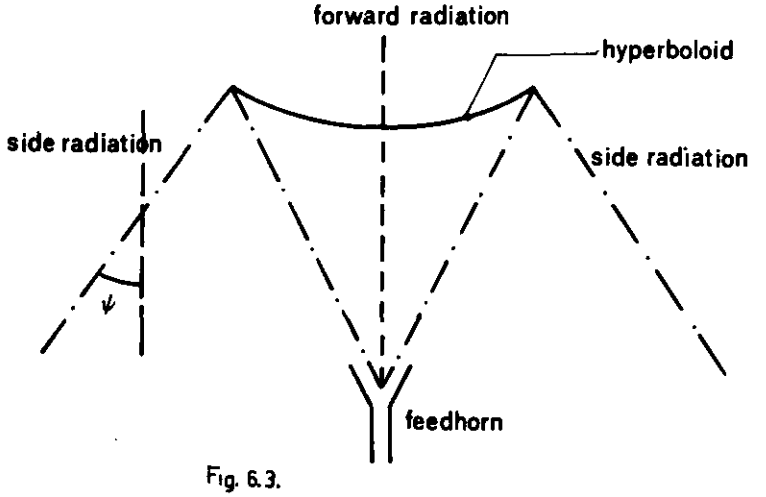

Fig. 6.3.

7. The modified cassegrain system

7.1 Introduction

Silver (lit. 16 p. 198) already reported the possibility of obtaining a specified pattern by modifying the reflector surface. The study of this subject has been continued by Kinber (lit. 12) especially on dual reflector systems. Others (lit. 7) also indicate the possibility of deviating from the standard hyperboloid and paraboloid of cassegrain systems to improve the reflected wavefront. A recent publication of Jet Propulsion Lab. (lit. 9) gives the impression that their present solution, providing the subreflector with a rim to decrease spillover losses, is not found ideal. Apparently other solutions are in preparation, proposing more radical modifications of the reflector surfaces. The problem of obtaining a dual antenna system with a specified amplitude and phase distribution in the aperture can be tackled in two ways;

(a) An arbitrary primary feed with a known radiation pattern illuminates a subreflector. The surfaces of main and subreflector must now meet certain requirements in order that the required aperture field may be obtained.

(b) An arbitrary main reflector is available and a arbitrary aperture field is required. The feed must now possess a dictated radiation pattern and the subreflector needs modification. This paper only deals with possibility (a), as feeds with prescribed radiation patterns and large bandwidths (Sec. 5.2) are very difficult to realise or not at all (lit. 9). Pioneering work as to possibility (a) has been carried out by Galindo (lit. 11).

In this paper his methods of calculating the reflector surfaces are mainly applied. Calculations proposed by Green (lit. 50) and Williams (lit. 10) are also followed but only partially.

By modifying the reflector surfaces great advantages can be obtained over classical cassegrain antenna systems. First of all, uniform phase and amplitude distribution can be produced in the aperture, by which, theoretically, an aperture efficiency of 100% is obtainable. Secondly, the edge of the subreflector may be illuminated much lower than in classical cassegrain systems, as all the power radiated from

feed to subreflector is reflected by main and subreflector in such a way that uniform constant phase aperture distribution is obtained (Fig. 7.1).

Two clear advantages over the classical system are obtained by low edge illumination. First spillover at the subreflector edge will be very low. In Fig. 7.2 it is seen that a spillover efficiency of 99% is reached when illuminating the edge at -20 dB with the theoretical feed pattern

$$G(\phi_1) = 2(n+1)\cos^n \phi_1 \quad .$$

An actual feed, however, will have a spillover efficiency which is slightly less due to minor side lobes in the feed pattern. A classical cassegrain system demands an edge illumination of about -10 dB to obtain the maximum overall efficiency, but the spillover efficiency, will be only about 92%. Naturally, the antenna noise temperature will be affected unfavourably in the latter case.

A second advantage of low subreflector edge illumination will be the large decrease in diffraction losses. Calculations carried out by a computer using Eq. 3.83 shows this clearly. Curves are found in Fig. 7.3 where the diffraction efficiency is shown as a function of the edge illumination. This calculation has been carried out for classical cassegrain systems; however the strong similarity between classical and modified cassegrain systems and the work of Rusch on systems of Cassegrain and Gregory (lit. 51) make this approximation for modified systems plausible.

In the following sections analytical expressions are derived which can be used to calculate, the final shape of main and subreflector, if the primary feed pattern is known. An example with a primary feed pattern $G(\Psi_1) = 122 \cos^{60} \Psi_1$ is demonstrated later.

The radiation pattern, however, of an actual feed cannot be expressed in analytical form. The calculation should then be carried out by the computer with numerical methods using the feed pattern measured. The present computer programme available already takes this possibility into account.

7.2 The system's geometry

The design of a two-reflector system utilizes optical principles as

(1) Snell's Law applied to each reflector.

(2) Conservation of energy flow in any solid angle bounded by ray trajectories (Silver lit. 16 p.112)

(3) The surfaces of constant phase are normal to the ray trajectories even after a number of reflections (Theorem of Malus).
The application of these laws leads to a number of equations of constraint for the system.

Snell's law applied to the subreflector (Fig. 7.4) leads to the equation:

$$\frac{dy_1}{dx_1} = \tan \tfrac{1}{2} (\psi_1 - \psi_2) , \qquad (7.1)$$

where

$$\tan \psi_2 = \frac{x_2 - x_1}{\alpha+\beta-y_1+y_2} . \qquad (7.2)$$

Snell's law applied to the mainreflector leads to the equation

$$\frac{dy_2}{dx_2} = - \tan \tfrac{1}{2} \psi_2 . \qquad (7.3)$$

If we assume that the antenna system is circularly symmetrical, the relative power radiated by the primary feed between 0 and ψ_1 is equal to

$$2\pi \int_0^{\psi_1} G_1(\psi_1) \sin\psi_1 \, d\psi_1 ,$$

where $G_1(\psi_1)$ is the gain function of the primary feed.

According to the principle of energy conservation this power should be equal to the power radiated by the corresponding part of the aperture, viz.,

$$2\pi \int_0^{x_2} F(r) \cdot r \cdot dr \cdot ,$$

where F(r) is power density flow normal to the aperture. If uniform amplitude distribution has to be produced in the aperture, the function F(r) must be a constant. If both expressions are normalised by the total radiated power we obtain:

$$\frac{\int_0^{x_2} r\, dr}{\int_0^{x_{2\,max}} r\, dr} = \frac{\int_0^{\psi_1} G_1(\psi_1) \sin\psi_1 \, d\psi_1}{\int_0^{\Psi_1} G_1(\psi_1) \sin\psi_1 \, d\psi_1} \quad . \qquad (7.4)$$

In the aperture plane constant phase of all rays is required, The path length for each ray is therefore, given by

$$\rho_1 + \rho_2 + y_2 = \text{constant} \quad . \qquad (7.5)$$

It is assumed that all rays are coming from one common point and are in phase. If measured patterns show otherwise, Eq. 7.5 has to be extended by a term $\alpha(\psi_1)$ and the computer programme altered accordingly.

With the geometry of Fig. 7.4 we write Eq. 7.5

$$K = \frac{\beta - y_1}{\cos\psi_1} + y_2 + \left[(x_2 - x_1)^2 + (\alpha + \beta + y_2 - y_1)^2 \right]^{\frac{1}{2}} , \qquad (7.6)$$

K being a constant. By means of Eq. 7.2 is easely demonstrated that Eq. 7.6 can be written as

$$K = y_2 + \frac{\beta - y_1}{\cos\psi_1} + \frac{x_2 - x_1}{\sin\psi_2} \quad . \qquad (7.7)$$

Directly from Fig. 7.4 is found

$$\tan\psi_1 = \frac{x_1}{\beta - y_1} \quad . \qquad (7.8)$$

The boundary conditions are also found in Fig. 7.4, viz.,

$$\tan \Psi_1 = \frac{D_s}{2\beta} \quad , \tag{7.9}$$

$$\tan \Psi_2 = \frac{D-D_s}{2(\alpha+\beta)} \tag{7.10}$$

$$K = \frac{\beta}{\cos \Psi_1} = \frac{\alpha+\beta}{\cos \Psi_2} \quad . \tag{7.11}$$

After choosing Ψ_1, Ψ_2 and the ratio D_s/D the whole system is determined.

7.3 The solution of the equations

We shall choose the quantity ϕ_1 as a single independent variable. The remaining dependent variables will be considered as functions of ϕ_1. Therefore, we shall derive two differential equations

$$\frac{dy_1}{d\phi_1} = f_1 (\phi_1 , y_1 , y_2) , \tag{7.12}$$

and

$$\frac{dy_2}{d\phi_1} = f_2 (\phi_1 , y_1 , y_2) . \tag{7.13}$$

Upon solving these equations all the remaining dependent variables can immediately be found as functions of ϕ_1. From Eqs. 7.1 and 7.8 we find

$$\frac{dy_1}{d\phi_1} = \tan \tfrac{1}{2} (\phi_1 - \Psi_2) \frac{dx_1}{d\phi_1} \quad , \tag{7.14}$$

and

$$\frac{dx_1}{d\phi_1} = - \frac{dy_1}{d\phi_1} \tan \phi_1 + (\beta - y_1) \cdot \frac{1}{\cos^2 \phi_1} . \tag{7.15}$$

Substituting Eq. 7.15 in Eq. 7.14 we find

$$\frac{dy_1}{d\psi_1} = -\tan\tfrac{1}{2}(\psi_1-\psi_2)\cdot\tan\psi_1\cdot\frac{dy_1}{d\psi_1} + \frac{\tan\tfrac{1}{2}(\psi_1-\psi_2)}{\cos^2\psi_1}(\beta-y_1) \text{ or}$$

$$\frac{dy_1}{d\psi_1} = \frac{(\beta-y_1)\tan\tfrac{1}{2}(\psi_1-\psi_2)}{\{1+\tan\tfrac{1}{2}(\psi_1-\psi_2)\cdot\tan\psi_1\}\cos^2\psi_1} . \qquad (7.16)$$

Using the well-known formule $\tan\tfrac{1}{2}\alpha = \frac{\sin\alpha}{1+\cos\alpha}$ we obtain, instead of Eq. 7.16,

$$\frac{dy_1}{d\psi_1} = \frac{(\beta-y_1)\sin(\psi_1-\psi_2)}{\{\cos\psi_1+\cos\psi_1-\cos(\psi_1-\psi_2)+\sin\psi_1\cdot\sin(\psi_1-\psi_2)\}\cos\psi_1} \text{ or}$$

$$\frac{dy_1}{d\psi_1} = \frac{(\beta-y_1)\sin(\psi_1-\psi_2)}{\cos\psi_1(\cos\psi_1+\cos\psi_2)} . \qquad (7.17)$$

As will be explained in Sec. 7.4 the lower integration limits of the aperture integrals in Eq. 7.4 are replaced by $\frac{1}{2}D_s$ instead of zero. Eq. 7.4 is then written as

$$x_2^2 = \tfrac{1}{4}\left\{D_s^2+(D-D_s)^2\right\}\cdot\frac{\int_0^{\psi_1} G_1(\psi_1)\sin\psi_1\, d\psi_1}{\int_0^{\Psi_1} G_1(\psi_1)\sin\psi_1\, d\psi_1} . \qquad (7.18)$$

or, if $D_s/D = ds$

$$x_2 = \tfrac{1}{2}\sqrt{(ds)^2+(1-ds)^2}\cdot\frac{\int_0^{\psi_1} G_1(\psi_1)\sin\psi_1\, d\psi_1}{\int_0^{\Psi_1} G_1(\psi_1)\sin\psi_1\, d\psi_1} . \qquad (7.19)$$

From Eq. 7.18 we find

$$\frac{dx_2}{d\phi_1} = \frac{1}{8x_2}\,(1-ds)^2 \cdot \frac{G_1(\phi_1)\,\sin\phi_1}{\int_0^{\Psi_1} G_1(\phi_1)\,\sin\phi_1\,d\phi_1}\,, \qquad (7.20)$$

and by using Eq. 7.2

$$\frac{dy_2}{d\phi_1} = f_2(\phi_1, y_1, y_2)$$

$$= -\frac{\sin\phi_2}{1+\cos\phi_2}\cdot\frac{1}{8x_2}\cdot(1-ds)^2 \cdot \frac{G_1(\phi_1)\,\sin\phi_1}{\int_0^{\Psi_1} G_1(\phi_1)\sin\phi_1\,d\phi_1} \qquad (7.21)$$

If a subreflector edge illumination of -20 dB is chosen, the computer programme is built up as follows:

(1) Calculate Ψ_1 from $\cos^n\Psi_1 = 0{,}01$
(2) Choose the angle Ψ_2 and the ratio Ds/D = ds
(3) Calculate β from Eq. 7.9
(4) Calculate α from Eq. 7.10
(5) Calculate K from Eq. 7.11
(6) Calculate $\int_0^{\Psi_1} G_1(\phi_1)\,\sin\phi_1\,d\phi_1$
(7) Calculate x_2 from Eq. 7.19
(8) Calculate x_1 from Eq. 7.8
(9) Calculate ϕ_2 from Eq. 7.2 and substitute in Eqs. 7.17 and 7.21
(10) Solve Eqs. 7.17 and 7.21
(11) Check solutions with Eq. 7.6

7.4 Realisation of the maximum blocking efficiency

In chapter 3 much attention has been paid to the blocking efficiency in duel reflector systems. In conventional cassegrain antenna systems realisation of the maximum blocking efficiency is not possible;

however, both mainreflector and subreflector can be shaped in such a way that all the blocked power is properly intercepted by the aperture of the main reflector. In this way the relation (3.41) is theoretically obtainable, as

$$\left(\frac{\eta_B}{\eta_o}\right)_{max} = 1 - \frac{B}{A} \quad . \tag{3.41}$$

The areas indicated by B will only comprise the parts in the aperture blocked by plane waves, as by correct shaping no parts of the aperture will be blocked by spherical waves any longer. Both mainreflector and subreflector will have to be provided with grooves and rimples (as shown in an example for the subreflector in Fig. 7.5) to utilise the power blocked by the subreflector supports.

Mathematical expressions to calculate the surface shape of mainreflector and subreflector are still subjects of further study. To utilise the power blocked by the subreflector itself, this should have a cone shaped protuberance in the middle (Fig. 7.6), which can be alculated in a very simple manner. For this purpose it is sufficient to replace the lower integration limits of the aperture integrals in Eq. 7.4 by $\frac{1}{2} D_s$ instead of zero.

Therefore,

$$\frac{\int_{\frac{1}{2}D_s}^{\frac{1}{2}x_2} r\, dr}{\int_{\frac{1}{2}D_s}^{\frac{1}{2}D} r\, dr} = \frac{\int_0^{\psi_1} G_1(\psi_1) \sin\psi_1 \, d\psi_1}{\int_0^{\Psi_1} G_1(\psi_1) \sin\psi_1 \, d\psi_1} \quad . \tag{7.22}$$

Using the well-known theoretical feed pattern $G_1(\psi_1) = 2(n+1)\cos^n \psi_1$, Eq. 7.22 is written as

$$\frac{4x_2^2 - D_s^2}{D^2 - D_s^2} = \frac{1 - \cos^{n+1} \psi_1}{1 - \cos^{n+1} \Psi_1} \quad . \tag{7.23}$$

The cone shaped protuberance is clearly demonstrated in the calculated example of chapter 8, Fig. 8.1 .

It is expected, however, that some scattering will occur as the grooves and rimples will act as radiating line distributions. In the case of antennas for satellite communication, the dimensions of main reflector $D \approx 350\lambda$ and subreflector $D_s \approx 35\lambda$ are sufficiently large to keep the influence of diffraction small. The protuberance of the subreflector comprises only one singular point which will have little effect on the total radiation pattern.

The increase of the blocking efficiency obtainable is not important, however, the decrease in noise temperature will be very noticeable. The example of Fig. 3.10 shows that 1% and 3.5% of the power radiated by the feed is blocked by the subreflector and subreflector supports respectively. If the antennas points towards the horizon it may be expected that half of this power is scattered into the sky and the other half into the "hot" ground. The increase in noise temperature is therefore $0.5 \times 3^{\circ}K + 1.75 \times 3^{\circ}K = 6.75^{\circ}K$. Also Potter (lit. 9) explains the great importance of these noise contributions.

7.5 Conclusion

By modifying the surfaces of main and subreflector these can be adapted to any arbitrary primary feed pattern according to the mathematical relations of Sec. 7.2 . In this way it is possible to achieve a constant phase and amplitude distribution at the antenna aperture. Theoretically an aperture efficiency of 100% can be realised although some diffraction effects will take place as the ratio D/λ is not unlimited.

At the same time it is possible to illuminate the edge of the subreflector at -20 dB. This value is much lower than with the usual classical cassegrain antennas; a spillover efficiency of about 98% can now be realised. The product of spillover efficiency and aperture effiecency of classical cassegrain antennas is mostly of the order of 74% (chapter 3).

The increase in antenna efficiency by shaping the reflectors can therefore be considerable. The antenna gain can be increased by about 1 dB. This means that a modified cassegrain antenna with a main reflector diameter of 27 metres will have the same gain as a classical cassegrain system with a main reflector of 30 metres diameter.

The low spillover losses have no doubt a favourable influence on the antenna noise temperature. The losses by diffraction at the subreflector edge will also be much lower by decreasing the edge illumination, consequently the antenna noise temperature will be lower. A disadvantage is the fact that by illuminating the aperture uniformly, diffraction effects at the edge of the main reflector have to taken into account. In classical systems this contribution can be neglected as the illumination is tapered towards the edge. It is possible, however, to abandon the overall uniform illumination and leave a 1 metre ring along the main reflector edge under illuminated. The aperture efficiency will decrease, but on the other hand the contribution to noise temperature by this part of the scattered power also becomes less. Optimising this problem is now a subject of further study.

In an antenna system designed for satellite communication valuable advantages can further be obtained by having the power which is blocked by subreflector and supports, intercepted by the main reflector. This results in

(1) higher antenna efficiency
(2) decrease of the noise temperature.

Further theoretical and experimental study will be required to calculate the difficult diffraction effects of the grooves and rimples and to see whether this solution offers practical possibilities.

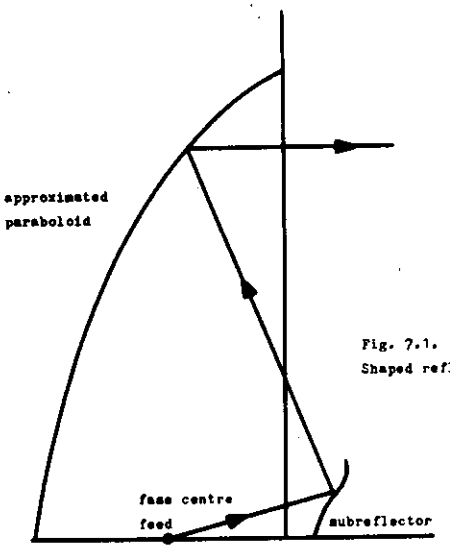

Fig. 7.1.
Shaped reflectors.

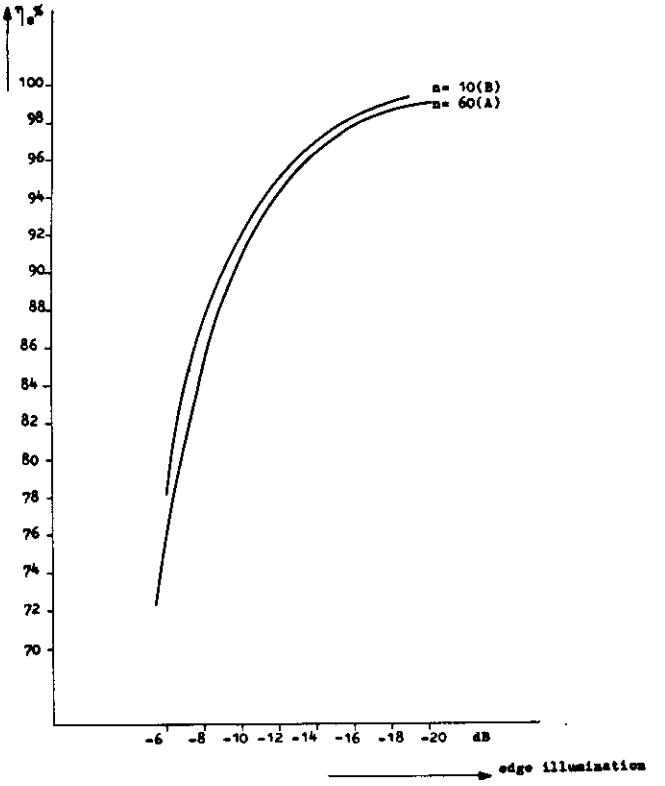

Fig. 7.2. The spillover efficiency η_s as function of the edge illumination of the subreflector.
Gain functions feed A $G(\psi_1) = 122 \cos^{60}\psi_1$
B $G(\psi_1) = 22 \cos^{60}\psi_1$

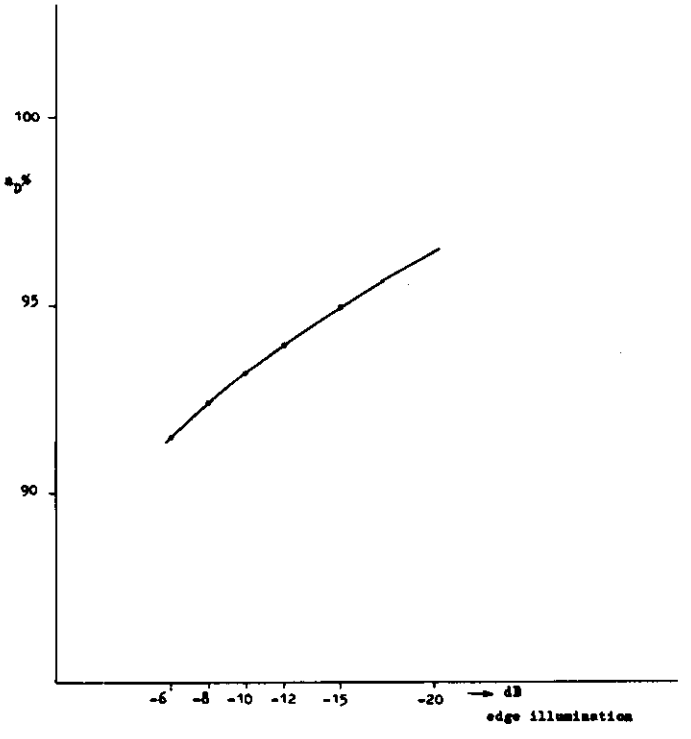

Fig. 7.3. The decrease of antenna efficiency by diffraction as function of the edge illumination at the subreflector.

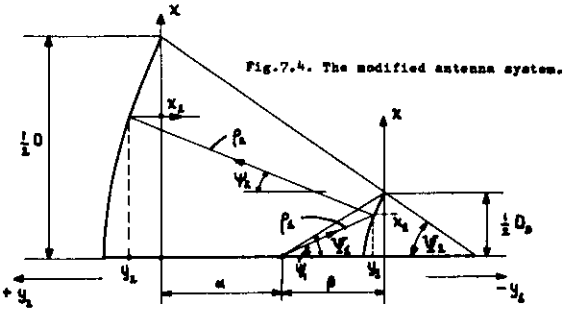

Fig.7.4. The modified antenna system.

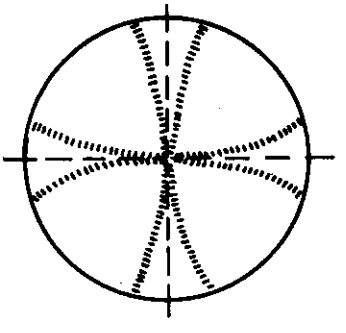

Fig. 7.5. Shaping the subreflector.

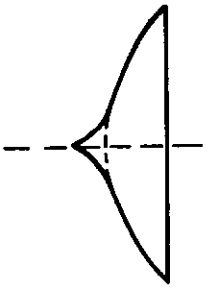

Fig. 7.6. cross-section of a shaped subreflector.

8. Proposal for an antenna system for satellite communication in the Netherlands

8.1. Introduction

The previous chapters have proved that a modified cassegrain antenna system should be proposed for satellite communication with stationairy satellites. The great advantage of this system as compared with the classical cassegrain system is increased aperture efficiency and a lower antenna noise temperature, because the power is spread over the aperture to obtain uniform illumination and because the edge of the subreflector is illuminated at a low level, resulting in low spillover losses. The calculations carried out by the computer indicate that in classical systems the angular aperture Ψ_2, i.e. the ratio F/D, and the maximum antenna gain are practically not related to each other.

If the reflectors are modified the antenna gain and antenna noise temperature can be calculated and optimised independently of each other. For the time being, an F/D ratio of 0.33 has been chosen, while the investigations carried out so far indicate the possibility of taking a higher F/D ratio without much loss in performance. The design proposed includes a modified conical horn antenna with properties specified elsewhere.

8.2. The feed

A feed has been prescribed in Sec. 5.4 (model H) which meets the specification with regard to the bandwidth. The aperture diameter is 6λ for a frequency of 3.7GHz. The shape of the beam in the H plane is very good, that in the E plane still needs some improvement. Judging from the experience met so far with special boundary conditions improvement may be expected by their introduction.

It is proposed to use a modified conical horn antenna, with the same dimensions as model H. The radiation pattern in the E plane is expected to be very similar to the pattern of Fig. 5.17.

The beamwidths in the E and H plane are expected to be similar to and slightly larger than those of Fig. 5.17. At the -20 dB points a beamwidth of about 44° is expected.

8.3. The shape of the reflectors

Chapter 7 gives detailed information as to the methods of shaping main and subreflector to obtain uniform constant phase aperture illumination at a given pattern. The results of a computer programme are shown in Fig. 8.1., where the coordinates of the reflector system are indicated. The function $G_1(\phi_1) = 122 \cos^{60}\phi_1$ served as primary feed pattern. This pattern corresponds very well with the pattern recommended in chapter 5. The diameter of the subreflector is 0.1D. The angle Ψ_2 corresponds with an F/D ratio of 0.33 if the cassegrain system had been classical. It will be clear that when the main reflector has been shaped no focus can be defined.

Apart from showing the shaped contours of main and subreflector, Fig. 8.1 also represents a true paraboloid with an F/D ratio of 0.33. By causing the edges of the two main reflectors to coincide, the differences are clearly demonstrated. Computer calculations indicate that the maximum deviation of the shaped paraboloid from the true paraboloid is about 0.01D. It is also possible to compare the shaped paraboloid with what is popularly known as a best-fit paraboloid, also called regression paraboloid, which can be found by the least square method.
The maximum difference between true and shaped paraboloid now reduces to about 0.0005D.

8.4. Calculation of the G/T ratio at 4 GHz and the antenna gain at 6 GHz

8.4.1. Power losses and noise contributions

Let us consider the antenna in transmitting condition and examine the power radiated outwards. We shall establish in succession all the losses that are found, and tabulate them in Table 8.1. It is possible to classify the contributions to loss and noise from Table 8.1. in three more or less independent groups. In this way, it is possible to distinguish the influence of each group.
Group I: The ideal mechanical antenna; containing all contributions affecting the ratio G/T in a quiet environment (without wind, no surface inaccuracies, etc.). These contributions will affect the electrical antenna properties.

Group II: contributions by mechanical imperfections of the antenna system and by the weather.

Group III: contributions of the components such as paramp. duplexer, polariser, etc.

Tables 8.3 and 8.4 show these contributions in more detail. Before explaining the figures given, however, the power balance within the antenna system should be determined. This power balance is tabulated in Table 8.2 (see also Fig. 8.2).

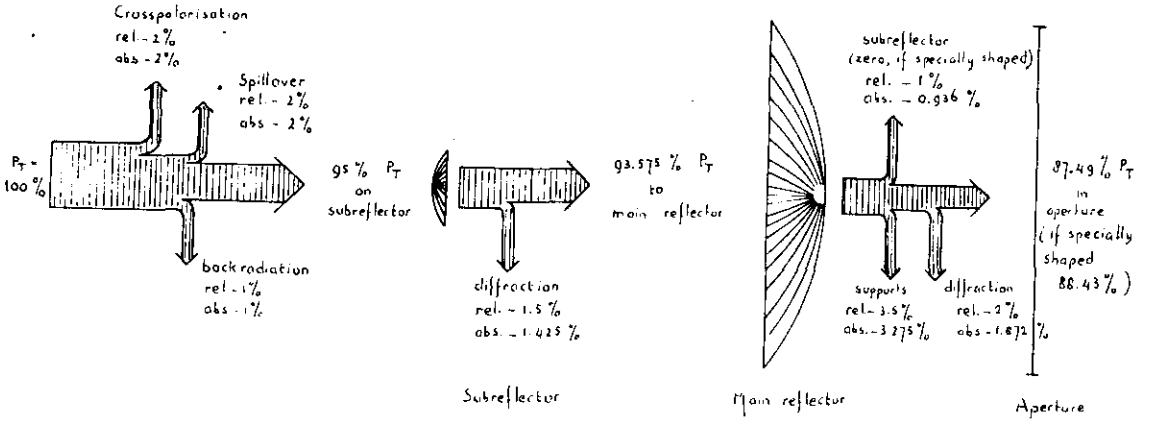

Fig. 8.2 Power equilibrium in a two-reflector system (modified cassegrain antenna)

Table 8.1

Characteristic	cause of power loss	cause of noise contribution
(1) microwave receiver	reflection loss	reflection (decrease of noise) amplifier noise temperature
(2) transmission between receiver and feed	reflection loss ohmic loss	reflection ohmic loss
(3) coupling of noise by cross coupler	coupling hole	radiation by coupling hole
(4) polariser	ellipticity	-
(5) feed + window	reflection loss ohmic loss cross polarisation backward radiation spillover loss	reflection loss thermal noise by losses sky noise by cross polarisation sky and earth noise by scattered backward radiation sky and earth noise by spillover
(6) subreflector	diffraction loss ohmic loss cross polarisation surface tolerance	scattering of diffraction power ohmic loss cross polarisation -
(7) main reflector	aperture efficiency phase efficiency surface tolerance cross polarisation blocking effects ohmic losses diffraction loss	sky noise by main beam and sidelobes only - - cross polarisation scattering of blocked power ohmic losses scattering of diffraction power
(8) various	loss by mispositioning of subreflector loss by pointing errors, paraboloid deviation by own weight loss by feed offset, wind shears, mode conversion, rain and clouds	

Table 8.2.

A. Power equilibrium of feed, if feed delivers 100% of the total power.

Characteristic	Power loss relative	Power loss absolute	relative efficiency
(1) loss by cross polarisation	2%	2%	
(2) loss by back radiation	1%	1%	0.95
(3) loss by spillover	2%	2%	
Total loss by feed		5%	0.95
Conclusion: 95% of the total power supplied to the feed is captured by the subreflector.			

B. Power equilibrium at the subreflector when 100% power is supplied to the subreflector.

(4) loss by diffraction	1.5%	0.95 x 1.5 = 1.425%	0.985
Conclusion: 93.575% of the total power supplied by the feed is captured by the main reflector.			

C. Power equilibrium at the main reflector when 100% power is supplied to the main reflector.

(5) scatter of the power blocked by subreflector	1%(nihil)*	0.936%(nihil)*	*if shaped according Sec. 7.4	
(6) scatter of the power blocked by the subreflector supports	3.5%	3.275%	0.935	0.945*
(7) scatter at the main reflector edge and contributions in far sidelobes	2%	1.872%		
Conclusion: 87.49% of the power supplied to the feed is radiated effectively by the main reflector, or 88.43% if the subreflector is shaped in accordance with Sec. 7.4				

Table 8.3.

Antenna efficiency and noise of the feed, feedsystem and antenna system.

		4 GHz					6 GHz		
	Feed (modified conical horn)	Losses dB	η	abs. power loss %	Noise 0° elev. $^\circ K$	Noise 10° elev. $^\circ K$	Losses dB	η	
1.	Reflection losses of feed VSWR $\leq$ 1.2	0.044	0.990		see also 25		0.044	0.990	
2.	Ohmic losses of feed + window	0.009	0.998		0.5°	0.5°	0.009	0.998	
3.	Mode conversion	-	-	-	-	-	-	-	
4.	Cross polarisation max. 2% (see also 8 and 13)	0.088	0.980	2.0	3.0	0.75°	0.088	0.980	
5.	Back radiation max. 1%	0.044	0.990	1.0	1.5	1.35	0.044	0.990	
	Subreflector D_s = 0.1D								
6.	Relative spillover efficiency at - 20 dB edge illumination	0.088	0.980	2.0	3.0	2.7	0.088	0.980	
7.	Relative diffraction efficiency	0.132	0.970	1.425	2.14	1.92	0.132	0.970	
8.	Cross polarisation (see 4)	-	-	-	-	-	-	-	
9.	Surface tolerance and ohmic losses (see table 8.4)	-	-	-	-	-	-	-	
	Main reflector								
10.	Aperture efficiency (amplitude)	0.269	0.940	-	-	-	0.706	0.85	
11.	Aperture efficiency (phase)	0.223	0.950	-	-	-	0.458	0.900	
12.	Edge diffraction and far sidelobes 2%	0.088	0.980	1.872	2.81	2.53	0.088	0.980	
13.	Cross polarisation (see 4)	-	-	-	-	-	-	-	
14.	Blocking, ohmic losses, surface tolerance, pointing errors, etc. (see table 8.4)	-	-	-	-	-	-	-	
15.	Noise contribution from main lobe and near sidelobes ($-5^\circ < \theta < +5^\circ$)	-	-	-	150	13.5	-	-	
16.	Radiation by sun and stars (not in main lobe!)	-	-	-	1.0	1.0	-	-	
	Totals		0.797			24.25	1.657	0.683	

Table 8.4.

Losses by mechanical imperfections, blocking and weather.

		4 GHz					6 GHz	
		losses dB	η	abs. power loss %	Noise 0° elev. °K	Noise 10° elev. °K	losses dB	η
17	Surface tolerance of subreflector 0,3 mm r.m.s.	-	neglected		-	-		
18	Surface tolerance main reflector 2 mm r.m.s.	0.487	0.894		-	-	1.101	0.776
19	Blocking subreflector 1%	0.044	0.99		-	-	0.362	0.920
	supports 3.5%	0.315	0.93	3.275	4.91	4.42		
20	Losses by feed offset, pointing errors, deviation paraboloid by own weight	0.101	0.977				0.2	0.955
21	= 20 at wind shears		calculations still to be carried out.					
22	Increase noise temperature in rainy and cloudy weather		not important for I.C.S.C. specification.					
23	Ohmic losses of the reflectors				0.5°	0.5°	0.017	0.996
	Totals		0.804		5.41	4.92	1.680	0.679

Losses and noise contributions of the system components.

		4 GHz					6 GHz	
		Losses dB	η	abs. power loss %	Noise 0° élev.	Noise 10° elev.	losses dB	η
24	Noise temp.paramp. + $\frac{T_{PA} + T_{TD}/G_{PA}=16+2.1}{2^{nd}}$ + 3rd stage	-	-		18.10	18.10	-	-
25	Reflection loss paramp = 4% -VSWR=1.5 Paramp noise by reflection of feed (f_3)	0.177	0.960	-	0.14	0.14	-	-
26	Ohmic losses: wave guide duplexer, circulator coax. filter (f_2)	0.20	0.955		12.65	12.65	0.301	0.933
27	Losses by mode conversion in the wave guide system							
28	Noise by cross coupler (23 dB) and tracking system (f_4)	0.022 0.01	0.995 0.998		2.16	2.16	-	-
29	Ellipticity losses	0.056	0.987	-	-	-	0.056	0.987
	Totals		0.898		33.05	33.05	0.357	0.921

Explanation of Table 8.3.

(1) The maximum VSWR of 1.2 introduces a power loss of 1%. Noise power increases and decreases also, if the power flow is considered from receiver to feed and from space to feed. In this design both contributions are nearly accidentally the same.

(2) The ohmic losses in feed and window are average values of an internally gilded feed closed by a melinex window as a protection against weather influences.

(4) The total amount of cross polarisation is 2%. It is assumed that the cross polarisation power is radiated into a small solid angle centred around the antenna axis (lit. 16, p. 423).

(5) The model discussed in Sec. 4.5.4.2. is used for the calculation of the noise contributions by spillover, back radiation and diffraction.

(7) The figures in the third columm are the power losses with respect to the total power supplied. These figures are important for calculating the noise temperature.

(10) Uniform illumination is proposed in this design except for a ring of about 1 metre width around the aperture edge. The field over this ring is tapered towards the edge to -10 dB to avoid that high diffraction losses occur around the main reflector edge, resulting in a decrease of antenna temperature. The value of 1 metre can be found by the principle of stationary phase. The aperture efficiency found will be 0.98 according to the method explained by Fig. 8.3. A figure of 0.94 has been put down in Table 8.3, as ray optics, by which the shaped reflectors have been calculated, can only be used to a certain extent. Moreover, the fact that the radiation of the feed is not be truly circular has been taken into account as well.

(11) Generally speaking, it is not possible to define an efficiency caused only by phase errors. Silver (lit. 16, p. 186), however, has shown that the problem can be approximated by a small quadratic error. In the design proposed a maximum quadratic error of about 20° is expected resulting in an efficiency of 0.95.

(12) The model of Sec. 4.5.4.2 has served again to calculate noise contributions of far side lobes and scattered diffraction power.

(15) According to Table 8.2, only about 87% of the total power supplied to the feed is radiated by the aperture. How this power is distributed is not exactly known as, it is difficult to predict what part of the power scattered by subreflector and support contributes to the main lobe and near side lobes (solid angle with flare angle of 5°). In this calculation it is therefore assumed that 90% of the total power supplied is radiated by the main reflector. The noise contribution by the main beam at an elevation angle of 10° will be 13.5° K as for an antenna without losses the average of this contribution would be 15° K (Fig. 4.3).

(16) The noise contribution due to radiation of the sun is 1° K at an average sidelobe level of -50 dB.

Explanation of Table 8.4.

(18) Considerable losses are introduced by surface inaccuracies. The loss in efficiency can be calculated by Ruze's formula (lit. 55)

$$\eta_A/\eta_o = \exp\left(-\frac{4\pi\varepsilon}{\lambda}\right)^2 \qquad \varepsilon = \text{rms error}$$

(19) Calculation of the blocking coefficient can be found in section 3. The model discussed in Sec. 4.5.4.2 has served to find the noise contributions by scatter from subreflector and supports.

(20) The losses by feed offset and subreflector mispositioning are estimated to be 0.1 dB. Additional calculations will be required after the mechanical designer has finished the strength calculations.

(23) According to lit. 13, for alluminium reflectors an additional noise contribution of 0.5° K has to be taken into account by absorption.

(24-29)

The data mentioned in this table have been placed at our disposal by third parties and are independent of the electrical antenna design. However, they place an important rule in the design of the complete system. More details of the contribution of these components are found in Sec. 4.6.2.

8.4.2. Final results

Noise contribution at 4 GHz in ^{o} K at 10^{o} elevation

(1) main lobe	13.5
(2) ground noise	13.67
(3) radiation of sun	1.-
(4) ohmic losses	1.-
Total noise T_A =	29.17^{o}K

The noise T_A is measured at the input terminals of the feed. At the input terminals of the parametric amplifier (Sec. 4.6.2) this noise will be

$$T_A' = T_A \cdot g_2(1-|\rho_1|^2)\,(1-|\rho_2|)^2 = 26.48^{o}\ K.$$

(5) noise paramp + 2nd and 3rd stage	18.1^{o}K	
(6) noise due to components	14.95^{o}K	(Table 8.4)
Total noise temperature	59.53^{o}K or 17.75 dB	

relative to 1^{o}K .

Table 8.5 Antenna efficiency

characteristic	4 GHz	6 GHz
electrical antenna efficiency, table 8.3.	0.797	0.683
blocking efficiency	0.920	0.920
aperture efficiency main reflector	0.894	0.776
component efficiency	0.898	0.921
feed offset and ohmic losses	0.977	0.955
Total efficiency	0.575	0.429
Total efficiency in dB	2.40	3.67

Maximum antenna gain $20 \log \frac{\pi D}{\lambda}$

D = 25 m. at 4 GHz G_{max} = 60.40 dB

D = 25 m. at 6 GHz G_{max} = 63.92 dB.

Net gain at 4 GHz at terminals of parametric amplifier
(60.40 - 2.40) = 58.00 dB.
Net gain at 6 GHz at transmitting terminals of duplexer
(63.92 - 3.67) = 60.25 dB.
Figure of merit G/T_s at 4 GHz at 10° elevation
(58.00 - 17.75) = 40.25 dB.

8.4.3. Expected antenna gain as a function of the frequency

So far it has been assumed that the beamwidth of the feed is independent of the frequency. In calculating the aperture efficiency a factor taking that the main beam is not exactly circularly symmetrical has been introduced. The (ideal) frequency-independent radiation pattern of the feed will give the same aperture efficiency over the entire frequency band.

The gain of the antenna as a function of the frequency is

$$G = 20 \log. \frac{f}{4} \quad (f \text{ in GHz})$$

This relationship is shown in Fig. 8.4. There will be no problem for frequencies higher than 4 GHz but at a frequency of 3.7 GHz the gain of the proposed antenna will be 0.66 dB lower. As the antenna dimensions relative to the wavelength will decrease with decreasing frequency, the diffraction effects have the tendency to increase. The noise temperature is, therefore, expected to increase by about 1° K.

The feed proposed will have a beamwidth slightly dependent on the frequency (Fig. 5.16). Generally speaking the beamwidth tends to increase at decreasing frequency. Therefore, spillover will increase at lower frequencies resulting in a higher noise temperature. The phase ics characteristics of the feed will not be entirely frequency independent either; the final computer programme will, therefore, be based on an average phase characteristic.

At higher frequencies the aperture efficiency will be somewhat lower as the beamwidth of the main lobe of the feed tends to decrease. This factor has already been taken into account when calculating the antenna gain at 6 GHz, indicating an aperture efficiency of only 85%.

The gain is expected to be 20 log $(\frac{6}{5.9})$ = - 0.14 dB lower at 5.9 GHz, in respect of 6 GHz and > 60 dB at frequencies higher than 6 GHz. The figure of merit G/T will be higher than 40 dB at frequencies higher than 4 GHz, and 0.8 dB lower at 3.7 GHz.

8.5. Conclusion

The calculations carried out so far indicate clearly the great difficulties in obtaining the required figure of merit. Most the stations existing at the moment (Jan. 1968) do not meet the specifications. A recent investigation (lit. 13) shows that most designers increase the antenna diameter to 27.5 metres for future stations; probably the specification is too severe for a 25-metre paraboloid, especially with the present parametric amplifiers as these have high noise temperatures.

It is recommended for the Dutch ground station to increase the antenna diameter likewise to 27.5 meter. The gain will increase by about 0.84 dB (Fig. 8.4), giving some margin in the figure of merit.

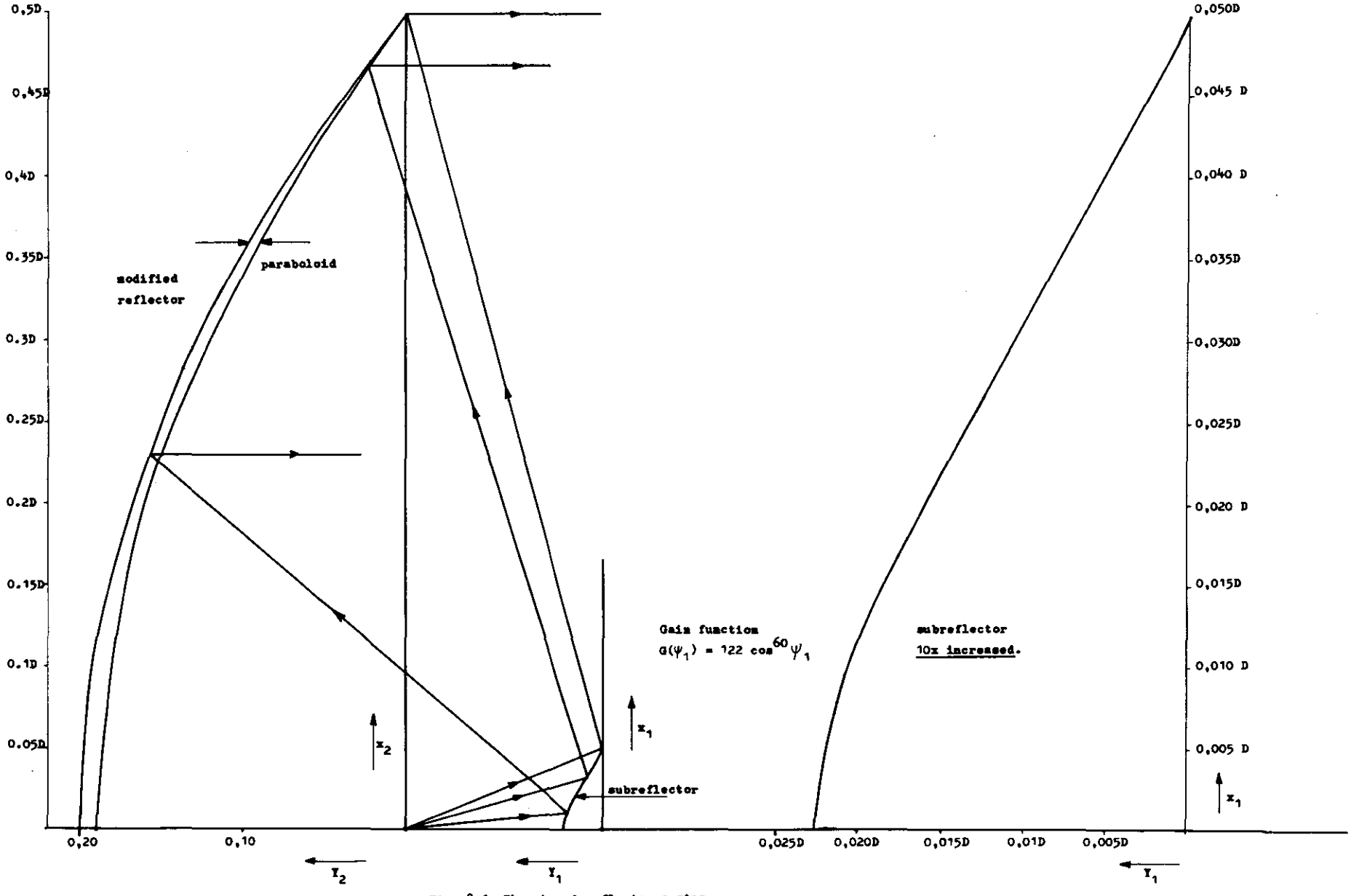

Fig. 8.1. The shaped reflector system

Fig. 8.3 Aperture efficiency integration paper.

relative fieldstrength
relative power

A_v = area under voltage plot
A_p = area under power plot
A_{tri} = area of entire angle

$$\eta_a = \frac{A_v^2}{A_p \cdot A_{tri}} \quad \text{(lit. 26)}$$

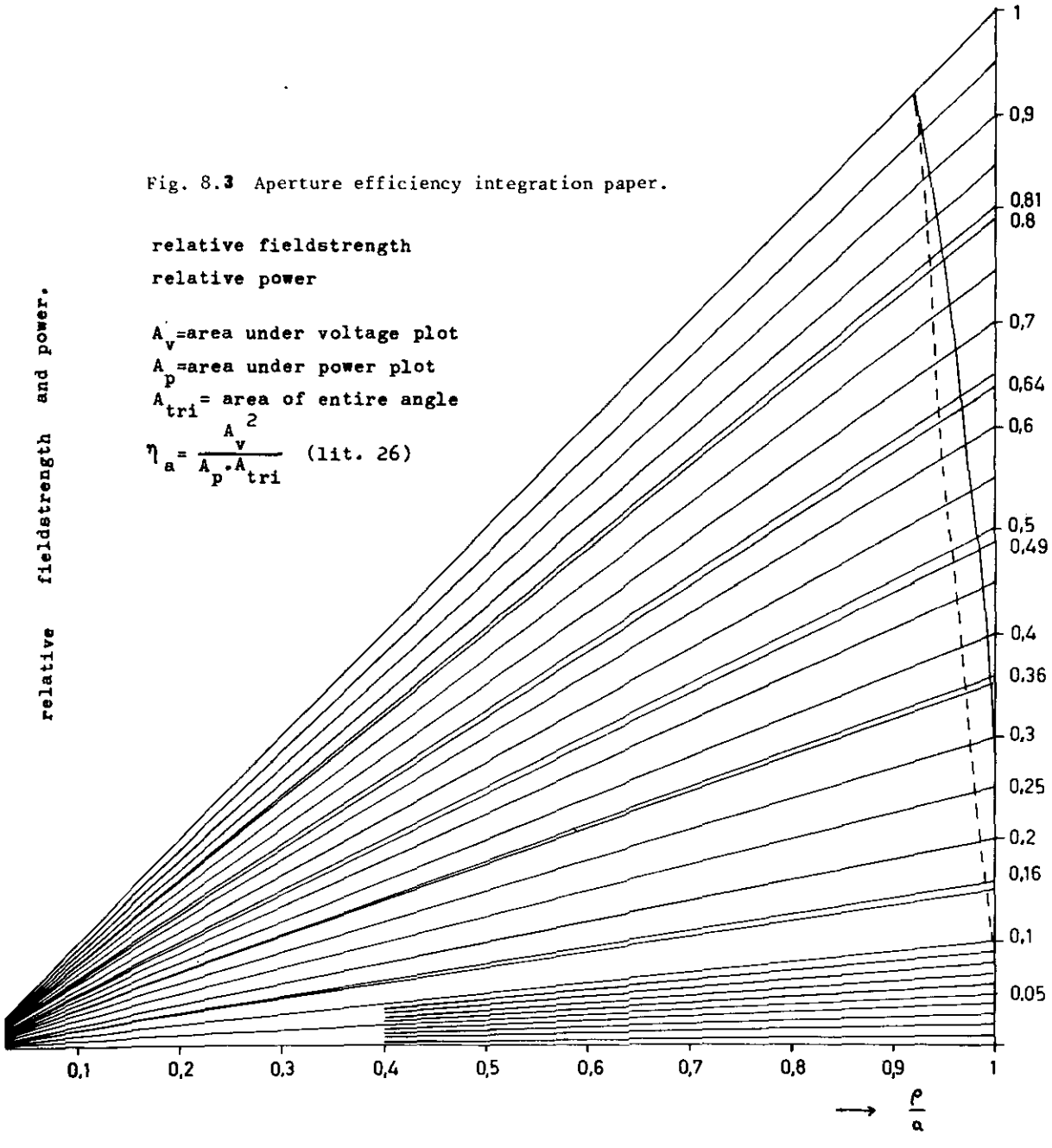

Fig. 8.4 The antenna gain as a function of the aperture diameter and the frequency.

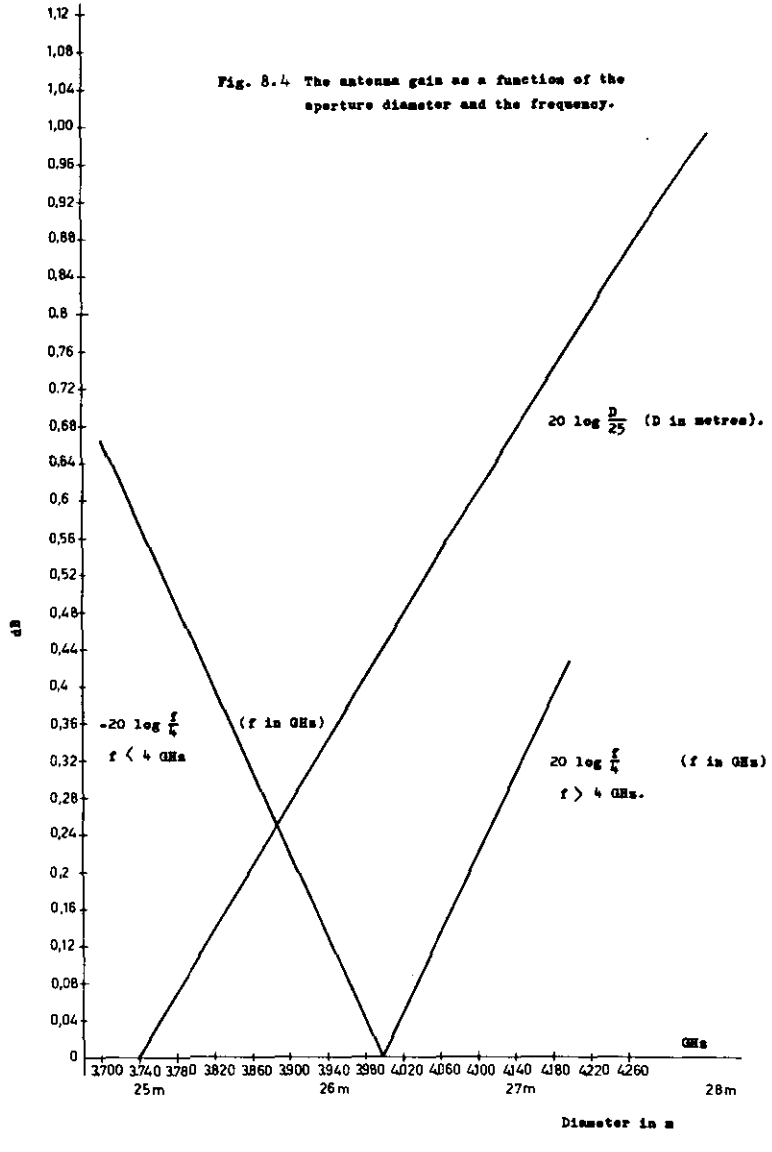

9. Literature.

1. C.F. Davidson and I.A. Ravenscroft:
"Design considerations for a centre fed paraboloidal aerial system for a satellite-communication earth station",
Conference on large steerable aerials, London, June 6-8 1966, pp.289-303.

2. F. Taylor:
"The Goonhilly project",
The Inst. of Electrical Engineers, Savoy Place, London, 1964.

3. P.W. Hannan:
"Microwave antennas derived from the cassegrain telescope",
Trans. IRE AP-9, no.2, pp. 140-153, March 1961.

4. M.E. Viggh:
"Cassegrain antennas",
Elteknik, 5, no.5, pp.83-87, May '62.

5. M.E. Viggh:
"Designing for desired aperture illuminations in Cassegrain antennas",
I.E.E.E., AP-11, no.2, pp. 198-199, March 1963.

6. P.D. Potter:
"Design and performance of the NASA/JPL 210 ft steerable paraboloid",
Design and construction of large steerable aerials, I.E.E. Conference, June 6-8, 1966.

7. E. Gillitzer:
"Die Cassegrain-Parabolantenne und andere Antennes für breitband-Richtfunk bei 6 GHz",
Frequenz, 16, Nr. 11, S.459-468, Nov. 1962.

8. G. von Trentini ,K.P. Romeiser und E. Jatsch:
"Dimensionierung und Elektrische Eigenschaften der 25 M. Antenne der Erdefunkstelle Raisting usw.",
Frequenz, 19, Nr.12, S.402-421, Dec. 1965.

9. G. von Trentini:
"Erregersysteme für Cassegrain-Antennen",
Frequenz/Sonderausgabe, 17, S.491-599, Dec. 1963.

10. W.F. Williams:
"High efficiency antenna reflector",
Microwave Journal, pp. 79-82, July 1965.

11. V. Galindo:
"Design of dual reflector antennas with arbitrary phase and amplitude distributions",
I.E.E.E. Trans. on Antennas and Propagation, pp.403-408, 1964.

12. B.Y. Kinber:
"On two reflector antennas",
Radio Engrg Electronic Phys. 7, pp.914-921, June 1962.

13. J. Dijk:
"Overzicht van grondstations voor satelliet communicatie",
Intern rapport, TH Eindhoven, Mei 1967.

14. D.O. Woodbury:
"The glass giant of Palomar",
Dodd Mead and Co., New York, N.Y. 1957.

15. P.D. Potter:
"Aperture illumination and gain of a cassegrainian system",
I.E.E.E. Transactions on Antennas and Propagation, pp.373-375, May '63.

16. S. Silver:
"Microwave antenna theory and design",
New York, 1949.

17. M.S. Afifi:
"Scattered radiation from microwave antennas and the design of a paraboloid-plane reflector antenna",
Thesis, July 1967, TH Delft, Netherlands.

18. W.V.T. Rusch:
"Scattering from a hyperboloidal reflector in a cassegrainian feed system",
I.E.E.E., AP-11, no. 4, pp.414-421, July 1963.

19. P.D. Potter:
"Unique feed system improves space antennas",
Electronics, pp.36-40, June 22, 1962.

20. F.J. Sheftman:
"Experimental study of subreflector support structures in a cassegrainian antenna",
M.I.T. Technical Report 416, 23 september 1966.

21. J.H. Nested:
"Shadow and diffraction effect of spars in a cassegrainian system",
Design and construction of large steerable aerials, I.E.E.E. Conference , London, June 6-8, 1966.

22. C.L. Gray:
"Estimating the effect of feed support member blocking on antenna gain and side-lobe level",
The Microwave Journal, p. 88-91, March 1964.

23. E.G. Doidge:
"Antenna gain as it applies to satellite communication earth stations",
U.S. Seminar on Communication Satellite Earth Station Technology, Washington D.C., May 16-27, 1966.

24. P.D. Potter:
"The application of the cassegrainian principle to ground antennas for space communications",
I.R.E. Transactions on Space Electronics and Telemetry , p. 154-158, June 1962.

25. A. Sciambi:
"Instant antenna patterns",
Microwaves, 48-60, June 1966.

26. A. Sciambi:
"The effect of the aperture illumination on the circular aperture antenna pattern characteristics",
Microwave Journal, p. 79-84, Aug. 1965.

27. G. Doundoulakis:
"Far field patterns of circular paraboloid reflectors",
General Bronze Corporation, Garden City, L.I.N.Y.

28. A. Giger and R.H. Turrin:
"The triply-folded horn reflector",
The B.S.T.J., p. 1229-1253, Sept. 1965.

29. Lamont V. Blake:
"Low noise receiving-antennas",
Microwaves, p. 18-27, March 1966.

30. D.C. Hogg:
"Effective antenna temperatures due to oxygen and water vapour in the atmosphere",
Journal of Applied Physics, vol. 30, nr 9, p. 1417-1419, Sept. 1959.

31. D.C. Hogg and W.W. Mumford:
"The effective noise temperature of the sky",
The Microwave Journal, p. 81-84, March 1960.

32. D.C. Hogg, R.A. Semplak:
"The effect of rain and water vapor on sky noise at centimeter wavelengths",
The B.S.T.J., p. 1331-1348, Sept. 1961.

33. M. Hoffman:
"Antenna noise temperature",
U.S. Seminar on satellite communications earth station technolog.,
May 16-27, 1966 Washington D.C.

34. P. Foldes:
"The capabilities of cassegrain microwave optics systems for low noise antennas",
Solid State Electronics, vol. 4, p. 319-356, Oct. 1962.

35. A.D. Kuz'min and A.E. Salomonovich:
"Radioastronomical methodes of antenna measurements",
Academic Press, New York and London, 1966.

36. J. Tischer:
"Basic theory of space communications",
D. van Nostrand Comp. Inc., Princeton, New Yersey, 1965.

37. J.H. Piddington:
"The origin of galactic radio-frequency radiation",
Mon. Not. Roy. Astron. Soc., Vol 111, p. 45-63 Jan. 1951.

38. R.H. Dicke, P.J.E. Peebles, P.G. Roll and D.T. Wilkinson:
"Cosmic black-body radiation",
Astrophys. J. (USA) Vol 142 no 1, p. 414-419, July 1965.

39. J.O. Artman and J.P. Gordon:
"Assorption of microwaves by oxygen in the millimeter wavelength region",
Physical Review, Vol. 96, p. 1237-1245, Dec. 1954.

40. J.H. van Vleck:
"The absorption of microwaves by oxygen",
Physical Review, Vol. 71, p. 413-424, April 1947.

41. R.H. Dicke, R. Beringer. R.L. Kyhl and A.B. Vane:
"Atmospheric absurption measurements with a microwave radiometer",
Physical Review, Vol. 70, p. 340-348, Sept. 1946.

42. S.N.C. Chen:
"Apparent temperatures of smooth and rough terrain",
I.R.E. Transactions on antennas and propagation, p. 567-572, March 1960.

43. E. Weger:
"Apparent thermal noise temperatures in the microwave region",
I.R.E. Transactions on antennas and propagation, p. 213-217, March 1960.

44. H. Reed:
"Noise curves for high-gain antennas",
Microwaves, p. 46-49, April 1967.

45. C. Dragone and D.C. Hogg:
"Wide-angle radiation due to rough phase fronts",
The B.S.T.J., p. 2285-2296, Sept. 1963.

46. D.H. Shinn:
"The effect on gain and sidelobes of errors in the profile of a parabolic reflector",
Design and construction of large steerable aerials, I.E.E. Conference, London, June 6-8 1966.

47. L. Tartakovskii:
"Side radiation from ideal paraboloid with circular aperture",
Radio Engng. and Electronics Phys. 4, nr. 6, p. 14-28, 1959.

48. D.C. Hogg, R.A. Semplak:
"An experimental study of near-field cassegrainian antennas",
The B.S.T.J. p. 2677-2704, Nov. 1964.

49. P. Foldes e.a.:
"A cassegrainian feed for wide-band satellite communications",
R.C.A. Review, p. 369-399, Sept. 1965.

50. K.A. Green:
"Modified cassegrain antenna for arbitrary phase and amplitude illumination",
I.E.E.E. Transactions of Antennas and Propagation, p. 589-590, Sept. '63.

51. W. Rusch:
"A comparison of diffraction in cassegrainian and gregorian radio telescopes",
Proc. of the I.E.E.E., p. 630-631, April 1963.

52. J.S. Kikkert:
"Dimensionering van de cassegrain-antenne",
Report TH Eindhoven Jan. 1967

53. T.G. Williams, P.R. Cobb and H.L. Smith,
"Telecommunication antennas - design problems",
U.S. Seminar on Communication satellite earth station technology, p. 245-271, May 16-27 1966.

54. L.V. Blake, Private communication:
"Britisch Council post office course satellite communication",
Dec. 1965.

55. J. Ruze:
"Antenna tolerance theory - a review",
Design and construction of large steerable aerials I.E.E. conference, June 6-8 1966.

Appendix

To determine the power radiated into a solid angle the procedure to be followed should be:

(1) Redraw the radiation pattern (Fig. A. 1) on the special sin θ paper (Fig. A. 2 and A. 3).

(2) Determine the surfaces of the various parts of the pattern. (planimeter).

(3) The proportion of the surface of the required part to the total pattern surface is the relative power radiated within the specified solid angle corresponding to the required pattern surface.

In Fig. A. 1 the total surface is 0.3115. We want to know which part of the total power radiated, is contained within the -10dB points of the mainlobe of the pattern. We find a surface within the 10 dB points of 0.2715. Therefore:

$$\text{Relative power} = \frac{0.2715}{0.3115} \times 100\% = 87.1\%$$

Further we find that the relative power radiated within the -20 dB points is 94.9% and within the -30 dB points 97.0% .

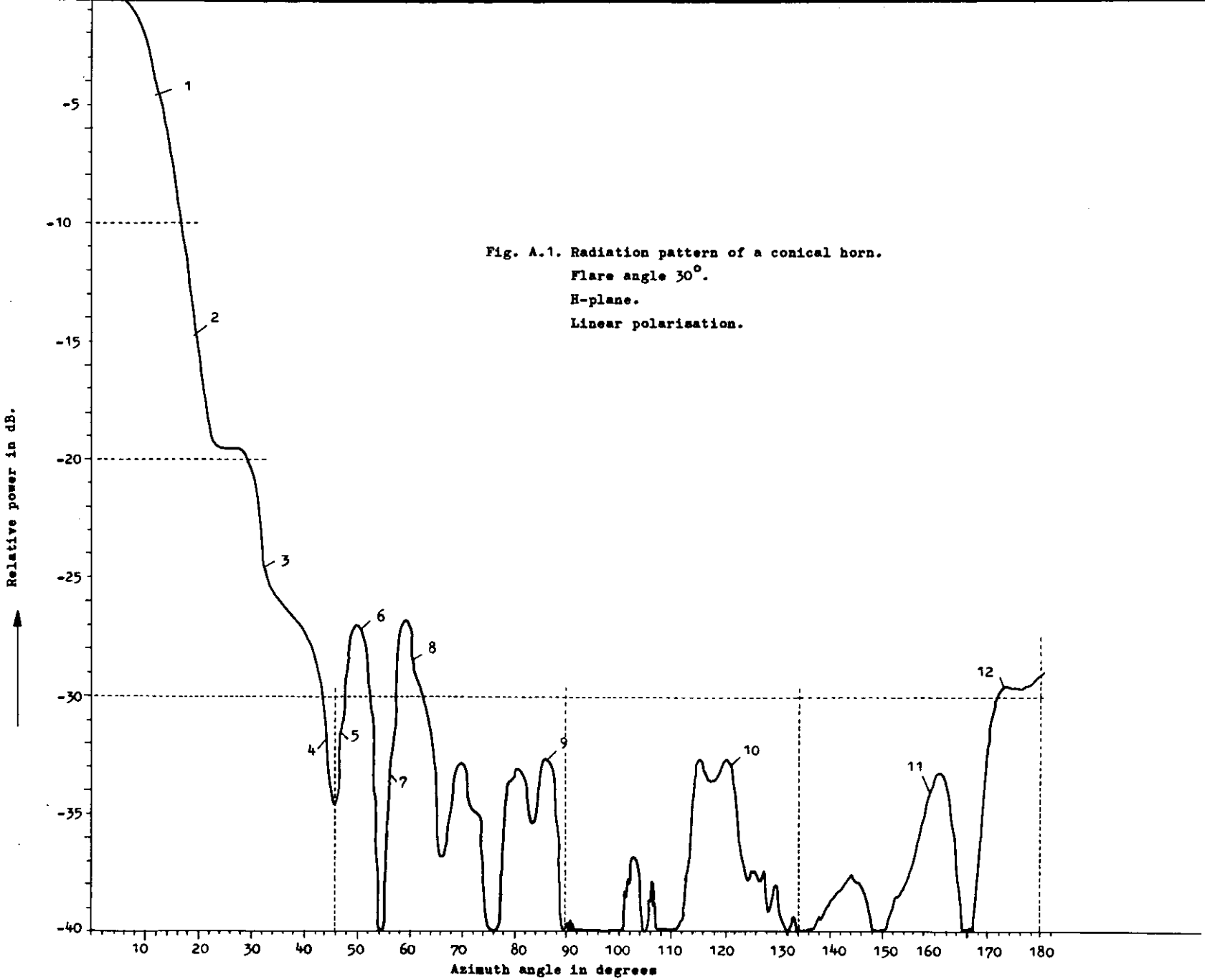

Fig. A.1. Radiation pattern of a conical horn.
Flare angle 30°.
H-plane.
Linear polarisation.

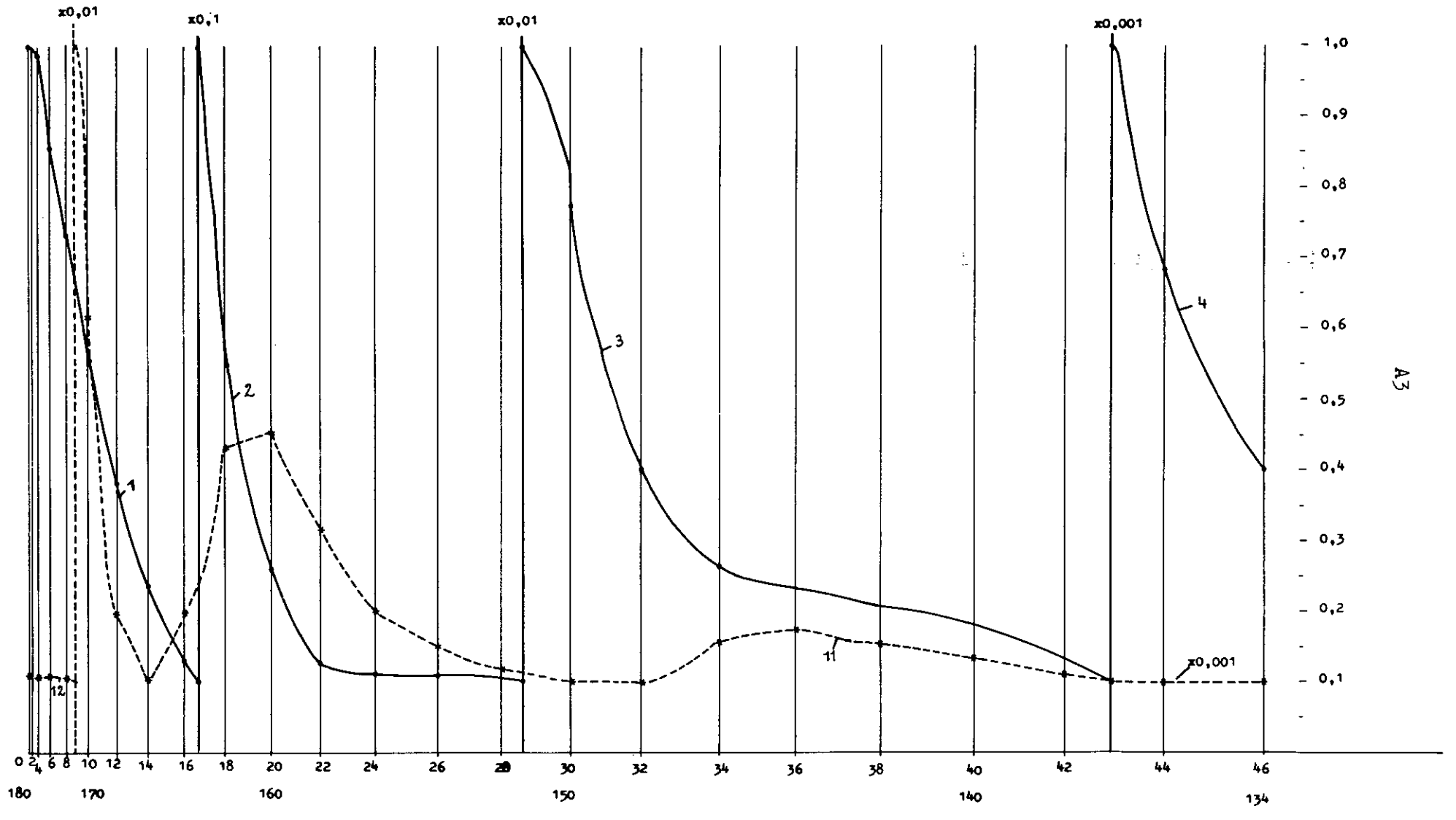

Fig. A.2. Conical horn.
Flare angle 30°.

Scale 2:1 (x axis)
Horizontally $\Delta\theta \sin\theta$ with $\Delta\theta = 2°$.

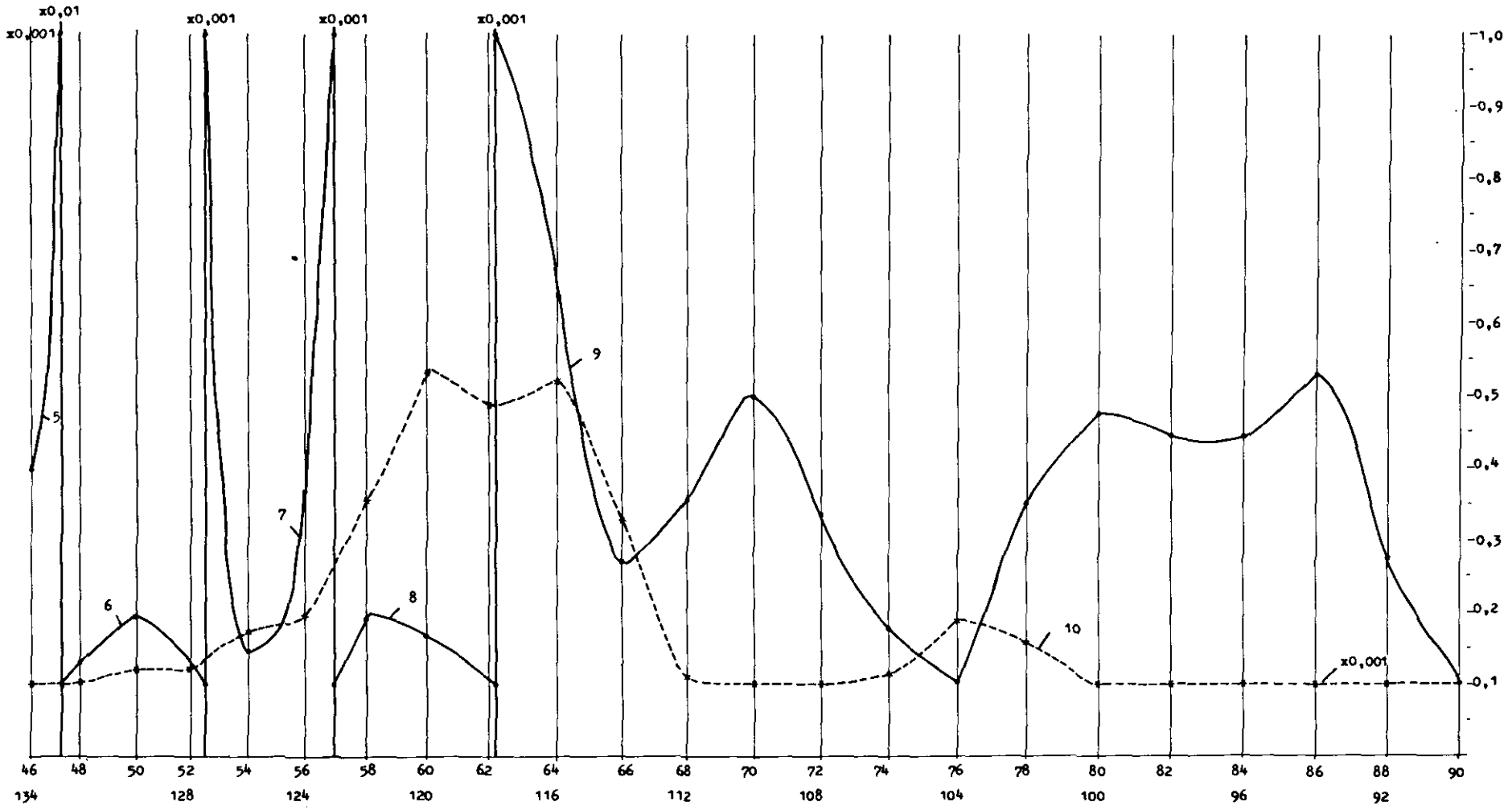

Fig. A.3. Conical horn. Flare angle 30°

Scale 1:1 (x-axis)

Horisontally $^{4}\theta_{min}\theta$ with $\Delta\theta = 2°$.